GROUNDWATER FLOW AND TRANSPORT MODEL SEASIDE GROUNDWATER BASIN MONTEREY COUNTY, CALIFORNIA

October 26, 2007

Prepared for:

RBF Consulting
3180 Imjin Road, Suite 110
Marina, CA 93933

Prepared by:

Timothy J. Durbin, Inc.
5330 Primrose Drive, Suite 228
Fair Oaks, CA 95628

Table of Contents

List of Figures

List of Tables

1.0 Introduction

1.1 Purpose and Scope of Report

The Seaside groundwater basin, which is located adjacent to and beneath Monterey Bay (Figure 1.1), has been the subject of an ongoing adjudication. Groundwater pumping exceeds the natural and secondary recharge, groundwater levels have been declining, and the adjudication has focused on the corresponding threat of seawater intrusion. While seawater intrusion has not been detected, except near Marina, the parties to the adjudication recognized the inevitability of eventual seawater intrusion were existing conditions to continue. However, the parties did dispute the best approach to addressing the threat, with respect to both the institutional setting and the physical solution.

A trial was held during late 2005 in the Monterey County Superior Court to adjudicate the disputed issues. The outcome was that the Court ordered the creation of a Watermaster, which was to be comprised of a collective of water users. The Watermaster was directed to monitor groundwater conditions, develop a physical solution, and implement the solution. The Court directed that the Watermaster report periodically to the Court on progress toward meeting it obligations.

An obligation of the Watermaster is to develop a groundwater model. During the trial, the testimony for the California-American Water Co. included the description of a groundwater model, which was used to evaluate the threat of seawater intrusion. In its post-trail decision, the Court ordered the creation of a groundwater model. Subsequently, the Watermaster decided the groundwater model developed for California American Water could meet the current basin-management needs. That model includes both groundwater flow and solute transport components. The trial testimony did not include written documentation of the model, which the Watermaster needs in order to use the model.

This report represents the needed documentation. The objective of the report is to describe the available data, the use of the data to develop the model, the predictive simulations, and the structure of the model input files. The documented model is the same as that presented to the court during the trial.

1.2 Description of Study Area

1.2.1 Physiographic Features

The Seaside groundwater basin underlies the hills and coastal plane at the northern end of the Sierra de Salinas (Figure 1.2). The principal drainages are Arroyo del Rey and El Toro Creek. Arroyo del Rey is a northwestward flowing tributary to Monterey Bay. El Toro Creek is a northeastward flowing tributary to the Salinas River.

While Arroyo del Rey and El Toro Creek drain mostly the upland areas overlying the groundwater basin, smaller streams drain the coastal plane toward Monterey Bay.

Yates and others (2005) examine the possible contributions of these streams to groundwater recharge. They concluded that El Toro Creek and Arroyo del Rey contribute insignificantly to groundwater recharge. Along limited reaches, these streams gain streamflow from groundwater discharge. However, the stream-aquifer exchanges are not important to either the groundwater budget or the response of the groundwater basin to pumping. Yates and others (2005) also concluded the smaller streams contribute insignificantly to groundwater recharge.

1.2.2 Hydrogeologic Features

The Seaside groundwater basin is underlain by six hydrogeologic units ranging from Miocene to Holocene age. From oldest to youngest, these units include the Monterey Formation of Miocene age, the Santa Margarita Formation of Miocene to Pliocene age, the Purisima Formation of Miocene to Pliocene age, the Paso Robles Formation of Pliocene to Pleistocene age, the Aromas Formation of Pleistocene Age, and surficial deposits of Pleistocene to Holocene age (Greene, 1970; Greene, 1977; Logan, 1982; Muir, 1982; Clark and others, 1997; Saucedo and others, 2000; Feeney and Rosenberg, 2002; Wagner and others, 2002). Figure 1.3 shows the surficial occurrences of these units, and Figures 1.4a-b show generalized cross sections through the groundwater basin. The map and cross sections represent generalizations derived for CH2M/Hill (2005) and Yates and others (2005).

While the Monterey Formation is essentially non-water-bearing, the younger units contain the active groundwater system. The Monterey Formation consists of low-permeability marine shale and mudstone, and locally is as much as 3,000 ft in thickness. The overlying Santa Margarita Formation consists of moderately-permeable sandstone, and locally is as much as 400 ft in thickness. The overlying Purisima Formation consists of poorly-permeable to moderately-permeable gravels to silty clays, which typically are poorly consolidated. The formation locally is as much as 1,000 ft in thickness. The overlying Paso Robles Formation consists of moderately-permeable to highly permeable gravels to silts, which typically are moderately consolidated. The formation locally is as much as 700 ft in thickness. The overlying Aromas Formation consists of highly-permeable sands deposited by wind and waves, and locally is as much a 200 ft in thickness. The contemporaneous and overlying surficial deposits consist of moderately-permeable to highly-permeably alluvial and other clastic deposits, and locally may be as much as 200 ft in thickness.

Figure 1.5a shows the extents and base altitudes of the Santa Margarita, Purisima, and Paso Robles formations. It shows also the extents and base altitudes of the surficial deposits and Salinas Valley clay. The Santa Margarita Formation underlies most of the landward part of the groundwater basin and the eastern seaward part (Figure 1.5a). The Purisima Formation underlies the northern landward part of the groundwater basin and eastern seaward part (Figure 1.5b) The Paso Robles Formation underlies all of the

landward part of the groundwater basin and the eastern seaward part (Figure 1.5c). The surficial deposits underlie the central part of the groundwater basin (Figure 1.5d). The Salinas Valley clay underlies a small area along the northern landward boundary of the groundwater basin (Figure 1.5e).

The base altitudes shown on Figures 1.5a-e were developed from various sources. For the landward part of the groundwater basin, the altitude contours represent extrapolations from the cross sections developed by CH2M/Hill (2005) and Yates and others (2005). For the seaward part of the groundwater basin, the contours represent a generalization and extrapolation from Greene (1970) and Greene (1977).

The top of the Monterey Formation represents the stratigraphic base of the groundwater basin, and the active groundwater system is limited to the overlying more-permeable formations. The altitude ranges from 1,800 ft below sea level to 1,600 ft above sea level. However, within much of the geographic area where the Monterey Formation is overlain, the base of the groundwater system is below sea level. Within most of the landward part of the groundwater basin, the Monterey Formation is overlain immediately by the Santa Margarita Formation, and the lowest interval of the groundwater system is contained in that formation. Along the eastern margin of the basin, the Monterey Formations is overlain immediately by the Paso Robles Formation, and there the lowest interval of the groundwater system is contained in that formation. Within the western seaward part of the groundwater basin, the Monterey Formation is overlain immediately by the Purisima Formation, and the lowest interval of the groundwater system is contained in that formation.

The groundwater basin is intersected by several significant northwest-trending faults as shown on Figure 1.3. The Chupines Fault is the most southerly. The Monterey Formation is displaced downward on the northeast side by about 100 ft. The Seaside Fault is located about 2,000 ft northeast of the Chupines Fault. There, the Monterey Formation is displaced downward on the northeast side by about 200 ft. The Ord Terrace Fault is located about 6,000 ft northeast of the Seaside Fault. There, the Monterey Formation is displaced downward on the northeast side by about 50 ft. The Reliz Fault is located near the Salinas River about 30,000 ft northeast of the Ord Terrace Fault. There, the Monterey Formation is displaced downward on the northeast side by as much as 1,000 ft.

While the vertical displacement along faults impact the geometry of the groundwater basin, they do not appear to have much influence on groundwater flow. However, the Ord Terrace Fault may represent an exception. Within the southeastern part of the groundwater basin, the Ord Terrace Fault appears to be responsible for abruptly lower groundwater levels on its north side relative to its south side, at least as interpreted by Yates and others (2005). However, the supporting water-level data are so sparse that the actual influence of the Ord Terrace Fault is uncertain.

1.2.3 Basin Boundary

Various investigators have variously delineated the boundary of the Seaside groundwater basin. The California Department of Water Resources (2003) defines two subbasins of the Salinas Valley groundwater basin within the Seaside area (Figure 1.6). The Seaside Area Subbasin extends along the Monterey Bay coastal plane from the Chupines Fault to the Reliz Fault, and it includes the communities of both Seaside and Marina. The Corral de Terra Area Subbasin comprises the upland areas east of the coastal plane. CH2M/Hill (2005) defined the Seaside groundwater basin (Figure 1.6) as consisting only of the southern one-half of the area defined by the California Department of Water Resources (2003) as the Seaside Area Subbasin. Yates and others (2005) similarly defines the Seaside groundwater basin (Figure 1.6), except that the northern boundary of his delineation is about 4,000 ft south of the CH2M/Hill (2005) boundary. Both CH2M/Hill and Yates located the northern boundary based not on a hydrologic feature but on the assumed occurrence of a groundwater divide. While such a divide would represent a no-flow boundary, CH2M/Hill (2005) and Yates and others (2005) both inconsistently ascribe northward groundwater flow across the boundary.

For the development of the groundwater model, the Seaside groundwater basin (Figure 1.6) includes both Seaside Area Subbasin and Corral de Terra Area Subbasins as generally described by the California Department of Water Resources (2003). The southwestern boundary is represented by segments of the Chupines, Seaside, and Ord Terrace faults, the northeastern boundary is the Reliz Fault, the southeastern boundary is the surface contact between the Monterey Formation and the overlying formations, and the offshore boundary is the subsea contact between the Monterey Formation and the overlying formations (Greene, 1970; Greene, 19977). Except at the Reliz Fault, the boundaries are no-flow boundaries because the Monterey Formation impedes cross-boundary groundwater flow. However, cross-boundary flow occurs between the Seaside basin and 180/400-Foot aquifer sub-basin of the Salinas Valley groundwater basin (California Department of Water Resources, 2003). Within the boundaries of the Seaside basin, groundwater flows in response to recharge, pumping, and the hydraulic interactions with Monterey Bay, including groundwater flow across the northern boundaries defined by CH2M/Hill (2005) and Yates and others (2005).

The groundwater divide used by CH2M/Hill (2005) and Yates and others (2005) is not used as a boundary for the development of the groundwater model. This is the case firstly because neither CH2M/Hill (2005) nor Yates and others (2005) considered it to be a no-flow boundary, because both quantify northward groundwater flow across the divide. This is the case secondly because the divide is not a stationary hydrologic boundary. Even if the divide were to be a no-flow boundary, such a no-flow boundary would tend to move in response to groundwater pumping. Correspondingly, the northern model boundary is the Reliz Fault. Even though that is not a hydrologic boundary, the Reliz Fault is sufficiently distant from the principal groundwater pumping that its actual characteristic is not important.

The boundary used for the model development is not the adjudication boundary. The adjudication boundary encloses a smaller geographic area than the model boundary, and the adjudication boundary is mostly contained within the model boundary.

1.2.4 Cultural Features

The communities of Seaside, Del Ray Oaks, and Marina overlie the basin. However, the majority of the groundwater basin is overlain by mostly undeveloped land. That land represents native vegetation and minor residential development. Figure 1.7 is a 2000 false-color infrared satellite image on which the communities and undeveloped land can be identified. The developed areas appear as light blue on the image, and the undeveloped areas appear as pink to red. The more reddish areas correspond to more verdant vegetation.

1.2.5 Water Use

Groundwater is the water supply for communities within the Seaside groundwater basin. However, groundwater pumping can be different than the water use because the regional water-distribution system has interconnections that cross the southeastern basin boundary. Water can be conveyed through the interconnections from or to the Seaside basin to or from the areas otherwise served from the Carmel River basin, and the net transfers in recent years have been from the Seaside basin to the areas otherwise served from the Carmel River basin. Considering just basin boundaries defined by CH2M/Hill (2005), the water use within the Seaside groundwater basin was 6,000 acre-ft (CH2M/Hill, 2005, Terry Foreman, written communication). However, the groundwater pumping was about 6,200 acre-ft (CH2M/Hill, 2005), which suggests a net transfer of 200 acre-ft . The groundwater pumping within the Seaside basin is supported by annual natural recharge of about 4,200 acre-ft and secondary recharge of about 400 acre-ft (CH2M/Hill 2005), which suggests that the 2002 pumping exceeded the natural and secondary recharge by about 1,800 acre-ft.

Little agricultural water use occurs within the Seaside groundwater basin. Some agricultural water use occurs immediately adjacent to the northern basin boundary. However, the groundwater pumping for that water use has essentially no impact on the Seaside groundwater basin with respect to the adjudicated area.

1.2.6 Groundwater Conditions

Groundwater flows northwestward and northward within the Seaside basin, and this pattern occurs within both the Paso Robles and Santa Margarita formations. This is expressed in the groundwater-level contours shown on Figures1.8a-b, where the contours are modified from Yates and others (2005, Figures 13 and 15). Within both the Paso Robles and Santa Margarita formations, groundwater levels within the southeast corner of the Seaside basin have an altitude of about 180 ft, and groundwater flows radially from that corner toward Monterey Bay and the Salinas Valley. The pattern of radial groundwater flow results from the boundary effects produced by the hydraulic interactions between the Seaside basin, Monterey Bay, and the Salinas Valley.

However, pumping from wells within Seaside and Marina has produced local groundwater levels lower than sea level. Within the Paso Robles Formation, groundwater levels are below sea level underlying Seaside, where groundwater levels are as much as 30 ft below sea level. Groundwater levels are below sea level within a roughly circular area that is about 7,000 ft in diameter and is located entirely landward of Monterey Bay. Within the Santa Margarita Formation, groundwater levels are below sea level underlying both Seaside and Marina, where groundwater levels respectively are as much as 40 ft and 50 ft below sea level. Underlying Seaside, groundwater levels are below sea level within an area that is about 10,000 ft in diameter and is located partly beneath Monterey Bay. Underlying Marina, groundwater levels are below sea level within an area that is about 4,000 ft in diameter and is located entirely landward of Monterey Bay.

Little groundwater-level data are available for the Purisima Formation. Similarly, little data are available for the surficial deposits, except adjacent to the northern boundary of the Seaside basin. However, the groundwater conditions within the Purisima Formation and surficial deposits most likely are similar to the corresponding local conditions within the Santa Margarita and Paso Robles formations.

Except for areas underlying Marina, seawater intrusions has not been detected within the Seaside groundwater basin. The impacted area as reported by the Monterey County Water Resources Agency (2001) are shown on Figures 1.8a-b, which delineate the extent of intrusion within both 180-Foot and 400-Foot aquifers. The maximum southward extent is about 6,000 ft from the Reliz Fault, where the extent represents areas with chloride greater than 500 mg/L.

1.3 Model Code Used

The groundwater model was developed using a modified version of the U. S. Geological Survey computer program *FEMFLOW3D,* Version 1.0 (Durbin and Bond, 1998), which is referred to as *FEMFLOW3D,* Version 3.0, (Durbin, 2007) *FEMFLOW3D* is a program for simulating three-dimensional groundwater systems using the finite-element method. *FEMFLOW3D* includes a module for vertically expanding or contracting the model grid to follow a fluctuating groundwater table as described by Durbin and Berenbrock (1985), which is a feature not included within *FEMFLOW3D,* Version 1.0. With respect to groundwater flow, the mathematical basis and source code of *FEMFLOW3D,* Version 3.0is the same as described by Durbin and Bond (1998) and Durbin and Berenbrock (1985). The simulation of groundwater flow is based on the governing equation

$$\frac{\partial}{x_i}\left(K_{ij}\frac{\partial h}{\partial x_j}\right)+W=S_s\frac{\partial h}{\partial t} \qquad (1.1a)$$

with the free-surface boundary condition

$$K_{ij}\frac{\partial h}{\partial x_j}n_i = -S_y\frac{\partial h_f}{\partial t}n_3 \qquad (1.1b)$$

for

$$i = 1,2,3$$
$$j = 1,2,3$$

where h is the hydraulic head (ft), h_f is the water-table altitude (ft) K_{ij} is a component of the hydraulic conductivity tensor (ft/d), W is the source injection rate per unit volume (1/d), S_s is the specific storage (1/ft), n_i is component of the outward normal on the water-table surface, S_y is the specific yield (ft^0), x_i is an axis of a right-hand Cartesian coordinate system (ft), and t is time (d).

However, with respect to solute transport, new modules have been added with a mathematical basis as described by Pinder and Gray (1977). The modules allow the simulation of a non-reacting solute with linear sorption and decay according to the governing equation

$$\phi\left(1+\frac{\rho_b K_s}{\phi}\right)\frac{\partial c}{\partial t} = \frac{\partial}{\partial x_i}\left(\phi D_{ij}\frac{\partial c}{\partial x_j}\right) + \frac{\partial}{\partial x_i}\left(q_i c\right) + \phi W c^* - \phi\lambda c \qquad (1.2)$$

for

$$i = 1,2,3$$
$$j = 1,2,3$$

where c is the solute concentration (mg/ft^3), ϕ is the effective porosity (ft^0), D_{ij} is a component of the dispersion tensor (ft^2/d), q_i is a component of the groundwater flux (ft/d), c* is the concentration of injected water (mg/ft^3), ρ_b is the aquifer bulk density (mg/ft^3), K_s is the partitioning coefficient (ft^3/mg), and λ is the decay coefficient (1/d)

Equations 1.1 and 1.2 are solved within *FEMFLOW3D* using the finite-element method (Pinder and Gray, 1977; Wang and Anderson, 1995; Huyakorn and Pinder, 1983). The solution uses linear four-node tetrahedral elements (Huyakorn and Pinder, 1983, p. 88-91). However, a mesh is input to *FEMFLOW3D* using three-dimensional wedge elements that subsequently are decomposed into tetrahedrons within *FEMFLOW3D*. The mathematics of the solution are identical to those described by Pinder and Gray (1977, pp.126-199). The shape functions for the tetrahedral elements were derived from Zienkiewicz and Taylor (1989, pp. 135-139).

FEMFLOW3D, Version 3.0 is described in a user's manual (Durbin, 2007). The manual describes the mathematical bases and input formats for simulating groundwater

flow and solute transport. Additionally, the manual describes the application of *FEMFLOW3D* to test problems for which the solution is known.

The transport and ground-water flow simulations do not account for the density effects normally associated with seawater intrusion. Those effects were not included because they were assumed to be unimportant to the simulation of potential landward seawater intrusion into the Seaside groundwater basin. This assumption is based on simulations that were made with the computer program *FEMWATER* (U.S. Army, 1995), which simulates density-dependent groundwater flow. *FEMWATER* was used to simulate two-dimensional groundwater flow in a generalized cross section. The section was perpendicular to the Monterey Bay shore and extended beneath the bay. The simulation results were that the seaward part of the groundwater basin contains only dilute seawater, except for the immediately contact zone between Monterey Bay and the underlying groundwater system. Therefore, the potential for seawater intrusion can be simulated without considering density aspects.

2.0 Data Used

2.1 Previous Work

A large number of reports have been prepared on the geology and water resources of the Seaside groundwater basin and adjacent areas, and selected reports were obtained and reviewed during the development of the groundwater model. The reviewed materials include reports on geologic and hydrogeologic investigations by Wagner and others (2002), Clark and others (1997), Greene (1970 and1977), Stall, Gardner & Dunn (1987, 1988, 1990a, and 1990b), Logan (1982). They include reports on water-resource investigations by CH2M/Hill (2005), Yates and others (2002 and 2005), Yates and Rosenberg (2005), Hanson and others (2002), Yates and others (2002), Yates (1988), Durbin and others (1978), and Muir (1982). Additionally, geospatial information was obtained from the California Geological Survey, California Spatial Information Library, California Department of Water Resources, and U. S. Geological Survey.

However, the development of the groundwater model relied mostly on the reports by CH2M/Hill (2005) and Yates and others (2005).

The report "Hydrogeologic Assessment of the Seaside Groundwater Basin" was prepared by CH2M/Hill (2005) for the California-American Water Co. The report was prepared to facilitate the development of a groundwater management strategy for the Seaside groundwater basin. The report contains a compilation of hydrogeologic information, including maps and cross sections. The report describes the groundwater levels and quality within the Seaside basin. Finally, the report describes the quantification of natural recharge, groundwater pumping, and secondary recharge. Much of this information was incorporated into the model. CH2M/Hill provided data used in preparing the report but not tabulated in the report (CH2M/Hill, Terry Forman, written communication, 2005), including the computational details of the recharge estimates.

The report "Seaside Groundwater Basin: Update on Water Resource Conditions" was prepared by Yates and others (2005) for the Monterey Peninsula Water Management District. The report was prepared to assist the District in developing a comprehensive groundwater-management plan of the Seaside groundwater basin, implementing management actions, and securing grant funding. The report is similar to the CH2M/Hill (2005) report in that it: contains a compilation of hydrogeologic information, including maps and cross sections; describes the groundwater levels and quality within the Seaside basin; and describes the quantification of natural recharge, groundwater pumping, and secondary recharge. Much of this information was incorporated into the model or otherwise significantly influenced the model development.

2.2 Hydrogeologic Information

To develop a hydrogeologic model for the groundwater model, hydrogeologic information was extracted from CH2M/Hill (2005), Yates and others (2005), Greene

(1977), Greene (1970). Within the CH2M/Hill (2005) report: Figure 3-5 shows fault locations, except for the Reliz Fault; Figures 3-6 through 3-11 show geologic cross sections; and Figure 3-12 and 3-13 respectively show the regional and surficial geology. Within the Yates and others (2005) report: Figure 3 shows the regional geology and the location of the Reliz Fault; and Figures 3 and 4 show geologic cross sections. This information was supplemented with topographic and bathymetric information downloaded from the U. S. Geological Survey as DEMs (digital elevation model). Additionally, geologic information was downloaded from the U. S. Geological Survey as isopach maps representing the offshore geology (Wong and Eittreim, 2001).

The hydrogeologic model incorporated within the groundwater model was constructed from Figures 1.5a-e, which show the base altitude for each of the hydrogeologic units represented in the model. Contours of base altitude were developed from extrapolations of the cross sections constructed by CH2M/Hill (2005) and Yates and others (2005). They also were developed from the geologic descriptions of Greene (1970) and Greene (1977), and Wong and Eittreim (2001). To translate Figures 1.5a-e into the model mesh, the contours were converted to raster grid files using the 3D Analyst and Spatial Analysis extensions of ArcGIS.

Aquifer-parameter information has been compiled by CH2M/Hill (2005) and Yates and others (2005). The compiled aquifer-test data suggest an average hydraulic conductivities of 100 ft/day for the Paso Robles Formation and 130 ft/day for the Santa Margarita Formation. However, because wells tend to be screened in the more conductive intervals of a formation, the aquifer-test results likewise tend to overstate the depth-averaged conductivity for the entire formation thickness. Accordingly, Yates and others (2005) derived hydraulic conductivities of 2 ft/day for the Paso Robles Formation and about 4 ft/day for the Santa Margarita Formation, based on the calibration of a groundwater model, where these conductivities represent the entire thicknesses of the respective formations. Yates and others (2005 also derived from the model calibration a specific yield of 0.08 and specific storages in the range 10^{-5} to 10^{-6} ft^{-1}.

2.3 Well Inventory

To define the monitoring and production locations within the Seaside groundwater basin, a well inventory was compiled. CH2M/Hill (Terry Foreman, 2005, written communication) provided information on the location and construction of monitoring and production wells within the Seaside groundwater basin. The provided information was supplemented with data extracted from Yates and others (2005, Appendix C). Table 2.1 lists the information compiled on the monitoring wells actually used in developing the model, and Figure 2.1 shows the well locations. Table 2.2 lists the information compiled on production wells, and Figure 2.2 shows the well locations. Additionally, Tables 2.1 and 2.2 identify the hydrogeologic units within the screened interval of the monitoring or projection well. As shown on Figures 2.1 and 2.2, the well inventory included wells outside the study areas used by CH2M/Hill (2005) and Yates and others (2005).

2.4 Groundwater Levels

To calibrate the groundwater model, data on groundwater levels were compiled. CH2M/Hill (Terry Foreman, 2005, written communication) provided water level measurements representing 1952-2004. Table 2.3 lists the measurements actually used in developing the model, which includes those measurements made during 1995 and later, and Figure 2.2 identifies the well locations. The model development was based only on the later measurements because they were considered to be the most reliable.

2.5 Groundwater Pumping

To specify the pumping rates to be assigned within the model, data on groundwater production was compiled. CH2M/Hill (Terry Forman, 2005, written communication) provided information on annual groundwater production from individual wells. The production from the California American Water Co., City of Seaside, County of Monterey, and private wells was provided for 1956-2002. The production from Marina Coast Water District wells was provided for 1993-2002. Table 2.4 lists the compiled production and identifies the well owners, and Figure 2.1 shows well locations. As shown on Figure 2.1, groundwater pumping outside the study areas by CH2M/Hill (2005) and Yates and others (2005) was incorporated into the model.

2.6 Groundwater Recharge

2.6.1 Prior Investigations

To specify the natural and secondary recharge rates to be assigned within the model, prior estimates of recharge were compiled. Both CH2M/Hill (2005) and Yates and others (2005) estimated the recharge to the Seaside groundwater basin. To estimate precipitation recharge, they used similar approaches, and they obtained similar results. They both used a soil-water budget approach. The approach involved simulating the inflow and outflow to the vegetative root zone. The inflow to the root zone is the precipitation infiltration, and the outflows are evapotranspiration and deep percolation. CH2M/Hill (2005) used a monthly time step to simulate these processes, and Yates and others (2005) used a daily time step. To estimate the secondary recharge from landscape irrigation, septic tanks, leaking pipes, and other sources, CH2M/Hill (2205) and Yates and others (2005) based their estimates on different approaches and data but produced similar estimates.

CH2M/Hill (2005) and Yates and others (2005) use slightly different study-area boundaries, and their respective recharge estimates differ in part due to that. The study area used by CH2M/Hill contains 12,600 acres, and the study area used by Yates and others contains 12,300 acres. Nevertheless, when the respective recharge rates are expressed in terms of the average rate per unit area, the separate recharge estimates are nearly identical. The average rate for CH2M/Hill is 0.35 ft/yr, and the average rate for Yates and Others is 0.32 ft/yr. However, the recharge rate estimated by CH2M/Hill (2005) was used in the model.

The natural recharge rates estimated by either CH2M/Hill (2005) or Yates and others (2005) are based on their estimates of the potential evapotranspiration within their respective study areas. Presumably, CH2M/Hill (2005) and Yates and others (2005) considered the dual effects of distance from Monterey Bay and altitude in characterizing the evapotranspiration over their study areas. Nevertheless, the region representing the groundwater model contains more coastal area and more higher-altitude area than within the CH2M/Hill (2005) or Yates and others (2005) study areas. These characteristics of the model area are counter balancing with respect to potential evapotranspiration. Therefore, the average natural recharge within the model area probably is similar to the average natural recharge estimated by either CH2M/Hill (2005) or Yates and others (2005).

Likewise, the secondary recharge rates estimated by either CH2M/Hill (2005) or Yates and others (2005) is based on the extent of the urbanized area within their respective study areas. The region representing the groundwater model is larger, but the proportion of urbanized area is not greatly different than within the study area used by CH2M/Hill (2005) or Yates and others (2005). Therefore, the average secondary recharge within the model area probably is similar to the average secondary recharge estimated by either CH2M/Hill (2005) or Yates and others (2005).

2.6.2 Satellite-Image Analysis

As preparation for 2005 trial on the Seaside basin adjudication, Timothy Durbin, Inc. (2005, written communication) evaluated the water-budget approach used by CH2M/Hill (2005) and Yates and others (2005). The approached used by them equates the precipitation recharge to the precipitation minus the evapotranspiration. Satellite imagery was analyzed by Durbin to estimate the consumptive use of the native vegetation, and a satellite analysis was used to evaluate the reasonableness of the prior recharge estimates.

Satellite imagery for the Seaside groundwater basin was related to consumptive use through the *NDVI* (Normalized Difference Vegetation Index) index (Gates, 1980). This index in turn is related to reflectances measurements acquired in the red and near-infrared spectral regions by the expression (Sellers, 1985; Myneni and others, 1995)

$$NDVI = \frac{\rho_{NIR} - \rho_R}{\rho_{NIR} + \rho_R} \tag{2.1}$$

where ρ_R is the red reflectance and ρ_{NIR} is the near-infrared reflectance. Work by Sellers (1985) and Myneni and others (1995) has shown the *NDVI* is related directly to the energy adsorption of plant canopies and hence to transpiration.

By design, *NDVI* values range from +1 (when $\rho_R = 0$) to -1 (when $\rho_{NIR} = 0$). However, the *NDVI* calculated from a particular satellite image and for a particular

vegetative condition depends on the atmospheric opacity when the image was acquired. The *NDVI** index corrects for the atmospheric and other factors (Huete and Liu, 1994; Liu and Huete, 1995), which has the form

$$NDVI^* = \frac{NDVI - NDVI_0}{NDVI_S - NDVI_0} \tag{2.2}$$

where $NDVI_0$ is the *NDVI* representing bare soil and $NDVI_S$ is the *NDVI* representing saturation. Saturation occurs in areas with the most verdant vegetation, such as irrigated crops. The $NDVI^*$ index has a range of 0 (for bare soil) to 1 (for verdant vegetation), and it enables the comparison of *NDVI* measured at different times with different atmospheric opacities.

The NDVI* index is related to actual evapotranspiration of the vegetative canopy by the relation (Baugh and Groeneveld, 2006)

$$ET = NDVI^* \cdot ET_0 \tag{2.3}$$

where *ET* is the actual evapotranspiration and ET_0 is the reference evapotranspiration. Equation 2.3 has the same form as the reference-crop equation used to compute crop consumption, where $NDVI^*$ is the crop coefficient. Equation 2.3 can be applied monthly, given a set of monthly satellite images and monthly ET_0 values.

Calendar year 1993 was selected for an analysis of evapotranspiration based on Equation 2.3. This year was selected because the annual precipitation was near normal and satellite images were readily available. Six 30-meter LANDSAT TM images, representing August, December, January, March, June, and October were used because these comprised the available cloud-free images. *NDVI* was calculated for each image using the Leica image-analysis extension for ArcGIS, and the *NDVI* values representing bare soil and verdant vegetation were extracted. The $NDVI^*$ index was then calculated using the map-calculator function within ArcGIS. Figures 2.3a-f show the resulting geographic distribution of $NDVI^*$ within the Seaside basin for the selected months.

The reference evapotranspiration within the Seaside basin decreases with increasing altitude and distance inland from Monterey Bay. Monthly ET_0 values are available from the California Irrigation Management Information System for three sites near Salinas, which have altitudes ranging from 9 to 146 ft, distances inland from Monterey Bay ranging from 4,800 to 107,000 ft, and annual ET_0 ranging from 36 to 46 inches. Figure 2.4 shows the site locations. Table 2.5 lists the station attributes, and Figure 2.4 shows the station locations.

The actual evapotranspiration was obtained by combining the geographic distribution of $NDVI^*$ (Figures 2.3a-f) with the respective ET_0 for the months represented by the satellite images. The geographic distribution of *ET* was calculated from Equation 2.3 using the map-calculator function within ArcGIS. The resulting *ET* for each satellite image is listed in Table 2.6, along with the corresponding annual *ET*. The resulting

annual *ET* for 1993 is 1.5 ft, within the study area used by CH2M/Hill (2005). Based on the precipitation, runoff, and irrigation for 1993 (CH2M/Hill, 2005; Yates and others ,2005) , the corresponding recharge is 0.46 ft. The average annual recharge estimated by CH2M/Hill (2005) for that study area is 0.32 ft, and the average annual recharge estimated by Yates and others (2005) for that study area is 0.35 ft. The recharge derived from the satellite-image analysis is similar, after accounting for the above average precipitation during 1993. Correspondingly, the average recharge estimated by CH2M/Hill (2005) was used in the model.

3.0 Model Development

The development of the groundwater model involved the steps of assembling and then calibrating the model. The assembly of the model involved firstly constructing a finite-element mesh and secondly assigning recharge, pumping, boundary conditions, and initial conditions to the mesh. The calibration of the model involved identifying the hydraulic conductivity, specific storage, and specific yield for the hydrogeologic units that comprise the groundwater system. These steps were applied to a model with a geographic extent congruent with the areas defined by the California Department of Water Resources (2003) for the Seaside and Corral de Tierra groundwater basins. These basins collectively are referred to in this report as the Seaside groundwater basin.

3.1 Model Assembly

3.1.1 Finite-Element Mesh

The computer program *FEMFLOW3D* uses a finite-element mesh to model the hydrogeologic conditions within a groundwater basin. The mesh is used to represent the geographic extent of a groundwater system and the thickness of the geologic units that comprise the system. Additionally, the mesh is used to specify the hydraulic properties, pumping, and recharge. The mesh for a groundwater model based on *FEMFLOW3D* is constructed by assembling a wire-frame mesh using wedge-shaped elements. The individual elements are oriented as shown on Figure 3.1, such that the triangular faces of the wedge are parallel (or sub parallel) with a horizontal plane. They are oriented additionally such that the rectangular (or trapezoidal) faces are parallel with a vertical plane. The results of this orientation are that an element appears as a triangle when viewed from above and as a rectangle (or trapezoid) when viewed from the side.

A wedge-shaped element has six vertices, which in the vernacular of groundwater modeling, are referred to as nodes (Figure 3.1). An individual element is located geographically and vertically by specifying the three-dimensional coordinates for each node. A mesh is constructed by creating an assemblage of nodes and by identifying which nodes define which elements.

Modified forms of the wedge-shaped elements also are used in the construction of the finite-element mesh. These forms are used where a hydrogeologic unit pinches out. Pinch-outs occur where the thickness of a hydrogeologic unit tapers to a zero-thickness along a boundary of the unit. Correspondingly, a wedge-shaped element adjacent to such a boundary would have a zero-height at the nodes located on the boundary. If a wedge-shaped element is oriented such that one node is located in a pinch-out boundary, the six-node wedged-shaped element is replaced with a five-node pyramid-shaped element as shown on Figure 3.1. If a wedge-shaped element is oriented such that two nodes are located in a pinch-out boundary, the six-node wedge-shaped element is replaced with a four-node tetrahedral-shaped element as shown on Figure 3.1.

The finite-element mesh is depicted in Figure 3.2 (map view), Figure 3.3 (perspective view), and Figures 3.4a-b (cross-sections through the mesh interior). The top surface of the mesh is the land surface, and the subsurface structure of the mesh corresponds to the hydrogeologic units that comprise the groundwater system. The mesh depicts the Santa Margarita, Purisima, Paso Robles, and Aromas formations, where the representation of the Aromas Formation includes the surficial deposits. The base elevations for these formations, as shown on Figures 1.5a-e, define the layers within the mesh. The mesh also portrays the Salinas Valley clay, which occurs within the upper part of the surficial deposits.

Node elevations for the base of each hydrogeologic unit were derived from Figures 1.5a-e, which shows contours of the base altitude for each hydrogeologic unit represented in the model. The contours firstly were translated into raster grids by using the 3D Analysist and Spatial Analyst extensions to ArcGIS. The nodal elevation secondly were interpolated from this raster grid by using the Spatial Analyst extension.

The only fault represented explicitly within this model is the Ord Terrace Fault. That fault dissects the landward part of the Seaside basin and the near-shore seaward part. The fault is represented in the model mesh as a narrow band of elements that extend vertically through the overall thickness of the groundwater system.

The mesh contains 30,361 nodes and 56,503 elements. To accommodate numerical requirements for the transport simulations, the horizontal nodal spacing is generally about 500 ft, and the vertical nodal spacing is generally about 50 ft. The number of element layers at a particular location depends on the number of hydrogeologic units occurring in the subsurface at the location and the number of element layers comprising the respective hydrogeologic units. The Santa Margarita Formation is represented in the model mesh with six element layers, the Purisima Formation is represented with six layers, the Paso Robles Formation is represented with 10 layers, and the Aromas Formation and surficial deposits are represented with six layers. At the locations where the mesh has the most layers, 34 layers occur.

FEMFLOW3D simulates changing groundwater-table conditions by adjusting the altitudes of mesh nodes. The mesh is expanded upward or collapsed downward such that the altitudes of the nodes representing the top surface of the model mesh equal the local altitude of the simulated groundwater table. However, the altitude adjustments typically involve more than just the top nodes. If a downward adjustment is large with respect to the thickness of an element layer, the bottom nodes for the element layer also are moved downward. Figure 3.5 shows the collapse of a element column due a water-table decline during time step t, where Δh is the water-table decline, z_{t-1} is the element height after time step t-1, z_t is the element height after time step t, and z_{min} is the specified minimum spacing between nodes. The quantity z_{min} is specified to flatten an element to effectively remove it from the hydraulics of the groundwater system but to maintain an element aspect ratio (horizontal to vertical dimensions) not larger than about 200.

3.1.2 Time Step, Simulation Periods, and Unit Dimensions

The model was developed based on annual time steps. Furthermore, the computational time step is annual, where $\Delta t = 365$ days for each step. The period used in the model calibration is the 47-year period 1956-2002, and the period used for future projections was the13-year period 2003-2015. Correspondingly, $t = 0$ is the start of 1956, $t = 365$ days (time step 1) is the end of 1956, $t = 17{,}155$ days (time step 47) is the end of 2002, and $t = 21{,}900$ days (time step 60) is 2015.

The 47-year period 1956-2002 was used in the model development in part because of data availability. More importantly, that period was used because the Seaside basin most likely was in a steady-state condition. The groundwater development was minimal with respect to the natural recharge, and in 1956 groundwater pumping most likely had not impacted groundwater levels. That steady-state condition was used as the initial condition for the model simulations. Data do not exist for describing an initial condition for the model (in 1956 or any other time), but an initial condition can be constructed by computing steady-state heads. The computed initial condition represents the start of 1956.

The model inputs and simulation outputs are in a consistent set of unit dimensions. Length is in feet, and time is in days. Concentrations are expressed in terms of the dimensionless equivalent seawater proportion. Correspondingly, the dimensionless concentration $c = 1$ is equivalent to a mass concentration of 35,000 mg/L, $c = 0.1$ is equivalent to 3,500 mg/L, and $c = 0.01$ is equivalent to 350 mg/L.

3.1.3 Recharge Volumetric and Solute Fluxes

Both recharge rates and salinity were assigned to the model. The recharge rate represents a water flux into the groundwater basin. When combined with water flux, the assignment of a recharge salinity represents a solute flux into the groundwater basin.

Groundwater Flow

Recharge was assigned to the model by specifying water fluxes to the top nodes within the model mesh. A geographically uniform recharge rate was applied to the model. Even though the rate for a particular year is variable, the average annual rate was applied to each time step within a simulation. The average annual rate is 11,900 ft/yr. This recharge rate is substantial larger than reported by either CH2M/Hill (2005) or Yates and others (2005) because the model areas is much larger then their study areas. Nevertheless, recharge rate per unit area used in the model is the same as that estimated by CH2M/Hill (2005), or 0.35 acre-ft/yr per acre.

While the average annual recharge corresponds to a volume per unit area of 0.35 acre-ft/yr per acre (ft/d), the nodal model inputs must be expressed the volumetric flux

(ft^3/d). The volumetric rate for a particular top node within the model mesh is given by the expression

$$R_{i,t} = \frac{1}{3} \sum_{e=\{j\}} A_e r_t \tag{3.1}$$

where $R_{i,t}$ is the volumetric flux assigned to node *i* for year *t*, A_e is the area of element *e* projected onto a horizontal plane, r_t is the recharge per unit area in year *t* and {*j*} is the set of all elements that share node *i*.

Solute Transport

Recharge salinity was assigned to the model by specifying a salinity corresponding to the water fluxes at each node. However, the assigned salinity equals zero for all landward top nodes and all times. Even though the recharge water has some salinity, the salinity equals essentially zero relative to seawater.

3.1.4 Pumping Volumetric and Solute Fluxes

Pumping rates were assigned to the model, but the pumping salinity is not a model input.

Groundwater Flow

Pumping represents a water flux from the groundwater basin. Pumping was assigned to the model by specifying fluxes to nodes within the model mesh. Annual pumping was assigned based on the well locations and constructions listed in Table 2.1 and the pumping rates listed in Table 2.4, except for the pumping for Marina. The Marina pumping is not included in the model because the wells are located very near the Reliz Fault, which as described later is represented in the model as a specified-head boundary. Whether the Marina pumping is or is not represented in the model, the boundary condition overrides the potential pumping effects.

Each production well was assigned to a collection of nodes corresponding to its well location and screened interval. The flux assigned to a particular node in the collection is a proportion of the total well pumping based on horizontal and vertical weightings. The horizontal weighting is based on the geographic location of the well within an element as shown on Figure 3.6, which shows the triangular top face of an element that is penetrated by a well. The vertices are labeled *A*, *B*, and *C* counterclockwise around the triangle. The horizontal weighting for node *A* is the perpendicular distance from the well to the line *BC* (quantity *a* on Figure 3.6) divided by the perpendicular distance from node *A* to the line *BC* (quantity *b* on Figure 3.6), the weighting for node *B* is the distance from the well to the line *CA* divided by the perpendicular distance from node *B* to the line *CA*, and the weighting for node *C* is the distance from the well to line *AB* divided by the perpendicular distance from node *C* to the line *AB*. The horizontal weights have the property that

$$\sum_{i=1}^{3} W_{hi} = 1 \tag{3.2}$$

where W_{hi} is the horizontal weight for node *i*. This property and the weighting scheme itself follow directly from the mathematical formulation of the finite-element method (Pinder and Gray, 1977).

The vertical weighting is based on the screen lengths within the elements penetrated by the well as shown on Figure 3.7, which shows the trapezoidal side faces for a stack of elements penetrated by a well. For nodes in the top face of element *e*, the vertical weight is given by the relation

$$W_{vi} = \left(\frac{L_e}{L}\right)\left(\frac{b_e}{\Delta z_e}\right) \tag{3.3a}$$

where W_{vi} is the vertical weight for node *i*, *L* is the total screen length for the well, L_e is the length of the screen segment within the element *e*, Δz_e is the vertical distance between the top and bottom faces of element *e* at the well location, and b_e is the distance from the bottom face of element *e* to the middle of the screen segment within the element. Likewise, for nodes in the bottom face of element e, the vertical weight is given by the relation

$$W_{vi} = \left(\frac{L_e}{L}\right)\left(1 - \frac{b_e}{\Delta z_e}\right) \tag{3.3b}$$

Finally, the vertical weight for a node with a contribution from screen segments within two vertically adjacent elements is the sum of the individual elemental contributions. As for the horizontal weighting scheme, the vertical weighting scheme follows from the mathematical formulation of the finite-element method (Pinder and Gray, 1977)

The proportion of the pumping from the well assigned to a node is the product of the vertical and horizontal weights for the node, or

$$p_i = W_{hi} \cdot W_{vi} \tag{3.4}$$

where p_i is the proportion of the total pumping from the well assigned to the node *i*.

Solute Transport

The salinity of pumped groundwater is not a model input. The combination of the pumping rate and the salinity of the pumped water represent a solute flux from the

groundwater basin. However, the pumpage salinity is identical to the local groundwater salinity, but the groundwater salinity is a calculated quantity.

3.1.5 Boundary Conditions

Boundary conditions were assigned to the model domain for both groundwater flow and solute transport. Boundary surfaces were assigned specified heads and specified fluxes to specify groundwater-flow conditions. Additionally, boundary surfaces were assigned specified fluxes to specify solute-transport conditions.

Groundwater Flow

For groundwater-flow, a specified-head boundary condition was applied to the bathymetric surface representing the bottom of Monterey Bay and the vertical surface representing the boundary between the Seaside groundwater basin and the Salinas Valley basin. The groundwater-flow simulations are configured in terms of fresh water, and the specified head for Monterey Bay corresponding are expressed as equivalent freshwater heads. The relation for translating from seawater to freshwater heads is

$$h_f = d_s\left(\frac{\rho_s}{\rho_f} - 1\right) \tag{3.5}$$

where h_f is the equivalent freshwater head, d_s is the seawater depth, ρ_s is the density of seawater, ρ_f is the density of freshwater. Based on a seawater density of 1,035 g/L and a freshwater density of 1,000 g/L, the freshwater head equals the seawater depth multiplied by 0.035. The heads derived from that relation were assigned to the model as temporally invariant heads over the Monterey Bay region shown on Figure 3.8.

The boundary between the Seaside groundwater basin and the Salinas Valley basin is the Reliz Fault, and specified heads were assigned to the fault plane from 5,000 ft offshore to where the eastern boundary of the Seaside basin intersects the Reliz Fault. Along that fault segment, which is identified on Figure 3.8, a specified-head boundary was assigned over the full thickness of the Seaside basin. While the assigned heads vary along the fault trace, they do not vary with depth at a particular location. The assigned heads represent the groundwater conditions on the north side of the Reliz Fault, where the heads were derived from a composite of the groundwater-level contour maps produced by Yates (1988) and Yates and others (2005). The derived heads were assigned to the model as temporally invariant specified heads as shown on Figure 3.9. The representation of the Reliz Fault as a specified head boundary allow unimpeded groundwater exchanges between the Seaside and Salinas Valley groundwater basins.

The remainder of the boundary surfaces are specified-flux boundaries. The boundary condition on the top surface of the landward part of the model domain is the precipitation and secondary recharge into the groundwater system, which was described previously. The boundary condition on bottom surface of the landward and seaward parts

of the model domain also is a no-flow boundary. Likewise, the boundary conditions on the landward and seaward vertical surfaces of the model domain, except for the segment of the Reliz Fault described above, are no-flow boundaries.

The leakances for the specified-head boundaries were assigned so as to produce a computed head almost identical to the specified head. Accordingly, the leakances were set to a somewhat arbitrary large value. The leakances were set sufficiently large to produce nearly identical specified and computed heads, but they were set also such that the difference between the specified and computed heads was with the precision of the computer.

Solute Transport

Where water crosses boundary surfaces as inward flows, due either to the assignment of specified-head or non-zero specified-flux groundwater-flow boundaries, the salinity of the inward flow is assigned. However, except for the boundary surface representing the bottom of Monterey Bay, the specified salinity equals zero. For the Monterey Bay surface, the specified salinity equals unity, which is the dimensionless concentration equivalent to seawater.

3.1.6 Initial Conditions

The groundwater-flow and solute-transport initial conditions is an assumed steady-state condition at the end of 1955. The groundwater development at the time was minimal at that time relative to precipitation recharge, and initial conditions were simulated based on the assumed steady state.

Groundwater Flow

The initial heads for groundwater flow are the calculated steady-state heads representing the long-term average annual recharge, the 1956 groundwater pumping, and the boundary conditions described above. *FEMFLOW3D* can calculate steady-state initial heads within a transient-state simulation, and that facility was used to specify the initial heads for the Seaside groundwater basin. The resulting steady-state groundwater levels are shown on Figures 3.10a-b. Because the steady-state heads depend on the hydraulic parameters assigned to the hydrogeologic units represented in the model, Figures 3.10a-b are derived from the model calibration, which is described later.

Solute Transport

The initial salinity for solute transport are the calculated nearly steady-state salinity again representing the long-term average annual recharge, the 1956 groundwater pumping, and the boundary conditions described above. By this construction of initial conditions, the seawater intrusion in the seaward part of the Seaside basin is assumed to be in equilibrium with the 1956 steady-state groundwater flow. Calculating steady-state solute-transport with *FEMFLOW3D* is not as convenient as for calculating steady-state

heads. The approach was to make a long-term simulation of solute transport based on the steady-state heads. A simulation period was selected such that near steady-state transport conditions occurred at the end of the simulation. This was achieved with a simulation period of 10,000 years. The resulting steady-state salinities are shown on Figures 3.11a-b. Because the steady-state salinities depend on the hydraulic and transport parameters assigned to the hydrogeologic units represented in the model, Figures 3.11a-b are derived from the model calibration, which is described next.

3.2 Aquifer-Parameter Identification

Aquifer-parameters for groundwater flow and solute transport were assigned to the model. The hydraulic parameters for groundwater flow include the hydraulic conductivity, specific storage, and specific yield for each hydrogeologic unit represented in the model. Likewise, the transport parameters include the effective porosity and dispersivity.

3.2.1 Identification Approach

Different approaches were used for the identification of the hydraulic and transport parameters. Groundwater-level data are available for the Seaside basin, and hydraulic parameters were identified by calibrating the model to groundwater-level measurements. The basin has been impacted little by seawater intrusion, and no basis exists for identifying the transport parameters by calibration. Correspondingly, transport parameters were assigned based on the textural characteristics of the individual hydrogeologic units.

Groundwater Flow

Two data sources were used in the identification of hydraulic parameters. With respect to the first data source, parameters were identified by formally calibrating the model to the groundwater levels listed in Table 2.3, which represent measurement is made within the wells listed in Table 2.2. The simulated head for a well follows from the assignment of mesh nodes to each monitoring well, and the simulated head is a weighted sum of the simulated heads for the assigned nodes. The weights are derived exactly as described in Section 3.1.4 for the assignment of well pumping to nodes. With respect to the second data source, parameters were identified by subjectively calibrating the model to qualitative characteristics of the groundwater-level contour maps produced by Yates and others (2005, Figures 12 through 15). Those maps show groundwater levels for Spring and Fall 2002 and respectively for the Paso Robles and Santa Margarita formations. Immediately landward from Monterey Bay and north of the Ord Terrace Fault, the maps show roughly circular areas where groundwater levels are below sea level. Within the Paso Robles Formation, the area is about 5,000 ft in diameter, and the area is contained entirely within the landward part of the groundwater basin, as shown on Figure 1.18a. Within the Santa Margarita Formation, the area is about 12,000 ft in diameter, and the area extends partly into the seaward part of the groundwater system, as

shown on Figure 1.18b. The model was calibrated in part to simulate similar areas where groundwater levels are below sea level.

Hydraulic parameters were identified from a weighted least-squares fit of the computed heads to the measured groundwater levels. The computer program *PEST* (Watermark Numerical Computing, 2002) was used to perform the calibration. *PEST* identifies parameter values such that the model fit minimizes the objective function

$$S = \sum_{i=1}^{n} \left[w_i \left(h_{ci} - h_{mi} \right) \right]^2 \tag{3.6}$$

where S is the sum of weighted squared residuals, h_{ci} is the computed head for a particular well and time, h_{mi} is the measured groundwater level for the particular well and time, w_i is the weight assigned to the measured groundwater level, and n is the number of measured groundwater levels. The weight assigned to a measurement is related to the uncertainty in the measurement according to the relation

$$w_i = \frac{1}{\sigma_i^2} \tag{3.7}$$

where σ_i is the standard error of the uncertainty in the measurement.

All groundwater-level measurements are uncertain, and the uncertainty has at least two sources. Firstly, uncertainty arises in measuring or recording groundwater depths and in measuring, estimating, or recording measuring-point altitudes. Additionally, uncertainty arises in the documentation of the location and construction of wells. However, for the Seaside groundwater basin, this uncertainty type most likely is small. Secondly, uncertainty arises because groundwater-level measurements represent spatial and temporal point processes, but the computed heads represent spatially and temporally average processes (Anderson and Woessner, 2002, pp.229-230, Gelhar, 1986), where the averaging depends on the effective spatial and temporal scales represented in the model. This uncertainty increases significantly with lower-permeability groundwater systems and with more heterogeneous and anisotropic groundwater systems. Because the Seaside groundwater basin can be characterized as a highly heterogeneous, highly anisotropic, and moderately permeable groundwater system, and because the effective model spatial and temporal scales are large, the second uncertainty type is large.

Within the groundwater-level data for the Seaside groundwater basin, the standard error for the combined effects of the two uncertainty types is about 16 ft. The first uncertainty type has a standard of perhaps 5 ft or less, the second error type has a standard error of most likely 15 ft or more. These combine according to the relation

$$\sigma_i = \sqrt{\sigma_{1i} + \sigma_{2i}} \tag{3.8}$$

where σ_i is the combined standard error, σ_{1i} is the standard error for the first uncertainty type, σ_{2i} is the standard error for the second uncertainty type. The effect of the combined error is that, even if the parameter values assigned to the model exactly match the actual characteristics of the groundwater system at the effective model scales, the fit of the model to the measured groundwater levels would have an expected standard error of 16 ft, which is the expected standard deviation of the residuals between the computed heads and measured groundwater levels.

The formal calibration was configured to identify for each hydrogeologic unit represented in the model the basin-wide average horizontal hydraulic conductivity, vertical hydraulic conductivity, specific storage, and specific yield. However, calibration involved identifying parameter values for just the Paso Robles Formation, because the parameter values for the other hydrogeologic units were assigned a fixed proportional relation to the Paso Robles Formation. For each of the other units, the horizontal hydraulic conductivity, vertical hydraulic conductivity, specific storage, and specific yield respectively are assigned a fixed ratio between the parameter value for the unit and the corresponding parameter value for the Paso Robles Formation. The assigned ratios are listed in Table 3.1. The ratios were assigned based on the review of aquifer properties compiled by CH2M/Hill (2005), Yates and others (2005), Davis (1969), Anderson (1984), Johnson (1967), Shepherd (1989), Morris and Johnson (1967), Lohman (1972), and others sources.

Solute Transport

The transport parameters for the model were selected from values published for similar aquifer parameters. The parameters include effective porosity, horizontal longitudinal dispersivity, horizontal transverse dispersivity, and vertical transverse dispersivity, where the dispersivities are related to the dispersion tensor in Equation 1.2 by the relations (Hydrogeologic, Inc., 1996)

$$D_{xx} = \alpha_{Lh}\frac{v_x^2}{|v|} + \alpha_{Th}\frac{v_y^2}{|v|} + \alpha_{Tv}\frac{v_z^2}{|v|} \tag{3.9a}$$

$$D_{yy} = \alpha_{Th}\frac{v_x^2}{|v|} + \alpha_{Lh}\frac{v_y^2}{|v|} + \alpha_{Tv}\frac{v_z^2}{|v|} \tag{3.9b}$$

$$D_{zz} = \alpha_{Tv}\frac{v_x^2}{|v|} + \alpha_{Tv}\frac{v_y^2}{|v|} + \alpha_{Lh}\frac{v_z^2}{|v|} \tag{3.9c}$$

$$D_{xy} = D_{yx} = (\alpha_{Lh} - \alpha_{Th})\frac{v_x v_y}{|v|} \tag{3.9d}$$

$$D_{xz} = D_{zx} = (\alpha_{Lh} - \alpha_{Th})\frac{v_x v_z}{|v|} \tag{3.9e}$$

and

$$D_{yz} = D_{zy} = (\alpha_{Lh} - \alpha_{Th})\frac{v_y v_z}{|v|} \tag{3.9f}$$

where

$$v_i = \frac{q_i}{\phi} \tag{3.10}$$

for

$$i = 1,2,3$$

and

$$|v| = \sqrt{v_x^2 + v_y^2 + v_z^2} \tag{3.11}$$

and where D_{ij} is a component of the dispersion tensor, α_{Lh} is the horizontal longitudinal dispersivity, α_{Lv} is the vertical longitudinal dispersivity, α_{Th} is the horizontal transverse dispersivity, α_{Tv} is the vertical transverse dispersivity, ϕ is the effective porosity, and q_i is a component of the groundwater-flux vector.

The dispersivities and porosity were assigned to each hydrogeologic unit represented in the model from a review of the parameter compilations by Davis (1969), Anderson (1984), Morris and Johnson (1967), and others sources. The resulting values are listed in Table 3.1.

3.2.2 Calibration Results

The calibration results are listed Table 3.1 and are shown on Figures 3.12a-b through 3.14a-b. Table 3.1 lists the hydraulic and transport parameters for the model. Figures 3.12a-b compare the computed heads and measured groundwater levels. Figure 3.13a shows the simulated heads within the Paso Robles Formation for 2002, and Figure 3.13b shows the simulated heads within the Santa Margarita Formation. Figure 3.14a shows the simulated salinity within the Paso Robles Formation for 2002, and Figure 3.14b shows the simulated salinity within the Santa Margarita Formation.

The hydraulic parameters derived from the calibration are mostly consistent with prior work. CH2M/Hill (2005) and Yates and others (2005) compiled aquifer-test data that suggests an average hydraulic conductivities of 110 ft/d for the Paso Robles Formation and 130 ft/day for the Santa Margarita Formation, but the variance of the

aquifer-test data would suggest no actual difference between the formations. Nevertheless, the aquifer-test values are larger than identified for the model. However, because wells tend to be screened in the more conductive intervals of a formation, the aquifer-test results likewise tend to overstate the depth-averaged conductivity for the entire formation thickness. Correspondingly, Yates and others (2005) derived hydraulic conductivities of 2 ft/d for the Paso Robles Formation and about 4 ft/d for the Santa Margarita Formation, based on the calibration of a groundwater model for the southern part of the Seaside groundwater basin, where these conductivities represent the entire thicknesses of the respective formations. Yates and others (2005) also derived from the model calibration a specific yield of 0.08 and specific storages in the range 10^{-5} to 10^{-6} ft^{-1}, which is similar to the storage properties listed in Table 3.1.

The work of Yates and others (2005) suggests a lower conductivity for the Paso Robles Formation than for the Santa Margarita Formation. However, such a discrimination probably cannot be identified from a model calibration. While the available data allow the identification of the overall transmissivity of the groundwater-water system, the data do not allow the identification of conductivities for individual formations.

The model fit to groundwater levels is reasonable, given the high uncertainty in the measured groundwater levels. Figure 3.12b shows a scatter diagram comparing the weighted computed heads to the corresponding weighted measured groundwater levels, where the weighting corresponds to Equation 3.7. The coefficient of determination (r^2) is 0.92, and the correlation coefficient (r) is 0.96. Likewise for the unweighted statistics, the coefficient of determination (r^2) is 0.92, and the correlation coefficient (r) is 0.96, which corresponds to Figure 3.12a. Hill (1998) suggests that the correlation coefficient should be greater than 0.9 for the model fit to be acceptable, which is the case for both the weighted and unweighted statistics. Hill (1998) further suggest not using weighting when the observation uncertainties are identical, but doing so results in incorrect assessments of some calibration statistics. In particular, while the standard error of the estimate for the unweighted observations is 29 ft, the standard error for the weighted observations is 0.13. Such differences occur furthermore with respect to the parameter and predictive statistics. Correspondingly, calibration statistics based on the weighted observations better characterize the model calibration than those based on the unweighted observations.

The contours of computed heads correspond to the geographic pattern identified by Yates and others (2005, Figures 13 and 15) and shown here on Figures 1.8a-b. For the Paso Robles Formation, Figure 3.13a shows an area underlying Seaside that has computed heads below sea level. The area is similar in size to that shown on Figure 1.8a, and the lowest groundwater levels are similar. For the Santa Margarita Formation, Figure 3.13b shows areas underlying Seaside has computed heads below sea level. The area is similar in size to those shown on Figure 1.8b, and the lowest groundwater levels are similar.

The contours of computed salinity correspond to the seawater intrusion shown on Figures 1.9a-b, which indicates the absence of observed intrusion within the Seaside area.

As shown on Figures 3.14a-b, simulated seawater-intrusion impacts are absent within the Seaside area. However, the seaward parts of the Seaside groundwater basin show seawater intrusion, but the simulated salinity tends to be limited to the upper depth intervals of the groundwater system.

4.0 Model Simulations of Future Conditions

To assess the potential for future seawater intrusion within the Seaside area, the model was used to simulate groundwater conditions in 2015. For this simulation, the annual groundwater pumping during 13-year period 2003-2015 was set equal to the 2002 pumping from the Seaside groundwater basin. The groundwater recharge was set equal to the 1956-2002 average annual rate. The 2002 pumping is 6,300 acre-ft/yr, and the average annual recharge is 11,900 acre-ft/yr.

The simulation indicates that groundwater levels will decline within the Seaside area but seawater intrusion will not occur. Figures 4.1a-b show contours of computed heads within Paso Robles and Santa Margarita formations for 2015. The computed heads are as much as 5 ft lower in the Paso Robles Formation than in 2002, and they are as much as 10 ft lower in the Santa Margarita Formation. However, sizes of the regions within the Paso Robles and Santa Margarita formations with groundwater levels below sea level increase from 2002 to 2015. Figures 4.2a-b shows contours of computed salinity within the Paso Robles and Santa Margarita formations for 2015. For both the Paso Robles and Santa Margarita formations, the computed salinity is similar to that simulated for 2002. The water budget for the simulation is listed in Table 4.1.

To evaluate the potential benefits of relocating some of the pumping, the model was used to simulate the groundwater conditions with relocated pumping. The basic configuration of the simulation was the same as for the first. However, the pumping from the Paralta well (Table 2.1) was transferred to a new well located 10,000 ft northeast from the Paralta well. The relocated pumping represented a pumping rate of 2,000 acre-ft/yr.

The simulation indicates that groundwater levels will recover within the Seaside area and seawater intrusion will not occur. Figures 4.3a-b show contours of computed heads within Paso Robles and Santa Margarita formations for 2015. Within the vicinity of the Paralta well, the computed heads are as much as 20 ft higher in the Paso Robles Formation than in 2002, and they are as much as 30 ft higher in the Santa Margarita Formation. Figures 4.4a-b show contours of computed salinity within the Paso Robles and Santa Margarita formations for 2015. For both the Paso Robles and Santa Margarita formations, the computed salinity is similar to that simulated for 2002. The water budget for the simulation is listed in Table 4.2.

5.0 Conclusions

A groundwater model has been constructed for the Seaside groundwater basin, using the basin boundaries as defined by the California Department of Water Resources (2003). The model simulates groundwater flow and solute transport using the groundwater-modeling software *FEMFLOW3D*, which is a variant of the modeling software *FEMFLOW3D* (Durbin and Bond, 1998). The development of the model for the Seaside basin is based mostly on the hydrogeologic interpretation and data tabulations developed by CH2M/Hill (2005). The resulting model is a generalized representation of the groundwater system. Simulation results derived from the model can be interpreted to phenomena with spatial scales several thousand feet or more and temporal scale of a year or more.

The model was used to make two simulation scenarios involving future conditions. The first scenario assumes that the 2002 pumping would be continued until 2015, and the second scenario assumes that the pumping from the Paralta well would be relocated inland. For the first scenario, the simulation results are that groundwater levels will decline relative to the 2002 conditions, but seawater intrusion will not occur within the landward part of the Seaside basin. For the second scenario, the simulation results are that groundwater levels near Monterey Bay will increase, and seawater intrusion will not occur within the landward part of the Seaside basin.

6.0 References Cited

Anderson, M. P., 1984, Movement of contaminants in groundwater, *in* Groundwater contamination: Washington, D. C., National Academy Press, pp. 37-45.

Anderson, M. P., and Woessner, W. W., 2002, Applied groundwater modeling: Simulation of flow and advective transport: New York, Academic Press.

Baugh, W. M., and Groeneveld, D. P., 2006, Broadband vegetation index performance evaluated for a low-cover environment: International Journal of Remote Sensing, vol. 27, pp. 4715-4730.

California Department of Water Resources, 2003, California groundwater: California Department of Water Resources Bulletin 118.

CH2M/Hill, 2005, Hydrogeologic assessment of the Seaside groundwater basin: Report prepared for Somach, Simmons & Dunn and California American Water Co.

Clark, J. C., Dupre, W. R., and Rosenberg, L. I., 1997, Geologic map of the Monterey and Seaside 7.5-minute quadrangles, Monterey County, California: U. S. Geological Survey Open-File Report 97-30.

Davis, S. N., 1969, Porosity and permeability in natural materials, in DeWiest, R. J. M., ed., Flow through porous media: New York, Academic Press, Inc., pp. 53-89.

Durbin, T.J., 2007, FEMFLOW3D—A finite-element program for the simulation of three-dimension aquifers, Version 3.0: Timothy J. Durbin, Inc., Fair Oaks, CA.

Durbin, T. J., and Berenbrock, C., 1985, Three-dimensional simulation of free-surface aquifers by the finite-element method: U. S. Geological Survey Water-Supply Paper 2270.

Durbin, T. D., and Bond, L. D., 1998, FEMFLOW3D: A finite-element program for the simulation of three-dimensional aquifers, Version 1.0: U. S. Geological Survey Open-File Report 97-810.

Durbin, T. J., and Delemos, D. W., 2007, Adaptive underrelaxation of Picard iterations in ground-water models: Ground Water, vol. 45, no. 5, pp. 648-651.

Durbin, T. J., Kapple, G. W., and Freckleton, J. R., 1978, Two-dimensional and tree-dimensional digital models of the Salinas Valley groundwater basin, California. U. S. Geological Survey Water-resources Investigations Report 78-113.

Feeney, M. B., and Rosenberg, L. I., 2002, Deep aquifer investigation: Hydrogeologic data inventory, review, interpretation and implications: Report prepared for WRIME, Inc.

Gates, D. M., 1980, Biophysical Ecology: New York, Springer-Verlag.

Gelhar, L. W., 1986, Stochastic subsurface hydrology from theory to application: Water Resources Research, vol. 22, no. 9, pp. 135-145.

Greene, H. G., 1970, Geology of southern Monterey Bay and its relationship to the groundwater basin and saltwater intrusion: U. S. Geological Survey Open-File Report 70-88.

Greene, H. G., 1977, Geology of the Monterey Bay region: U. S. Geological Survey Open-File Report 77-718.

Hill, M. C., 1998, Methods and guidelines for effective model calibration: U. S. geological Survey Water-Resources Investigations Report 98-4005.

Huyakorn, P. S., and Pinder, G. F., 1983, Computation methods in subsurface flow: New York, Academic Press.

Huete, A. R., and Liu, H. Q., 1994, An error and sensitivity analysis of atmospheric- and soil-correcting variants of the NDVI for the MODIS-EOS: Transactions on Geoscience and Remote Sensing, vol. 32, pp. 897-905.

Hydrogeologic, Inc., 1996, MODFLOW-SURFACT software documentation—Volume II, Transport modules:

Johnson, A. I., 1967, Specific yield—Compilation of specific yield for various materials: U. S. Geological Survey Water-Supply Paper 1662-D.

Lohman, S. W., 1972, Ground-water hydraulics: U. S. Geological Survey Professional Paper 708.

Liu, H. Q., and Huete, A. R., 1995, A feedback based modification of the NDVI to minimize canopy background and atmospheric noise: Transaction on Geoscience and Remote Sensing, vol. 33, pp. 457-465.

Logan, J., 1982, Hydrogeology of the Seaside area: Report prepared for the Monterey Peninsula Water Management District.

Monterey County Water Resources Agency, 2001, Water quality data:

Morris, D. A., and Johnson, A. I., 1967, Summary of hydrogeologic and physical properties of rock and soil materials as analyzed by the Hydrologic Laboratory of the U. S. Geological Survey: U. S. Geological Survey Water-Supply Paper 1839-D.

Muir, K. S., 1982, groundwater in the Seaside area, Monterey County, California: U. S. Geological Survey Water-Resources Investigations Report 82-10.

Myneni, R. B., Hall, F. G., Sellers, P. J., and Marshak, A. L., 1995, The interpretation of spectral vegetation indexes: *IEEE Transactions on Geoscience and Remote Sensing*, vol. 33, pp. 481-486.

Pinder, G. F., and Gray, W. G., 1977, Finite element simulation in surface and subsurface hydrology: New York, Academic Press, Inc.

Saucedo, G. J., Bedford, D. R., Raines, R. J., and Wentworth, C. M., 2000, GIS Data for the geologic map of California: California Division of Mines and Geology CD 2000-007

Sellers, P. J., 1985, Canopy reflectance, photosynthesis, and transpiration: International Journal of Remote Sensing, vol. **6**, pp.1335-1372.

Shepard, R. G., 1989, Correlations of permeability and grain size: Ground Water, vol. 27, no. 5, pp. 633-638.

Stall, Gardner & Dunne, Inc., 1987, Hydrogeologic investigation: Seaside coastal groundwater basin, Monterey County, California: Report prepared for Monterey Peninsula Water management District.

Stall, Gardner & Dunne, Inc., 1988, Phase II hydrogeologic investigation: Laguna Seca subarea, Monterey County, California: Report prepared for Monterey Peninsula Water management District.

Stall, Gardner & Dunne, Inc., 1990a, Hydrogeologic investigation: PCA well aquifer test, sand City, California: Report prepared for Monterey Peninsula Water Management District.

Stall, Gardner & Dunne, Inc., 1990b, Hydrogeologic update, Seaside coastal groundwater basins, Monterey County, California: Report prepared for Monterey Peninsula Water Management District.

Taraszki, M., and Craig, D. J., 2002, Hydrogeologic investigation of the Salinas Valley basin in the vicinity of Fort Ord and Marina, Salinas Valley, California: Report prepared for Monterey County Water Resources Agency.

U.S. Army, 1995, FEMWATER—A three-dimensional finite element computer model for simulating density-dependent flow and transport in variably saturated media, Version 3.0: U. S. Army Engineering Research and Development Center, Vicksburg.

Wagner, D. L. Greene, H. G., Saucedo, G. J., and Pridmore, C. L., 2002 Geologic map of Monterey 30'x60' quadrangle and adjacent areas: California Geological Survey CD 2002-04.

Wang, H. F., and Andersen, M. P.,1995, Introduction to groundwater modeling: New York, Academic Press.

Watermark Numerical Computing, 2002, Visual PEST-ASP Model-Independent Parameter Estimation: Distributed by Waterloo Hydrogeologic.

Wong, F.L., and Eittreim, S.E., 2001, Continental shelf GIS for the Monterey Bay National Marine Sanctuary: U.S. Geological Survey Open-File Report 01-179.

Yates, E. B., 1988, Simulated effects of ground-water management alternatives for the Salinas Valley, California: U. S. Geological Survey Water-Resources Investigations Report 87-4006.

Yates, E. B., Feeney, M. B., and Rosenberg, L. I., 2002, Laguna Seca Phase III hydrogeologic update: Report prepared for Monterey Peninsula Water Management District.

Yates, B. G., Feeney, M. B., and Rosenberg, L. L., 2005, Seaside groundwater basin: Update on water resource conditions: Report prepared for Monterey Penesula Water Management District.

Zienkiewicz, O. C., and Taylor, 1989, The finite element method, Fourth edition—Volume 1, basic formulation and linear problems: New York, McGraw-Hill.

Tables

Table 2.1 Location and Construction of Production Wells

Well Name	X[1] (m)	Y (m)	Depth Screen Top (ft)	Depth Screen Bottom (ft)	Aquifer
Bishop 1	-156707	-159577	--	--	Santa Margarita
Bishop 2	-158056	-159139	--	--	Paso Robles
City 1	-162854	-154839	245	275	Paso Robles
City 2	-162888	-154924	245	275	Paso Robles
City 3	-162585	-154416	340	540	Santa Margarita
Darwin	-163544	-154146	124	224	Paso Robles
Elm	-164076	-155163	--	--	Paso Robles
Fort Ord Golf Course	-163379	-153048	160	208	Paso Robles
Harding	-163660	-154271	141	225	Paso Robles
Hidden Hills Bay Ridge	-156744	-160552	--	--	Paso Robles
Hidden Hills Mutual	-156745	-160562	--	--	Santa Margarita
La Salle No. 2	-163682	-154078	178	326	Santa Margarita
Laguna Seca County Parks	-157771	-159247	--	--	Paso Robles
Laguna Seca Water Co.	-157302	-159473	--	--	Paso Robles
LS Golf Club	-158893	-159661	--	--	Santa Margarita
Luxton	-163841	-154173	150	277	Paso Robles
Luzern	-163410	-153752	212	266	Santa Margarita
MGT	-163463	-155597	187	307	Paso Robles
Military	-163289	-153553	184	264	Paso Robles
Ord Grove	-162643	-153924	353	478	Santa Margarita
Ord Village	-162595	-153979	205	707	Santa Margarita
Palm	-164084	-155106	--	--	Paso Robles
Paralta	-162164	-153558	440	810	Santa Margarita
Pasadera	-160235	-159061	--	--	Santa Margarita
Playa No. 3	-164172	-153829	188	218	Paso Robles
Plumas No. 2,3,4	-163631	-156193	105	275	Paso Robles
Ryan Ranch 10	-161543	-158708	--	--	Santa Margarita
Ryan Ranch 7	-161813	-158634	--	--	Santa Margarita
Ryan Ranch 9	-161709	-158624	--	--	Santa Margarita
Seaside Golf	-162572	-153526	--	--	Paso Robles
York School	-160618	-158589	--	--	Santa Margarita
El Toro W39-01	-151629	-155457	--	--	Paso Robles
El Toro W35	-151281	-155415	--	--	Paso Robles
El Toro W59-01	-151176	-155779	--	--	Paso Robles
Ambler Park #6	-153684	-158786	--	--	Santa Margarita
MCWD#10	-158966	-148168	--	--	Santa Margarita
SPCA	-157305	-159474	--	--	Paso Robles
Paddock #1	-158803	-159649	--	--	Paso Robles
Main Gate #2	-158897	-159662	--	--	Paso Robles
East Fence	-158059	-159140	--	--	Paso Robles
Tom Phillips	-164630	-154404	90	112	Paso Robles

[1]California State Spatial Library Albers projection.

Table 2.2 Monitoring Wells Locations and Aquifer

Well Number	Name	Aquifer	X[1] (m)	Y (m)
	Ambler Park #6	Paso Robles/Santa Margarita	-153683.6	-158785.7
	Beach	Salinas Valley 400-Foot Aquifer	-161234.4	-147312.6
T16S/R2E-05E02	Bishop No. 1	Paso Robles/Santa Margarita	-156707.4	-159577.5
T16S/R2E-05F06	Bishop No. 2	Paso Robles/Santa Margarita	-158055.6	-159139.1
T16S/R2E-09J02	Chamisal Tennis Club	Santa Margarita	-155828.0	-161164.7
T15S/R1E-36Rb	County MW-1D	Santa Margarita	-160617.7	-158588.7
T16S/R2E-09Bb	County MW-3D	Santa Margarita	-156725.7	-159573.3
T16S/R2E-09Bc	County MW-3S	Paso Robles	-156725.7	-159573.3
T16S/R2E-04Lc	County No. 3	Santa Margarita	-156725.7	-159573.3
T15S/R2E-32Ra	County TH-1 Range	Santa Margarita	-157429.1	-158609.3
T16S/R2E-05G04	County Park No. 3	Paso Robles	-158106.6	-159079.3
T16S/R2E-05G02	County Park No.1	Paso Robles/Santa Margarita	-157800.0	-159259.8
T15S/R1E-23E01	Darwin	Paso Robles	-163600.9	-154284.7
T16S/R2E-05F04	East Fence	Paso Robles	-158563.1	-159202.3
	El Toro Park W59-01	Paso Robles/Santa Margarita	-151176.2	-155779.1
	El Toro W35	Paso Robles/Santa Margarita	-151280.6	-155414.9
	El Toro W39-01	Paso Robles/Santa Margarita	-151628.9	-155457.3
	Fort Ord #10 Deep	Santa Margarita	-161197.68	-150823.51
	Fort Ord #10 Shallow	Paso Robles	-161197.68	-150823.51
	Fort Ord #11 Deep	Santa Margarita	-160345.98	-148631.00
	Fort Ord #4 Deep	Santa Margarita	-163391.00	-156636.00
T15S/R1E-12Fc	Fort Ord 10 deep	Santa Margarita	-161331.7	-150953.4
T15S/R1E-12Fa	Fort Ord 10 shallow	Paso Robles	-161331.7	-150953.4
T15S/R1E-7Bb	Fort Ord 11 deep	Santa Margarita	-159224.7	-150839.9
T15S/R1E-7Ba	Fort Ord 11 shallow	Paso Robles	-159224.7	-150839.9
T15S/R1E-13Lb	Fort Ord 7 deep	Santa Margarita	-161321.9	-153346.9
T15S/R1E-13La	Fort Ord 7 shallow	Paso Robles	-161321.9	-153346.9
T15S/R1E-12Qb	Fort Ord 8 deep	Santa Margarita	-160879.2	-152050.3
T15S/R1E-12Qa	Fort Ord 8 shallow	Paso Robles	-160879.2	-152050.3
T15S/R1E-11Pb	Fort Ord 9 deep	Santa Margarita	-163056.9	-151830.8
T15S/R1E-11Pa	Fort Ord 9 shallow	Paso Robles	-163056.9	-151830.8
T16S/R2E-09C02	Hidden Hills/Mutual	Paso Robles/Santa Margarita	-159384.2	-159192.4
T16S/R2E-09C03	Hidden Hills/Standex (QT	Paso Robles/Santa Margarita	-156741.3	-160560.6
T15S/R1E-27	Johann/Shea	Santa Margarita	-163404.0	-156408.1
T16S/R2E-06H02	L.S. Golf Course '98	Paso Robles/Santa Margarita	-158800.0	-159647.8
T15S/R1E-22H05	La Salle 2	Santa Margarita	-163771.3	-154180.3
T16S/R2E-04L04	LS Mutual No. 2	Paso Robles	-157301.6	-159472.5
15S/1E-22H01	Luxton	Paso Robles	-163883.8	-154271.5
T15S/R1E-14N04	Military	Paso Robles	-163309.4	-153669.0
T15S/R1E-15N02	Mont. Sand Co. deep	Santa Margarita	-164819.5	-153279.5
T15S/R1E-15N03	Mont. Sand Co. shal	Paso Robles	-164819.5	-153279.5
T15S/R2E-33Ca	MPWMD No. 3	Santa Margarita	-156480.8	-157153.8
T15S/R1E-26Nb	MPWMD No. 4D	Santa Margarita	-163350.7	-156655.9
T15S/R1E-26Na	MPWMD No. 4S	Paso Robles	-163330.5	-156653.3
T16S/R2E-04Hb	MPWMD No. 5D	Santa Margarita	-155848.9	-159175.1
T16S/R2E-04Ha	MPWMD No. 5S	Paso Robles	-155848.9	-159175.1

[1]California Spacial Information Library Albers projection.

Table 2.2 Monitoring Wells Locations and Aquifer

(Continued)

Well Number	Name	Aquifer	X (m)	Y (m)
T16S/R2E-04Fb	MPWMD No. 6D	Santa Margarita	-156613.3	-159295.0
T16S/R2E-04Fa	MPWMD No. 6S	Paso Robles	-156613.3	-159295.0
	MW-12-11-180L	Salinas Valley 400-Foot Aquifer	-161632.5	-148215.2
	MW-OU2-06-400	Salinas Valley 400-Foot Aquifer	-159639.6	-148568.1
	MW-OU2-07-400	Salinas Valley 400-Foot Aquifer	-159172.1	-148420.4
	MW-OU2-09-400	Salinas Valley 400-Foot Aquifer	-159799.8	-148838.1
	MW-OU2-22-400	Salinas Valley 400-Foot Aquifer	-159965.5	-148559.8
	MW-OU2-69-180	Salinas Valley 400-Foot Aquifer	-157263.0	-148917.1
	MW-OU2-72-180	Salinas Valley 400-Foot Aquifer	-156829.1	-149262.7
15S/1E-23B02	Ord Grove test	Santa Margarita	-162636.3	-154109.9
15S/1E-23Cb	Ord Ter - deep	Santa Margarita	-162943.8	-153933.9
15S/1E-23Ca	Ord Ter- shal	Santa Margarita	-162943.8	-153933.9
T16S/R2E-05M06	Paddock No. 1	Paso Robles/Santa Margarita	-157957.6	-159423.9
15S/1E-14R1	Paralta test	Paso Robles	-162243.9	-153680.6
T15S/R1E-15K04	PCA-E mult. Deep	Santa Margarita	-164068.1	-153221.9
T15S/R1E-15K05	PCA-E mult. Shal.	Paso Robles	-164068.1	-153221.9
15S/1E-22B03	Playa #3	Paso Robles	-164232.2	-153993.5
15S/1E-22B04	Playa #4	Santa Margarita	-164232.2	-153993.5
	PZ-12-01-180L	Salinas Valley 400-Foot Aquifer	-161527.1	-148331.3
	PZ-12-01-180L	Salinas Valley 400-Foot Aquifer	-161271.6	-148234.8
	PZ-12-02-180L	Salinas Valley 400-Foot Aquifer	-160957.6	-148231.6
T16S/R2E-09D01	Roerdan	Paso Robles	-157171.4	-160464.3
T15S/R1E-35Jx	Ryan Ranch Monitor M2S	Paso Robles	-162183.6	-158190.9
T16S/R1E-01C05	Ryan Ranch No. 10	Santa Margarita	-161542.7	-158708.3
T15S/R1E-36H02	Ryan Ranch No. 2	Santa Margarita	-162165.9	-158252.3
T15S/R1E-36N02	Ryan Ranch No. 9	Santa Margarita	-161708.5	-158624.1
T16S/R2E-06C02	SCS Deep	Santa Margarita	-159844.7	-158822.5
T16S/R2E-04E01	SPCA	Paso Robles	-157305.1	-159473.9
T16S/R2E-06M01	Subdivision	Santa Margarita	-160356.1	-159452.9
	Test2	Salinas Valley 400-Foot Aquifer	-155464.9	-150719.0
T16S/R2E-03L01	Tierra Meadows No. 1	Paso Robles	-154988.7	-159816.5
T16S/R2E-03L02	Tierra Meadows No. 2	Paso Robles	-155000.9	-159822.1
T16S/R2E-10E01	Vista El Encanto No. 1	Paso Robles/Santa Margarita	-155768.4	-160906.4
T16S/R2E-10E02	Vista El Encanto No. 2	Paso Robles/Santa Margarita	-155523.0	-160951.2
T16S/R2E-04L01	Xum Speegle	Paso Robles	-156747.1	-159553.6

Table 2.3 Merasured Groundwater Altitudes

(feet)

Well Number	Name	Aquifer	Measurement Time	
			Fall 95	Fall 02
	Ambler Park #6	Paso Robles/Santa Margarita	--	170.0
	Beach	Salinas Valley 400-Foot Aquifer	0.0	-5.3
T16S/R2E-05E02	Bishop No. 1	Paso Robles/Santa Margarita	0.0	186.0
T16S/R2E-05F06	Bishop No. 2	Paso Robles/Santa Margarita	0.0	169.9
T16S/R2E-09J02	Chamisal Tennis Club	Santa Margarita	0.0	227.3
T15S/R1E-36Rb	County MW-1D	Santa Margarita	0.0	215.2
T16S/R2E-09Bb	County MW-3D	Santa Margarita	192.2	178.8
T16S/R2E-09Bc	County MW-3S	Paso Robles	234.1	234.5
T16S/R2E-04Lc	County No. 3	Santa Margarita	210.8	197.3
T15S/R2E-32Ra	County TH-1 Range	Santa Margarita	219.4	213.2
T16S/R2E-05G04	County Park No. 3	Paso Robles	0.0	204.5
T16S/R2E-05G02	County Park No.1	Paso Robles/Santa Margarita	0.0	214.8
T15S/R1E-23E01	Darwin	Paso Robles	0.0	14.9
T16S/R2E-05F04	East Fence	Paso Robles	0.0	112.0
	El Toro Park W59-01	Paso Robles/Santa Margarita	0.0	-5.0
	El Toro W35	Paso Robles/Santa Margarita	0.0	-20.0
	El Toro W39-01	Paso Robles/Santa Margarita	0.0	-30.0
	Fort Ord #10 Deep	Santa Margarita	0.0	-1.3
	Fort Ord #10 Shallow	Paso Robles	0.0	-0.4
	Fort Ord #11 Deep	Santa Margarita	0.0	4.5
	Fort Ord #4 Deep	Santa Margarita	51.2	0.0
T15S/R1E-12Fc	Fort Ord 10 deep	Santa Margarita	-4.8	-1.3
T15S/R1E-12Fa	Fort Ord 10 shallow	Paso Robles	-3.0	-0.4
T15S/R1E-7Bb	Fort Ord 11 deep	Santa Margarita	0.0	4.5
T15S/R1E-7Ba	Fort Ord 11 shallow	Paso Robles	-5.0	-5.5
T15S/R1E-13Lb	Fort Ord 7 deep	Santa Margarita	-1.8	-15.7
T15S/R1E-13La	Fort Ord 7 shallow	Paso Robles	23.0	16.6
T15S/R1E-12Qb	Fort Ord 8 deep	Santa Margarita	-1.0	-14.7
T15S/R1E-12Qa	Fort Ord 8 shallow	Paso Robles	12.6	0.7
T15S/R1E-11Pb	Fort Ord 9 deep	Santa Margarita	-4.9	-17.1
T15S/R1E-11Pa	Fort Ord 9 shallow	Paso Robles	-0.8	5.1
T16S/R2E-09C02	Hidden Hills/Mutual	Paso Robles/Santa Margarita	0.0	205.6
T16S/R2E-09C03	Hidden Hills/Standex (QT	Paso Robles/Santa Margarita	0.0	209.6
T15S/R1E-27	Johann/Shea	Santa Margarita	0.0	44.1
T16S/R2E-06H02	L.S. Golf Course '98	Paso Robles/Santa Margarita	0.0	155.0
T15S/R1E-22H05	La Salle 2	Santa Margarita	0.0	-10.7
T16S/R2E-04L04	LS Mutual No. 2	Paso Robles	0.0	250.8
15S/1E-22H01	Luxton	Paso Robles	0.0	-9.3
T15S/R1E-14N04	Military	Paso Robles	0.0	-28.7
T15S/R1E-15N02	Mont. Sand Co. deep	Santa Margarita	-5.2	-14.3
T15S/R1E-15N03	Mont. Sand Co. shal	Paso Robles	-0.3	4.1
T15S/R2E-33Ca	MPWMD No. 3	Santa Margarita	149.4	144.7
T15S/R1E-26Nb	MPWMD No. 4D	Santa Margarita	51.8	56.5
T15S/R1E-26Na	MPWMD No. 4S	Paso Robles	52.3	57.2
T16S/R2E-04Hb	MPWMD No. 5D	Santa Margarita	193.2	185.0
T16S/R2E-04Ha	MPWMD No. 5S	Paso Robles	249.7	242.9

Table 2.4a California American Water Co. Annual Pumping

(acre-feet)

Year	Well																		
	Ord Grove	Military	Paralta	Darwin	La Salle No. 2	Luzern	Playa No. 3	Luxton	Harding	Plumas No. 2,3,4	MGT	Palm	Harcourt	Elm	Monte	Orange	Bishop Water Co.	Hidden Hills	Ryan Ranch	Laguna Seca Water Co.
1956				190	13						4									
1957				187	56						1									
1958				185					117											
1959				200	69				169	225										
1960				175	246			3	120	199										
1961				124	437			46	101	230	30									
1962				127	294			2	100	233	41									
1963				86	251			32	75	240	33									
1964				156	443			26	86	227	34									
1965				117	428			35	112	201	28									
1966		285		136	559	244	553	1	134	225	39	21	79	33	68	323				
1967		346		167	385	618	834		109	81	1	21	30	3	4	39				
1968		351		165	479	1,083	748		97	224	21	45	64	75	45	85				
1969	8	334		68	271	1,154	502		63	66	15	16	34	35	23	33				
1970	153	319		80	425	1,548	584		82	158	17	33	60	133	64	153				
1971	1,359	184		87	357	1,459	441		80	103	4	26	51	89	12	57				
1972	1,830	207		112	278	1,333	487		69	117		25	49	100	28	65				
1973	1,401	187		130	172	1,213	457		47	111		17	24	96	34	87				
1974	1,270	153		30	6	1,256	636		2	111						127				
1975	1,218	147		103	264	1,074	388		49	33		9	1	49		65				
1976	1,229	227		131	369	1,052	653		56	220		15	33	45		199				
1977	788	111		40	93	1,157	360		31	111		2								
1978	559	96		70		814	146			34										
1979	523					931	206													
1980	728	70		8	15	1,016	364			7										
1981	650	106		163		906	475			30										
1982	411	27				310	177													
1983	402	95		24	80	705	352			5										
1984	556	110		31	94	570	320			105										
1985	802	116		93	176	643	215			106										
1986	1,612	252		154	207	749	354			197										

Table 2.4a California American Water Co. Annual Pumping

(Continued)

Year	Well																		
	Ord Grove	Military	Paralta	Darwin	La Salle No. 2	Luzern	Playa No. 3	Luxton	Harding	Plumas No. 2,3,4	MGT	Palm	Harcourt	Elm	Monte	Orange	Bishop Water Co.	Hidden Hills	Ryan Ranch	Laguna Seca Water Co.
1987	1,520	177		99	172	748	434			173										
1988	1,563	197		82	151	580	450			324										
1989	1,550	185		67	118	613	425			270							95	113	21	26
1990	1,508	242		142	252	202	478			432							208	132	23	26
1991	1,347	111		78	119	485	480			221							265	138	23	27
1992	1,635	14		0	0	144	57			3							345	147	42	28
1993	1,372	106		34	64	221	177			66							360	162	47	28
1994	1,028	215		107	162	433	480			320							352	166	52	29
1995	1,404	134	1,656	68	90	344	529			183							304	154	63	29
1996	1,596	157	1,974	60	72		270			1							302	162	64	30
1997	534	162	1,336	70	245	208	462.3										192	180	67	31
1998	1,175	118	1,360	50	92	331	331			211							141	146	49	31
1999	1,609	70	1,609	37	70	349	303.5			191							89	179	59	32
2000	1,083	18	1,368	49	92	313	231			172							123	186	76	32
2001	1,360	106	1,866		105	321	187			142							165	213	81	32
2002	1,139	228	1,706		88	228	231			176							173	236	96	

Table 2.4B
City of Seaside Annual Pumping
(acre-feet)

Year	Well			Year	Well		
	City 1	City 2	City 3		City 1	City 2	City 3
1956				1980	100	151	234
1957				1981	299		158
1958				1982	303		187
1959				1983	338	19	157
1960				1984	155	152	207
1961				1985	30	251	211
1962				1986	61	192	224
1963				1987	48	73	29
1964				1988	238		22
1965				1989	252	8	3
1966				1990	222	23	55
1967	79	97		1991	260		33
1968	124	137		1992	110		210
1969	166	166		1993	153		153
1970	201	249		1994	124		155
1971	213	237		1995	149		185
1972	187	291		1996	7		300
1973	237	251		1997	23		310
1974	245	251		1998			
1975	175	203	136	1999			
1976	95	160	282	2000			
1977	56	67	110	2001			
1978	95	108	132	2002			
1979	63	206	167				

Table 2.4c Annual Pumping from Private Production Wells

(acre-feet)

Year	Well									
	Seaside Golf	Fort Ord Golf Course	Ord Village	Non-municipal	Misc. (L.S.)	LS Golf Club	Pasadera	York School	Laguna Seca County Parks	S.C. misc
1956				200						
1957				200						
1958				200						
1959			103	200						
1960			6	200						
1961			7	200						
1962			13	200						
1963			21	200						
1964			54	200						
1965			131	200						
1966			125	200						
1967			16	200						
1968		85	54	200						
1969		213	137	200						
1970		215	138	200						
1971		209	134	200						
1972		150	96	200						
1973		181	116	200						
1974		184	110	200						
1975		175	98	200						
1976		178	114	200						
1977		221	120	200						
1978		193	117	200						
1979		157	95	200						
1980		144	138	200						
1981		144		250						
1982		144		250						
1983		144		250						
1984		357		250						
1985		393		250						
1986		456		250						
1987		377		250						
1988		392		186						
1989		420		217						
1990		424		217	8	182			5	2
1991				200	13	138			5	3
1992				64	12	67			5	1
1993		423		55	12	4			5	1
1994		394		25	11	5			5	2
1995		233		28	10	0			5	1
1996		122		19	11	3			5	4
1997		282		39	14	79			5	4
1998		401		55	12	142			5	
1999	387				9	131			5	
2000	676				7	180	112		5	
2001	630				10	212	251		5	
2002					12	231	251	25	5	

Table 2.5 Attributes of CIMIS Stations

Station Number	Station Name	Altitude (ft)	Distance Inland (ft)	ET0 (inches/yr)
19	Castroville	9	4,800	36.20
89	Salinas South	120	86,000	46.00
115	Gonzales	146	107,000	45.72
116	Salinas North	61	35,000	36.88

Table 2.6 ET Corresponding to 1993 Satellite Images

Image Month	Period (mo)	Average NDVI*	Study Area Eto (ft/mo)	ET (ft/mo)	ET x Period (ft)
Jan	1.5	0.49	0.11	0.06	0.08
Mar	2.5	0.50	0.23	0.11	0.28
Jun	2.5	0.55	0.42	0.23	0.58
Aug	2.0	0.41	0.32	0.13	0.26
Oct	2.0	0.46	0.22	0.10	0.20
Dec	1.5	0.52	0.11	0.06	0.09
Total					1.50

Table 3.1 Parameter values Used in Model

Parameter	Paso Robles Ratio	Value	Units
Surficial Deposits			
Horizontal hydraulic conductivity (K_x)	1.5	7.4	ft/d
Vertical hydraulic conductivity (K_y)	1.5	0.23	ft/d
Specific storage (S_s)	1.0	0.00001	1/ft
Specific yield (S_y)	1.0	0.10	ft^0
Salinas Valley Clay			
Horizontal hydraulic conductivity (K_x)	0.051	0.25	ft/d
Vertical hydraulic conductivity (K_y)	0.051	0.0078	ft/d
Specific storage (S_s)	10.0	0.00010	1/ft
Specific yield (S_y)	1.0	0.10	ft^0
Paso Robles Formation			
Horizontal hydraulic conductivity (K_x)	1.0	4.9	ft/d
Vertical hydraulic conductivity (K_y)	1.0	0.15	ft/d
Specific storage (S_s)	1.0	0.00001	1/ft
Specific yield (S_y)	1.0	0.10	ft^0
Purisima Formation			
Horizontal hydraulic conductivity (K_x)	0.24	1.2	ft/d
Vertical hydraulic conductivity (K_y)	0.24	0.038	ft/d
Specific storage (S_s)	1.0	0.00001	1/ft
Specific yield (S_y)	1.0	0.10	ft^0
Santa Margarita Formation			
Horizontal hydraulic conductivity (K_x)	1.5	7.4	ft/d
Vertical hydraulic conductivity (K_y)	1.5	0.23	ft/d
Specific storage (S_s)	1.0	0.000001	1/ft
Specific yield (S_y)	1.0	0.10	ft^0
Ord Terrace Fault			
Horizontal hydraulic conductivity (K_x)	--	0.29	ft/d
Vertical hydraulic conductivity (K_y)	--	0.009	ft/d
All Units			
Horizontal longitudinal dispersivity (α_{Lh})	--	600	ft
Vertical longitudinal dispersivity (α_{Lv})	--	200	ft
Horizontal transverse dispersivity (α_{Th})	--	200	ft
Vertical transverse dispersivity (α_{Tv})	--	100	ft
Porosity (ϕ)		0.15	ft^0
Boundaries			
Monterey Bay leakance (C_{ch})	--	10,000	ft^2/d
Salinas Valley leakance (C_{ch})	--	10,000	ft^2/d

Table 3.2 Groundwater Budget for 2002

(acre-feet per year)

Component	Rate
Inflows	
Monterey Bay	1,600
Recharge	11,900
Total	13,500
Outflows	
Salinas Valley boundary	9,000
Pumping	6,300
Total	15,300
Storage Change	-1,800

Table 4.1 Groundwater Budget for 2015 With Continued Pumping

(acre-feet per year)

Component	Rate
Inflows	
Monterey Bay	1,700
Recharge	11,900
Total	13,600
Outflows	
Salinas Valley boundary	8,700
Pumping	6,300
Total	15,000
Storage Change	-1,400

Table 4.2 Groundwater Budget for 2015
With Relocated Pumping

(acre-feet per year)

Component	Rate
Inflows	
Monterey Bay	1,200
Recharge	11,900
Total	13,100
Outflows	
Salinas Valley boundary	8,100
Pumping	6,300
Total	14,400
Storage Change	-1,300

Figures

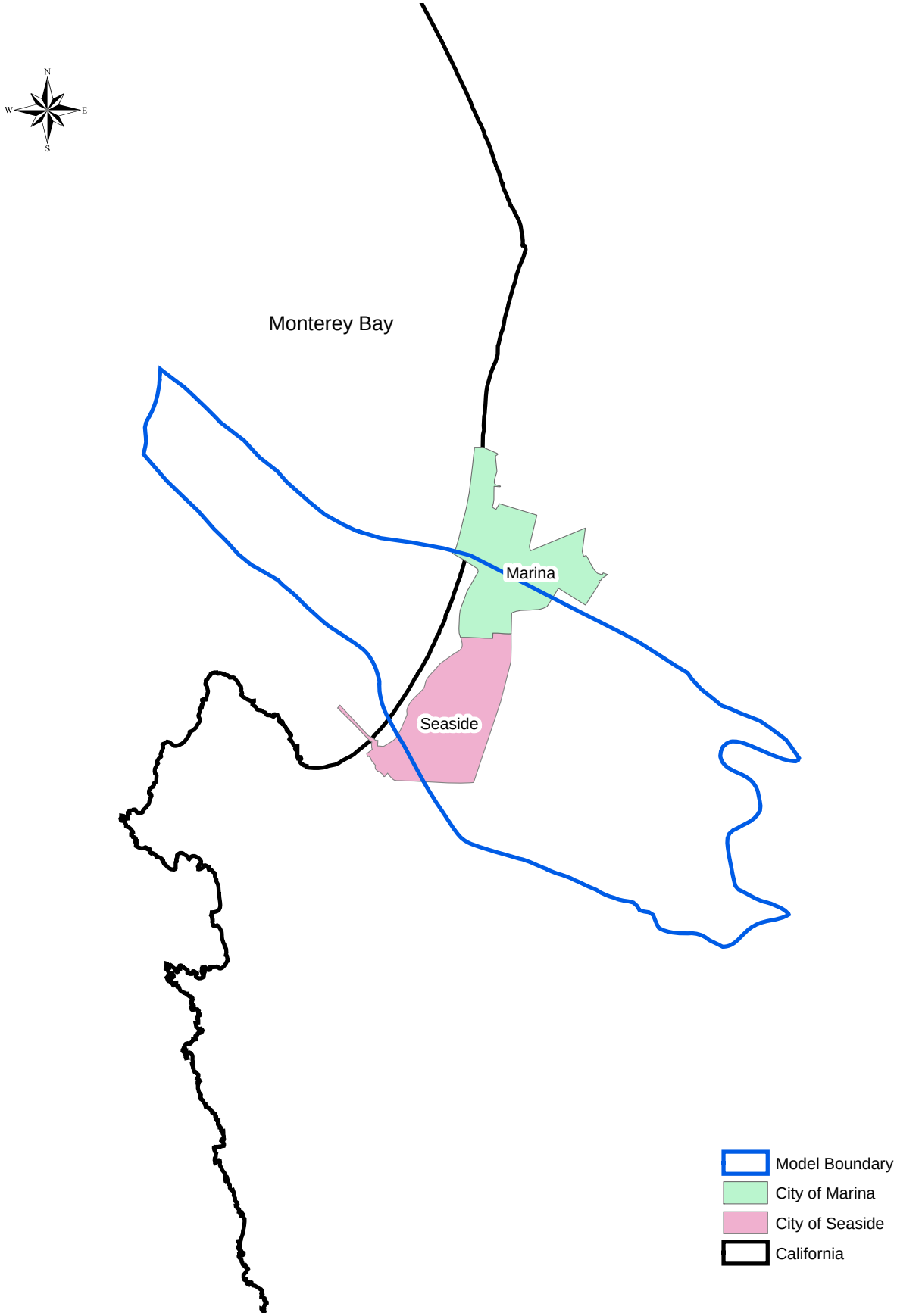

Figure 1.1 Location of Seaside Groundwater Basin

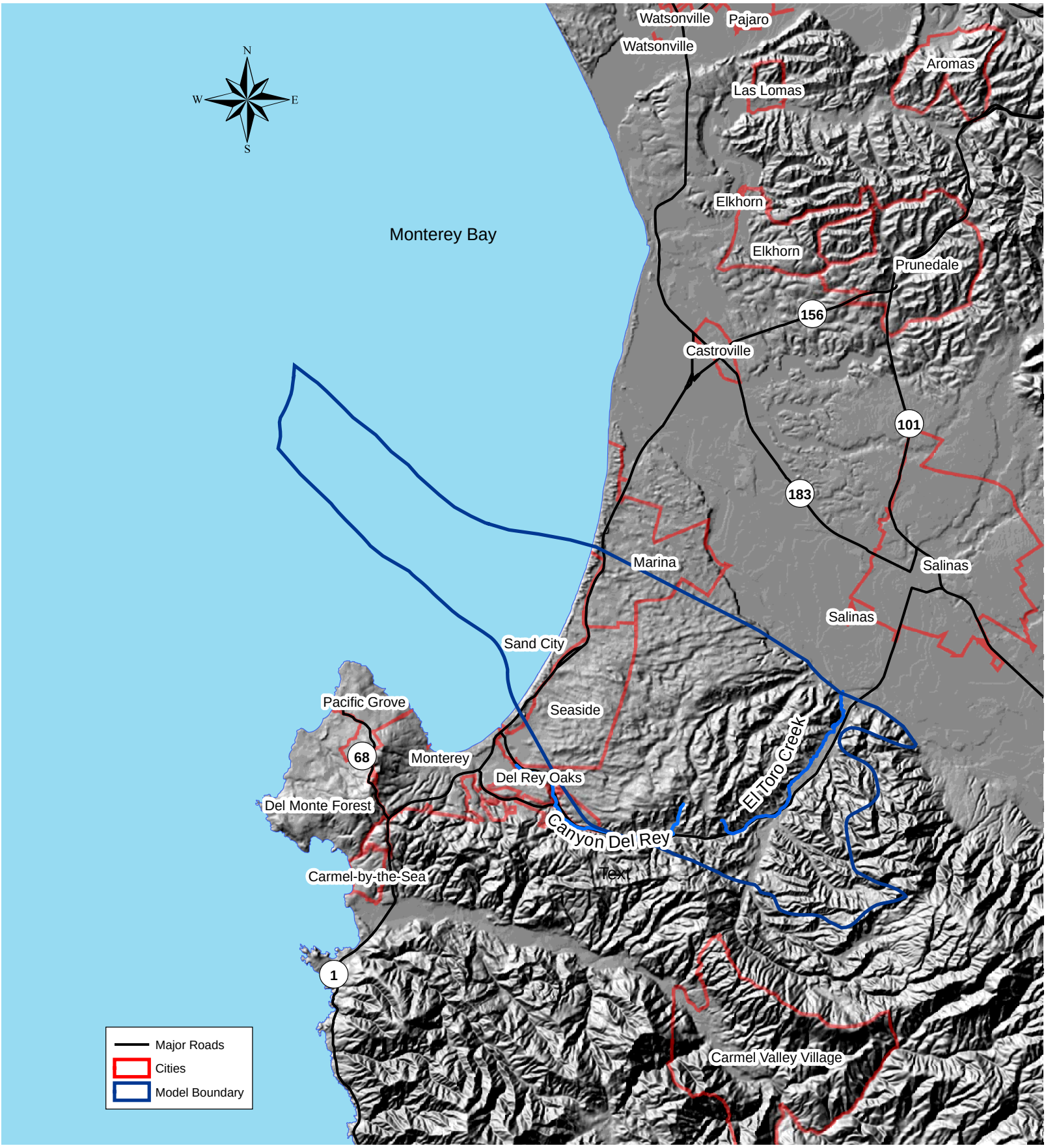

Figure 1.2 Physiographic and Cultural Features

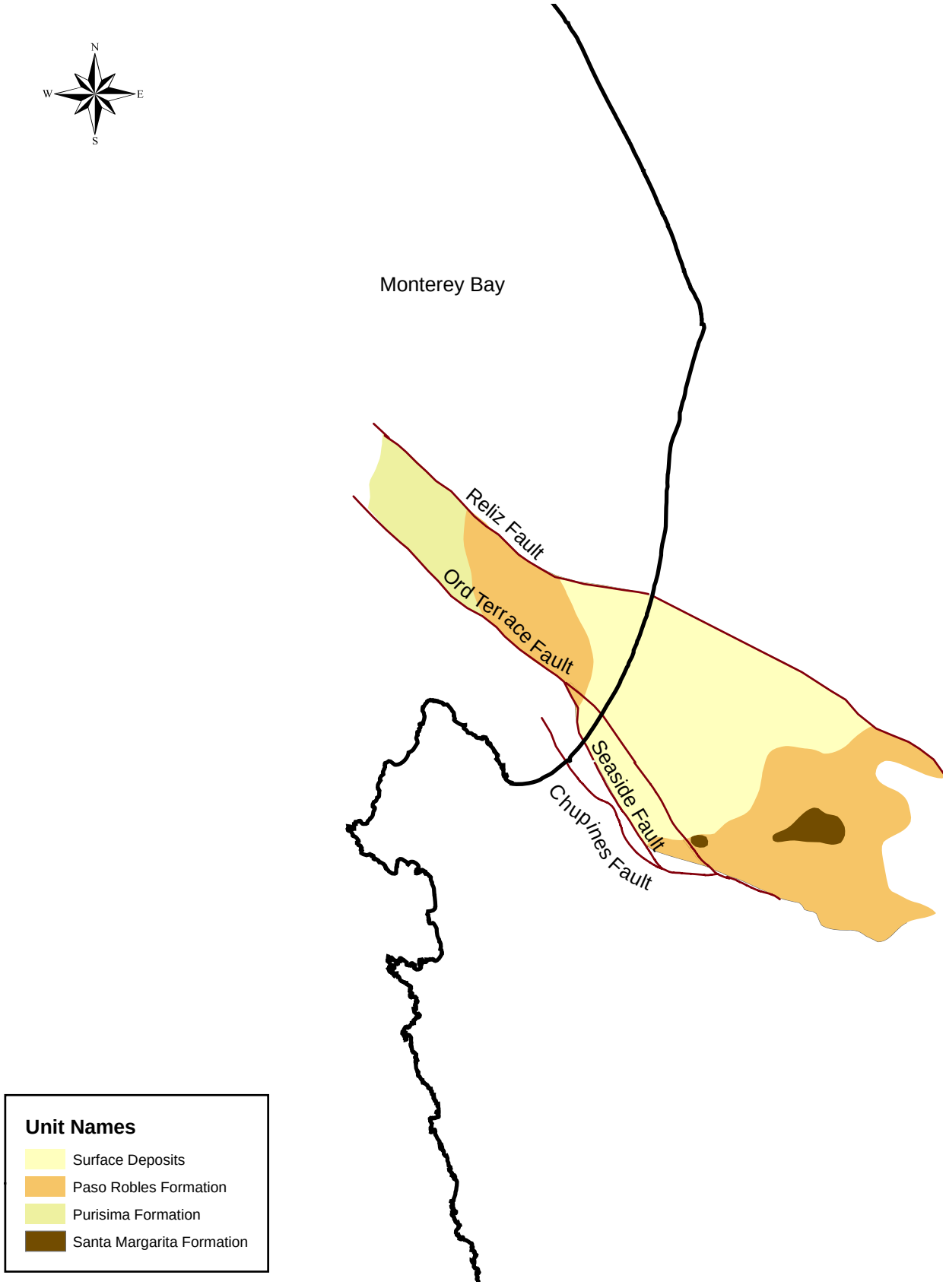

Figure 1.3 Hydrogeology of Study Area

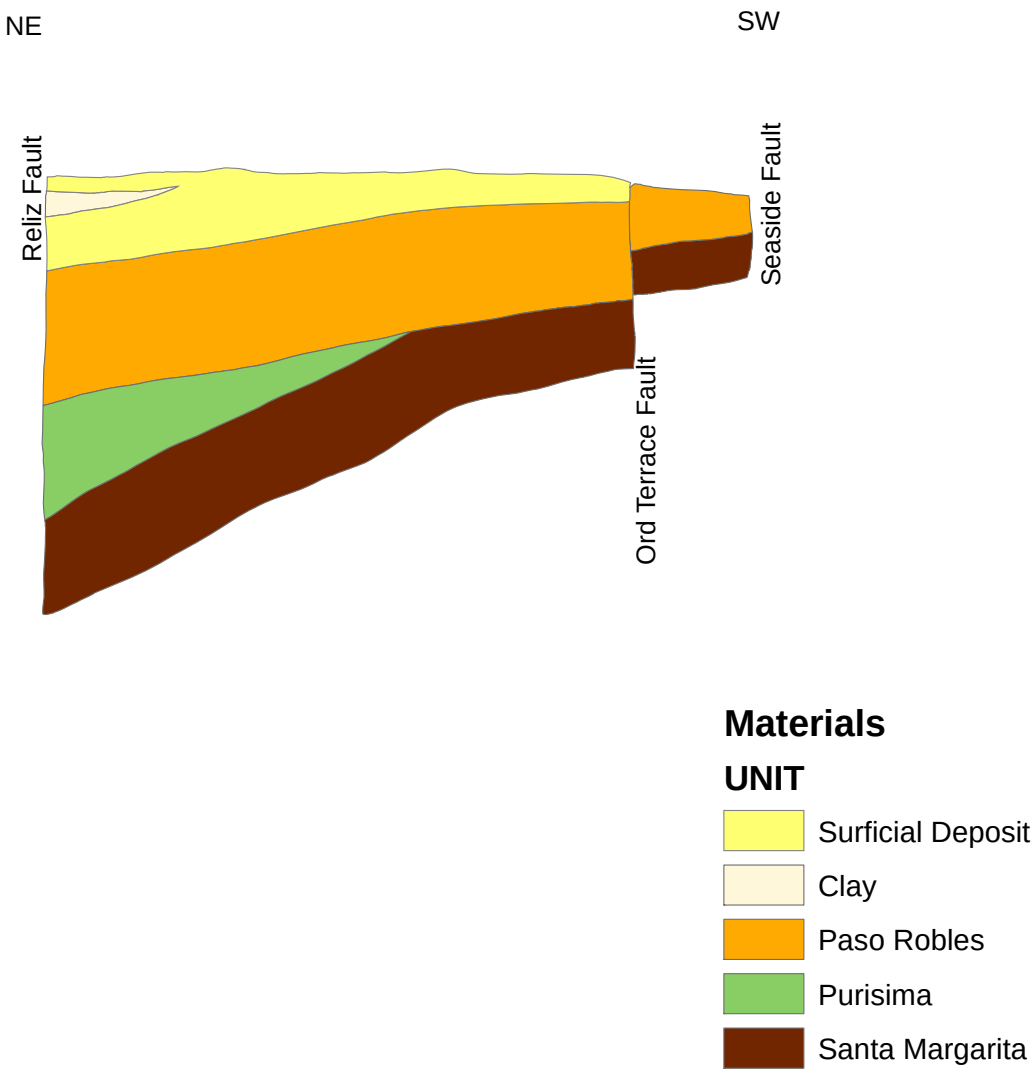

Figure 1.4a Northeast-Southwest Cross-Section of Seaside Groundwater Basin

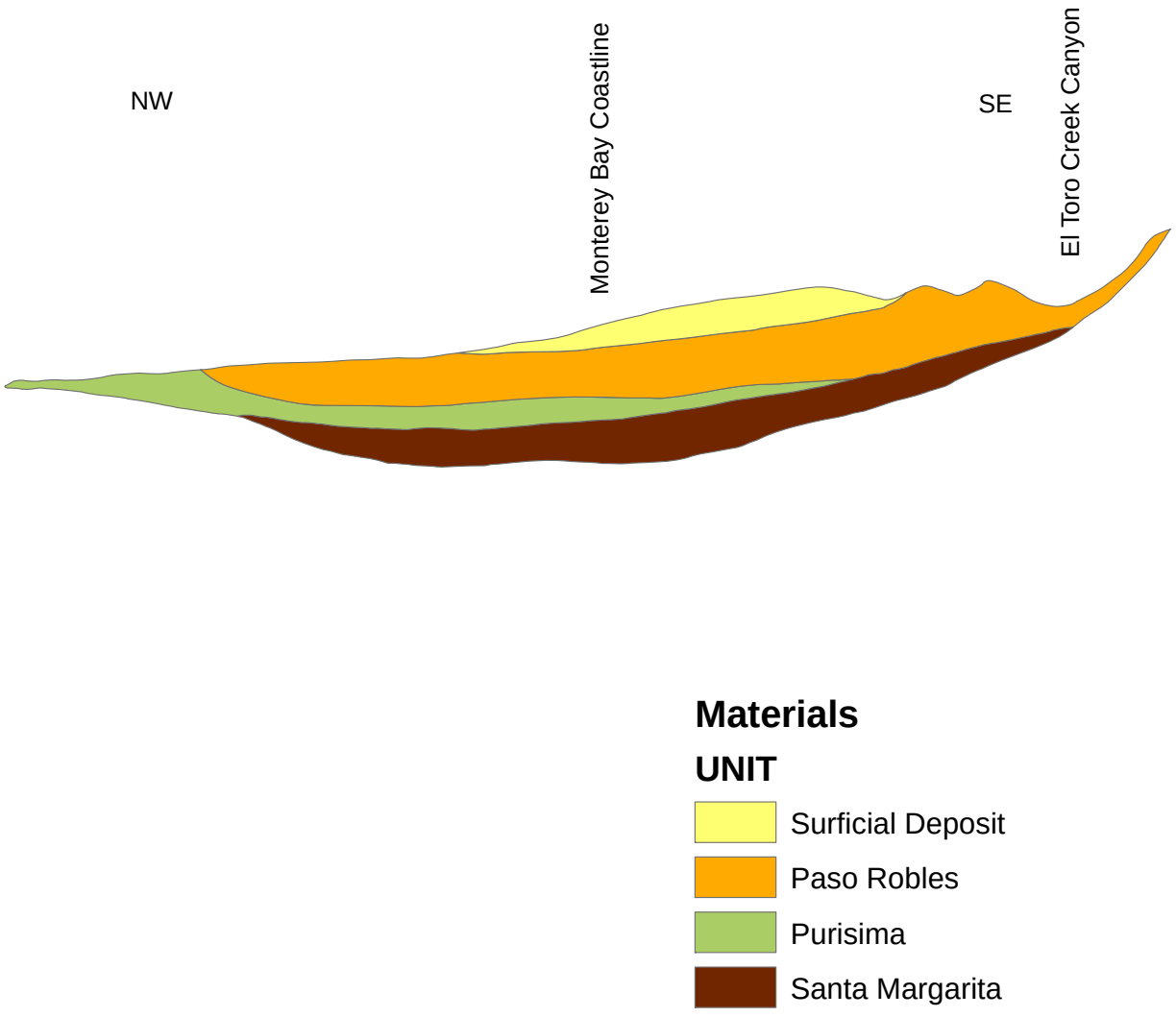

Figure 1.4b Northwest-Southest Cross-Section of Seaside Groundwater Basin

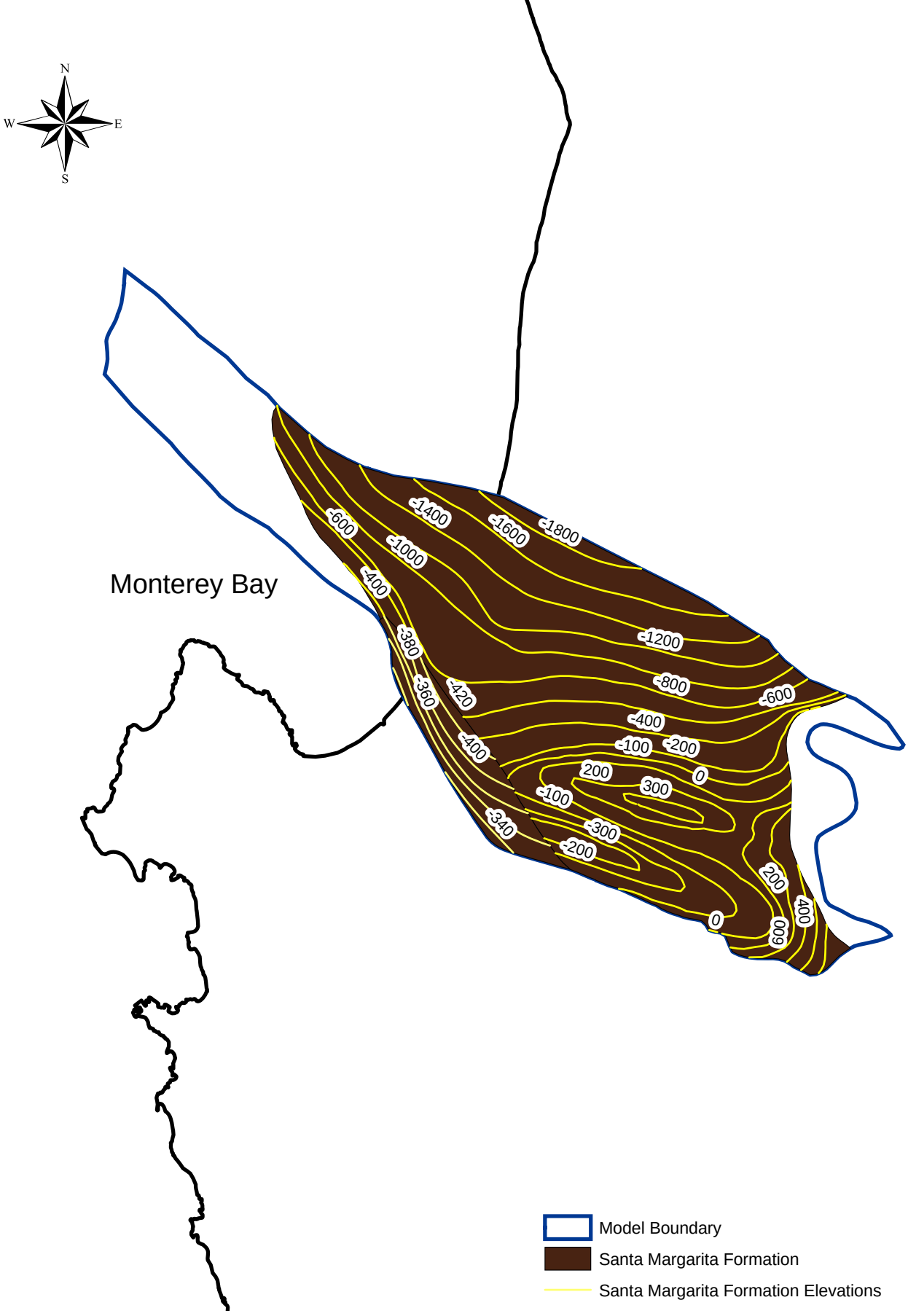

Figure 1.5a Base Elevation of Santa Margarita Formation

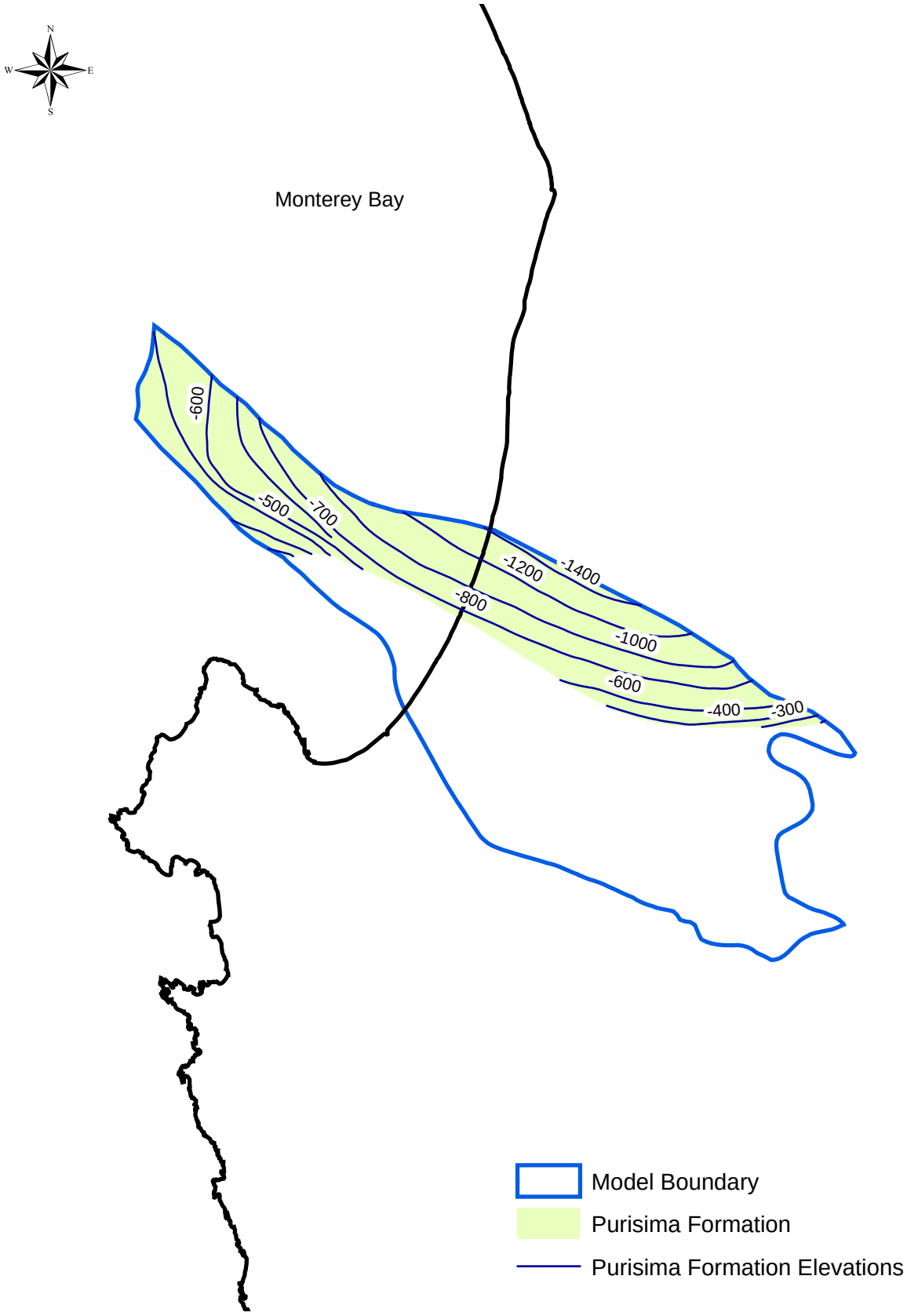

Figure 1.5b Base Elevation of Purisima Formation

Figure 1.5c Base Elevation of Pasa Robles Formation

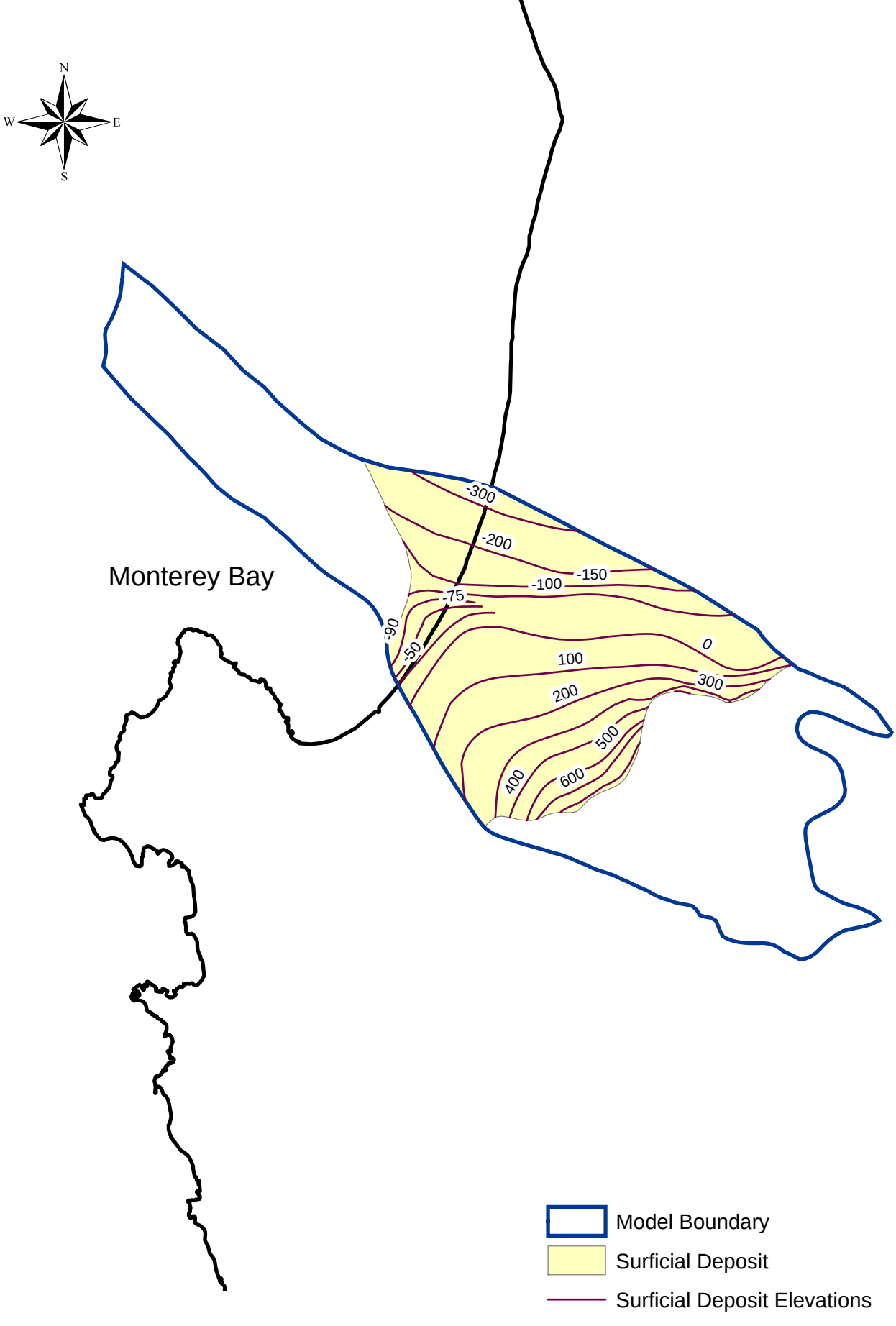

Figure 1.5d Base Elevation of Surficial Deposits

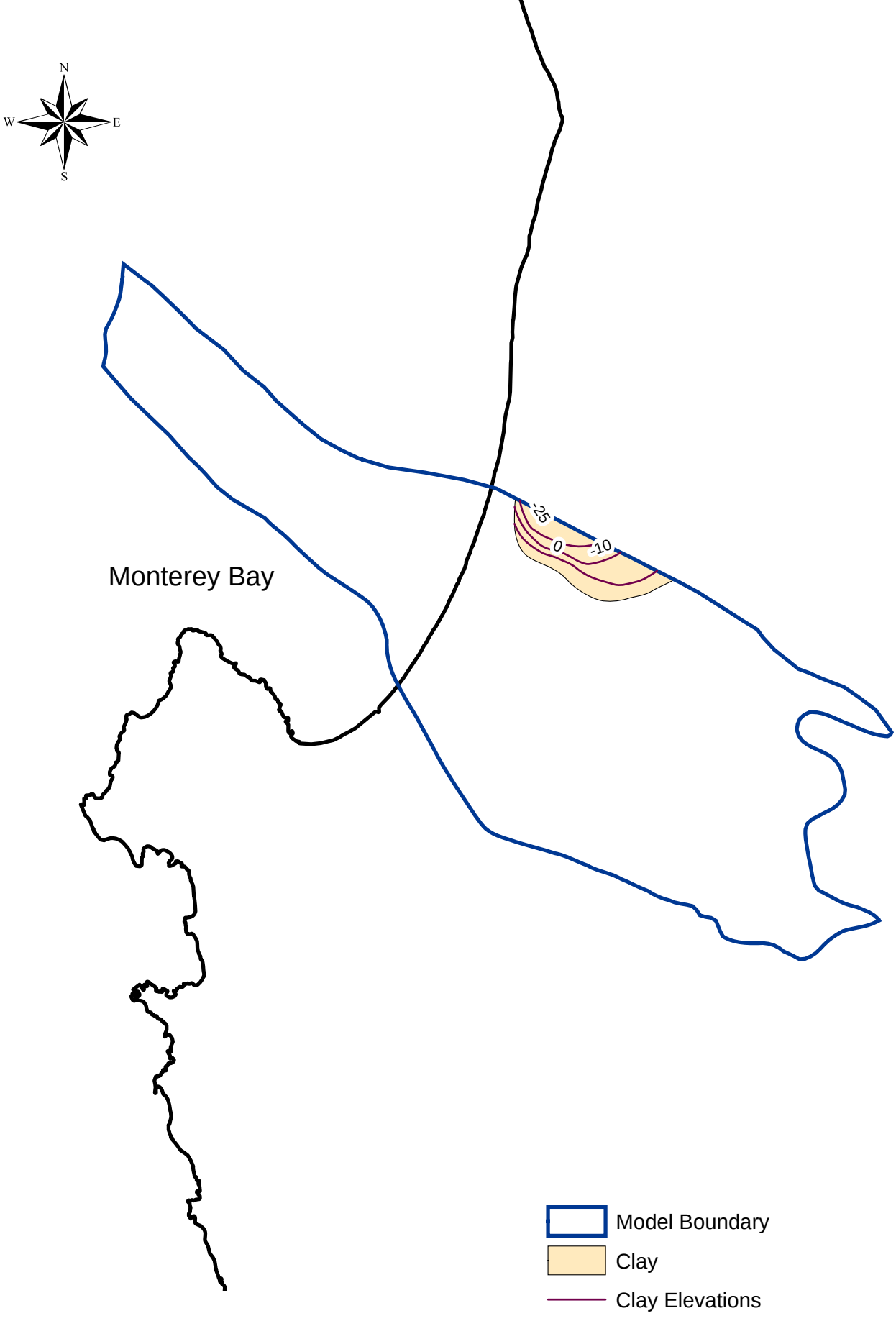

Figure 1.5e Base Elevation of Salinas Valley Clay

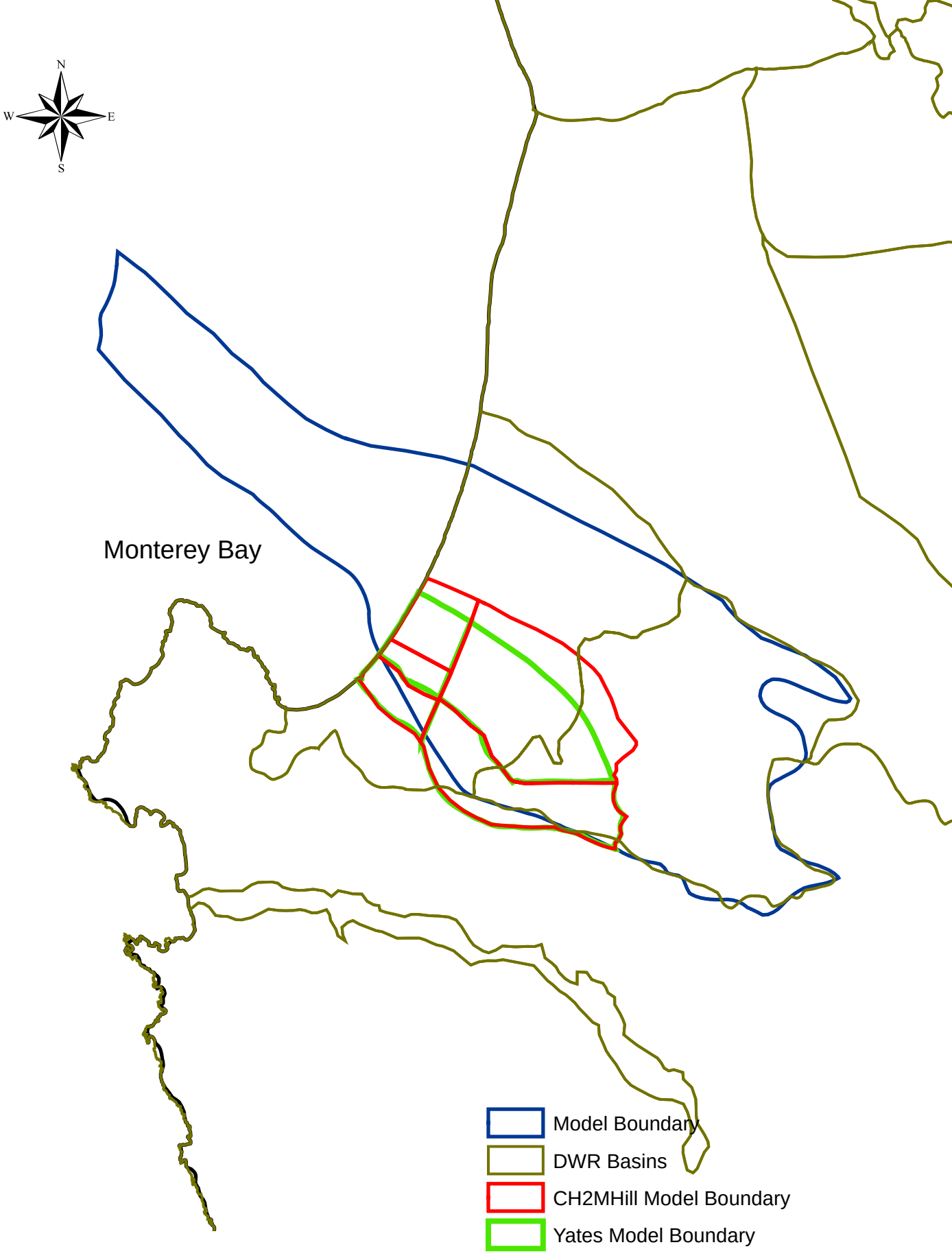

Figure 1.6 Model and Alternative Groundwater Boundaries

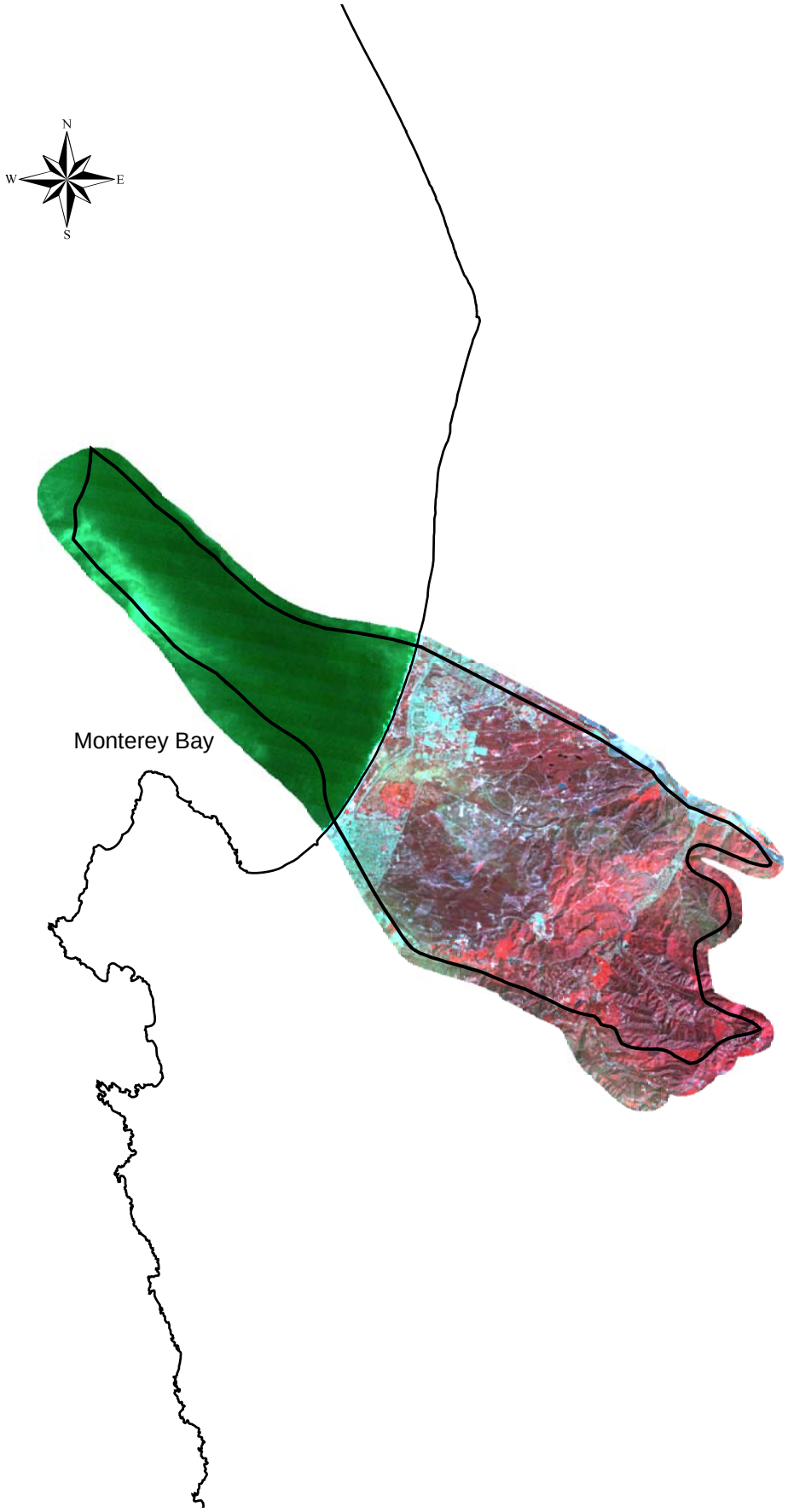

Figure 1.7 Satellite Image of Groundwater Basin, March 2000

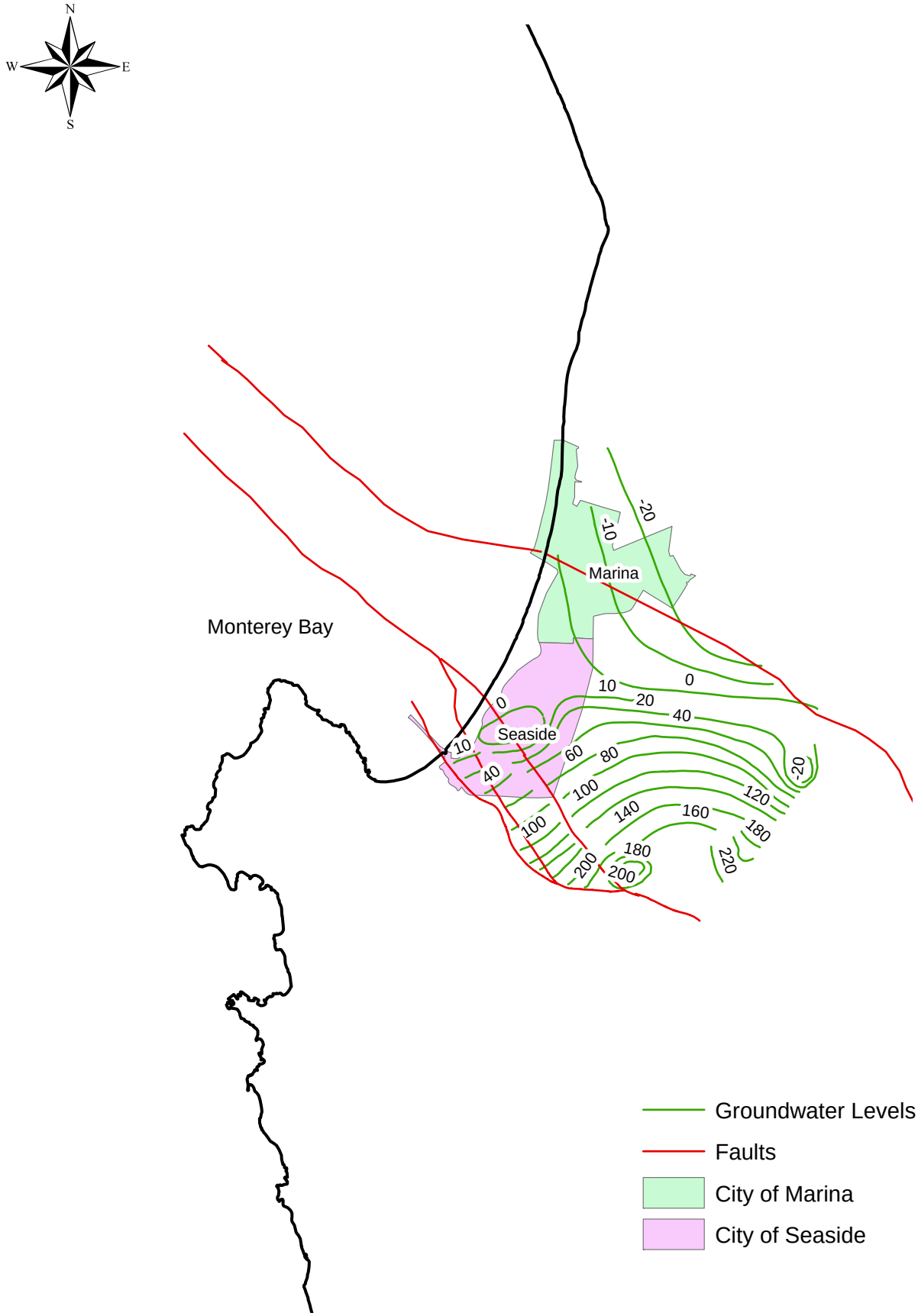

Figure 1.8a Groundwater Levels for Fall 2002, Paso Robles Formation

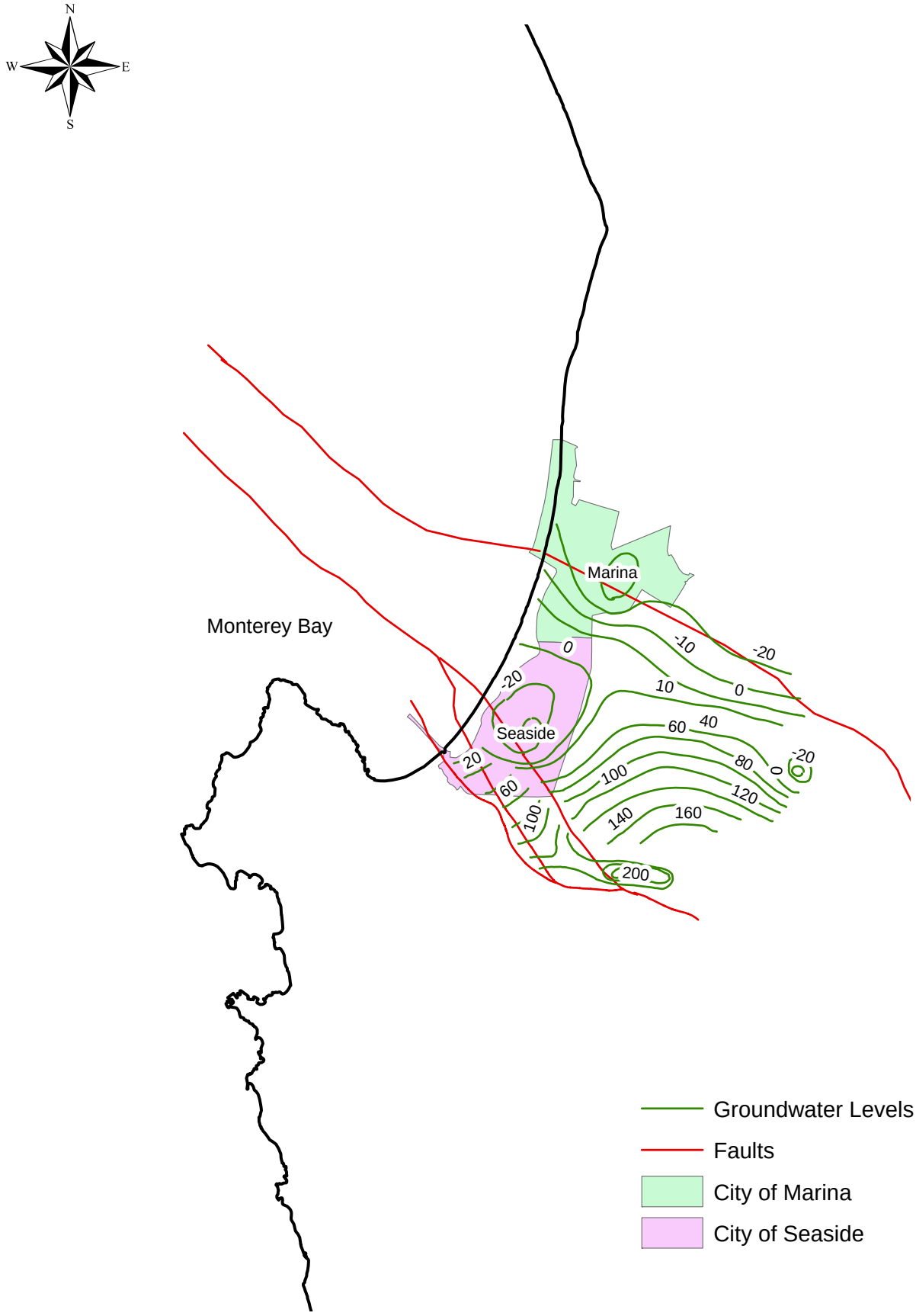

Figure 1.8b Groundwater Levels for Fall 2002, Santa Margarita Formation

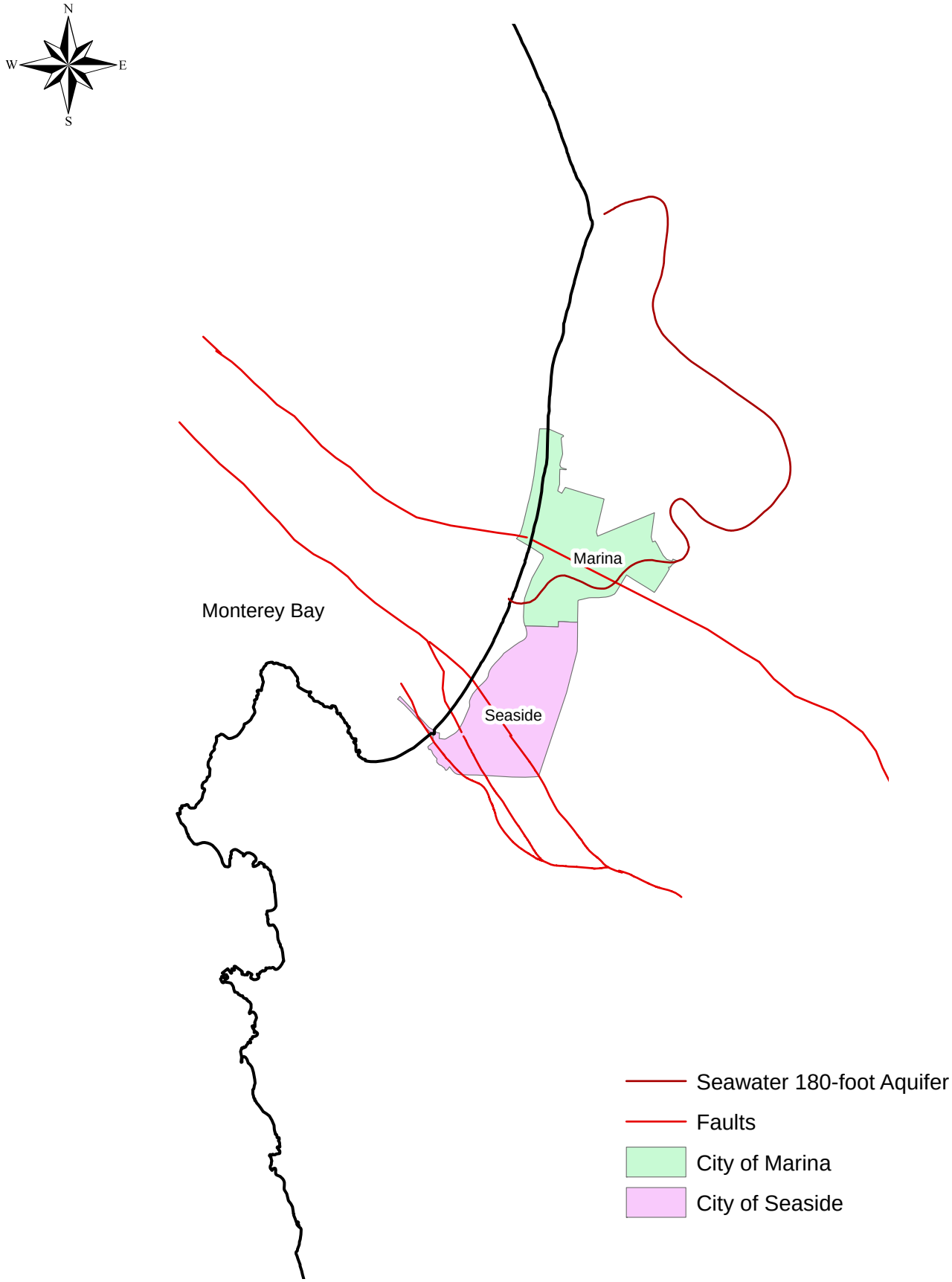

Figure 1.9a Extent of Seawater Intrusion for 2001, Salinas Valley 180-Foot Aquifer

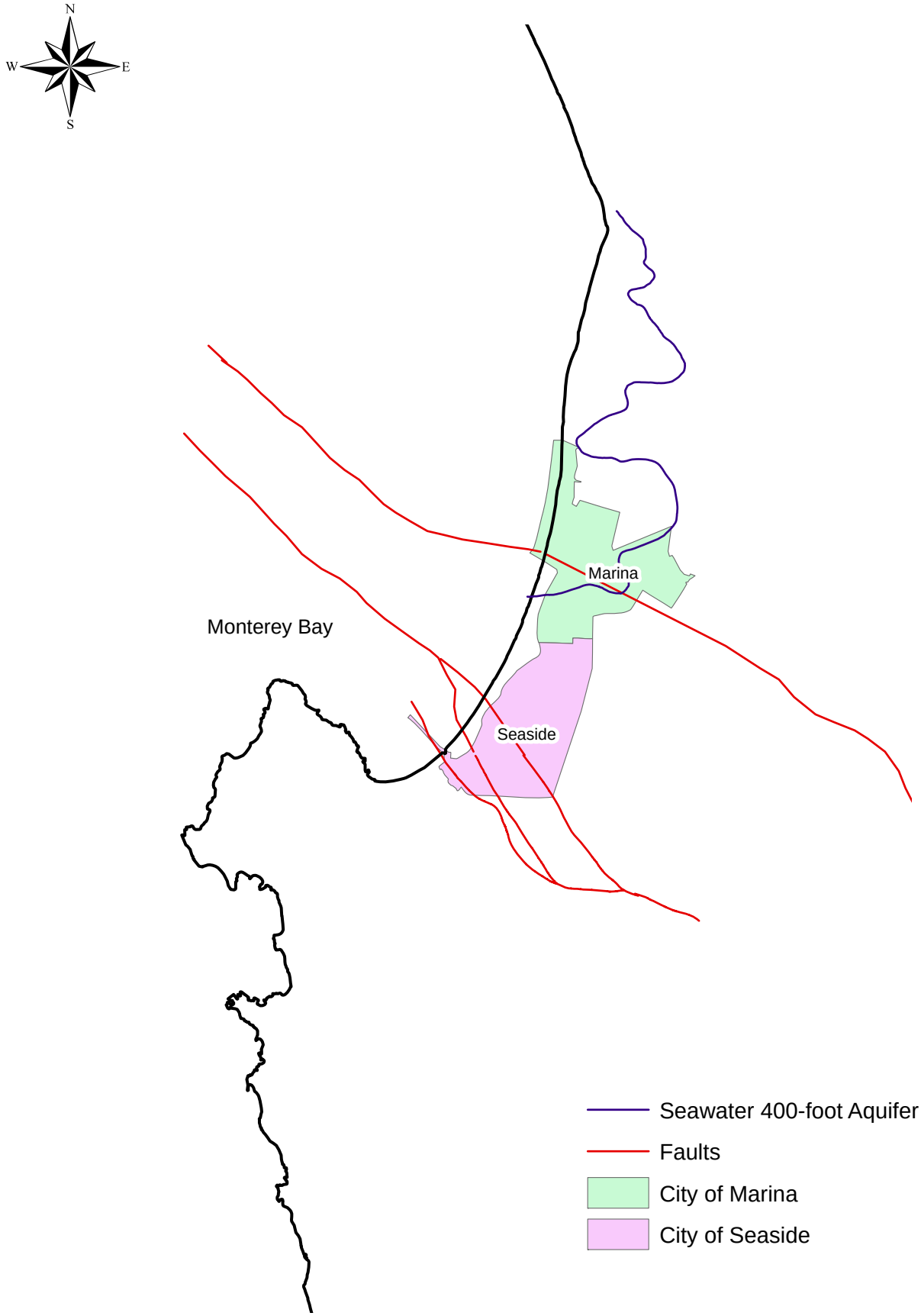

Figure 1.9b Extent of Seawater Intrusion for 2001, Salinas Valley 400-Foot Aquifer

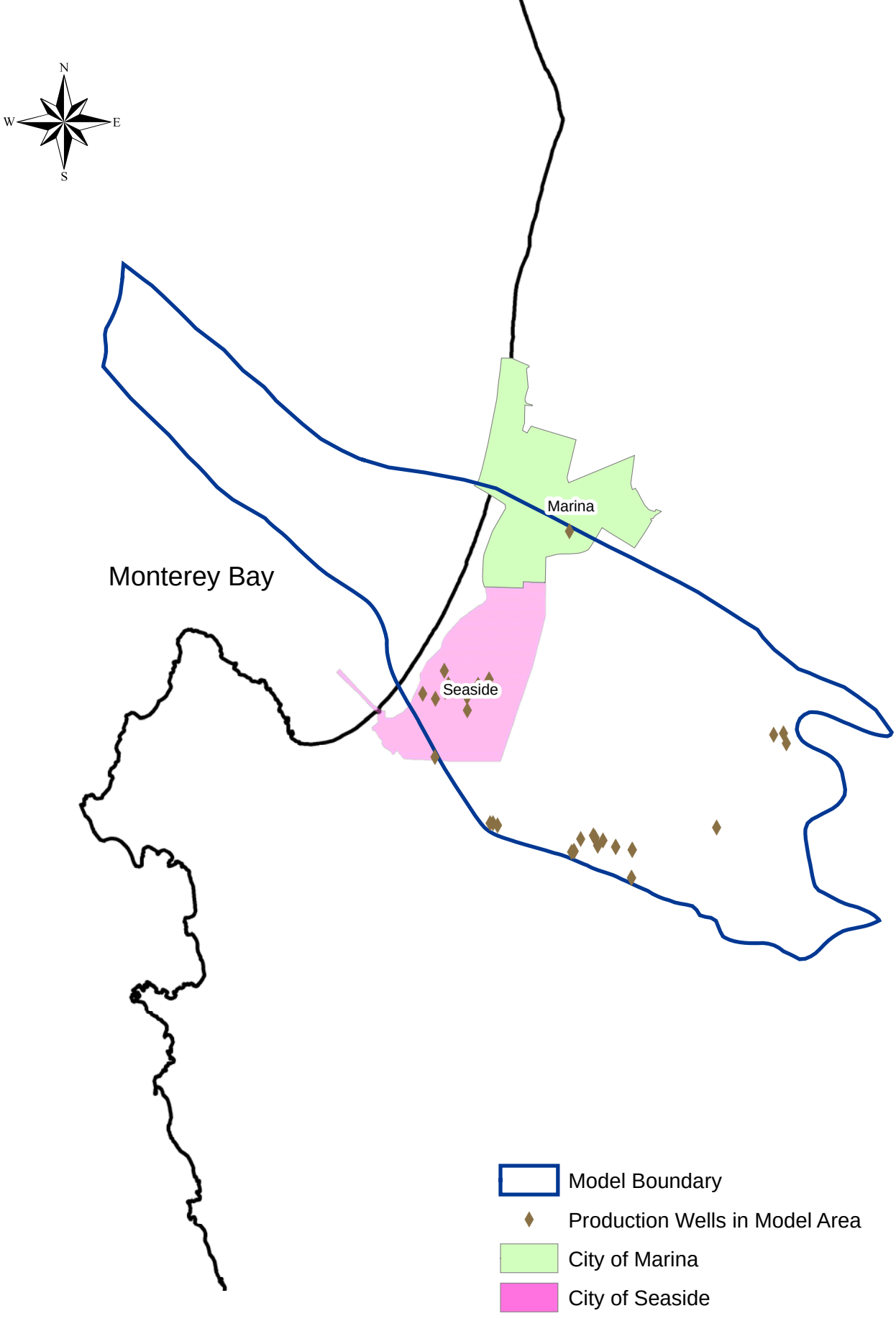

Figure 2.1 Production Wells in Model Area

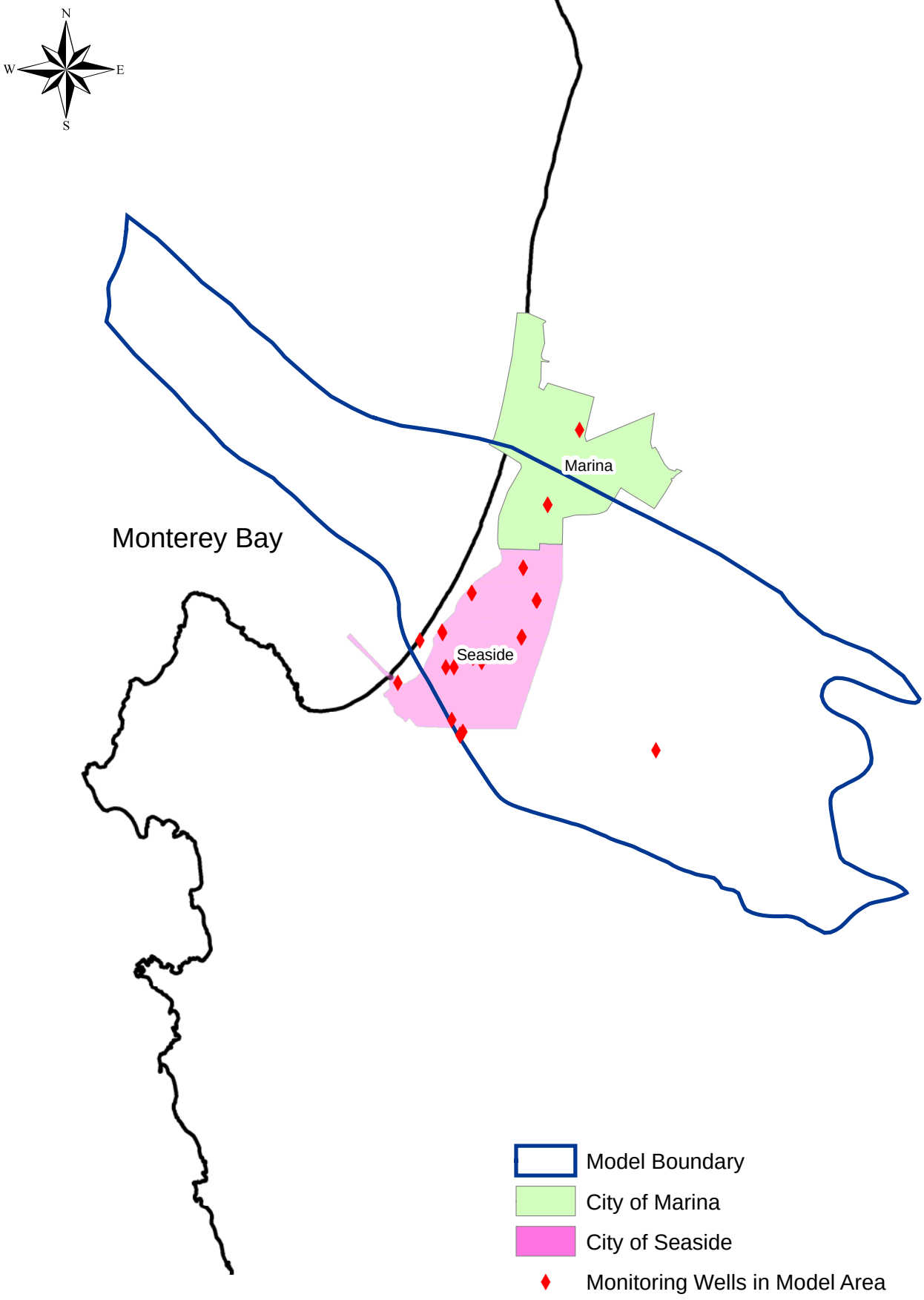

Figure 2.2 Monitoring Wells in Model Area

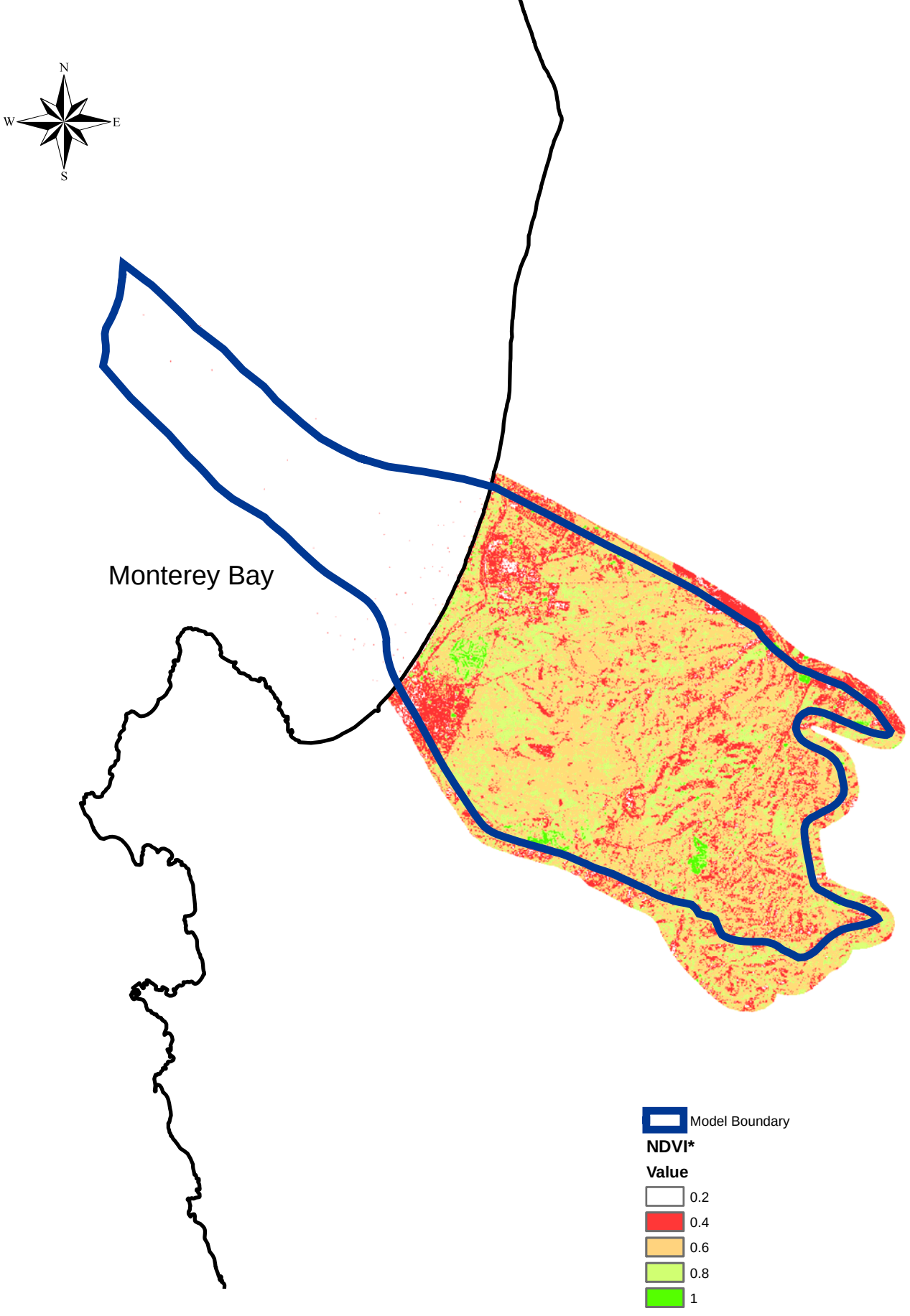

Figure 2.3a Geographic Distribution of NDVI*, January 1993

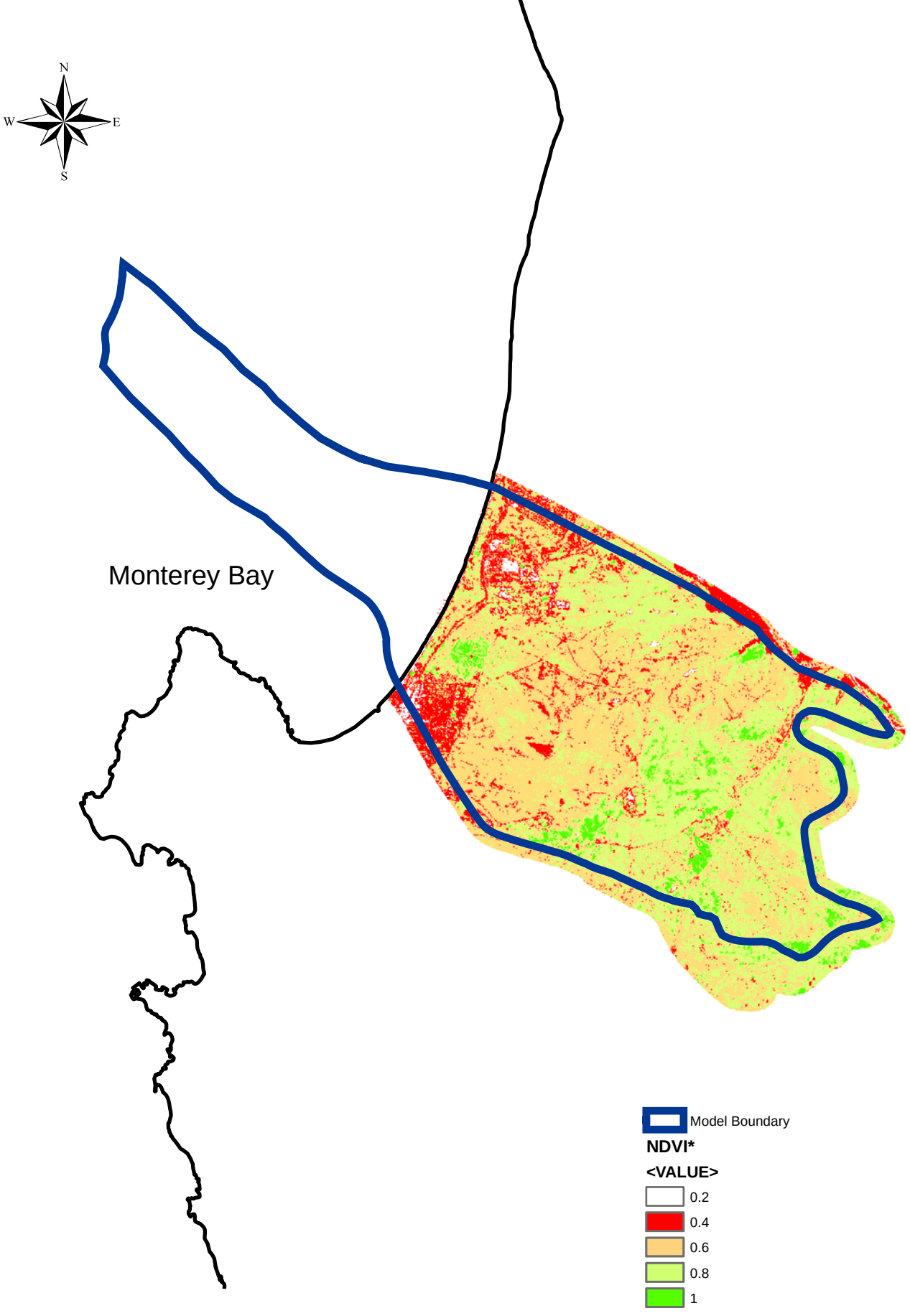

Figure 2.3b Geographic Distribution of NDVI*, March 1993

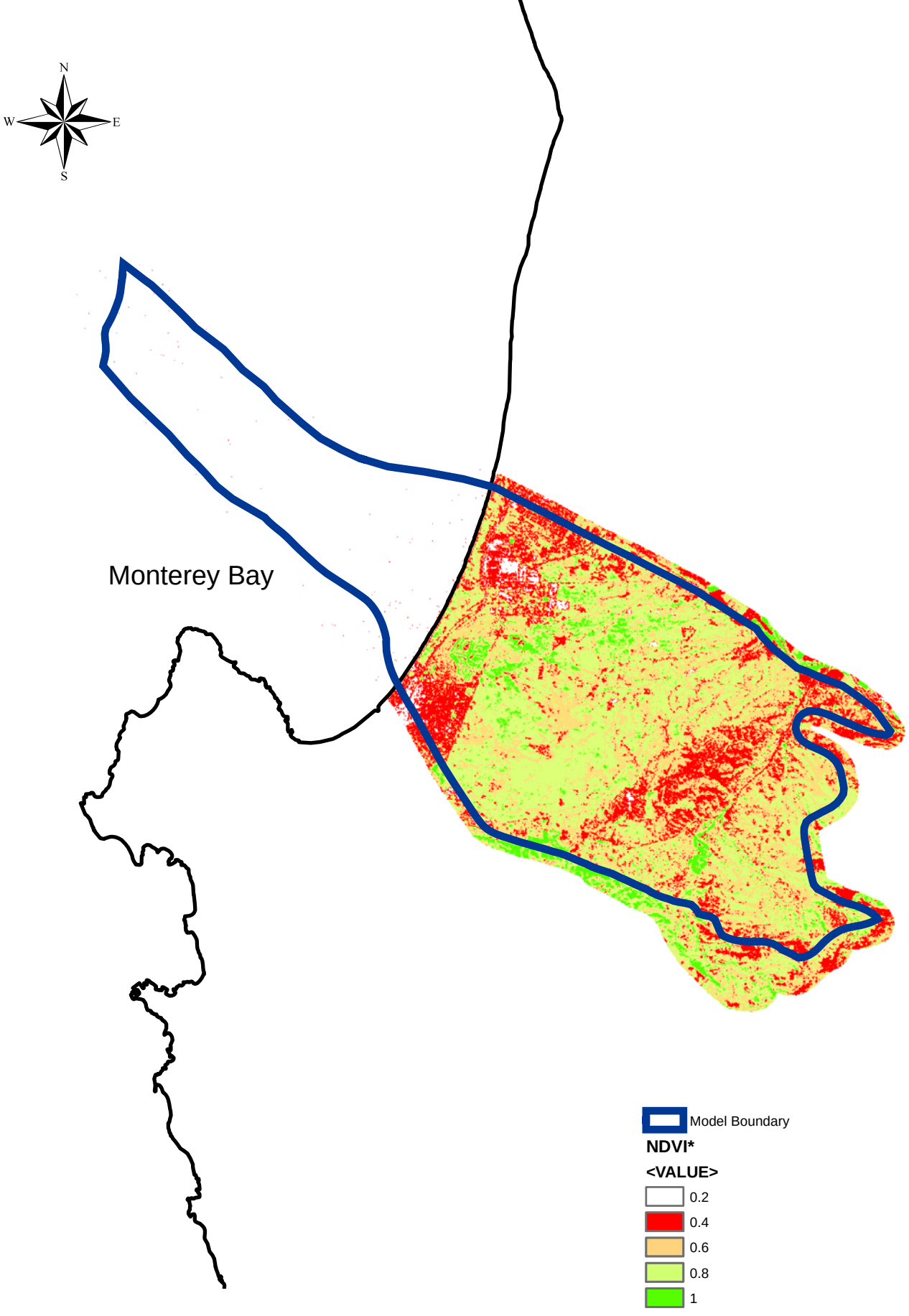

Figure 2.3c Geographic Distribution of NDVI*, June 1993

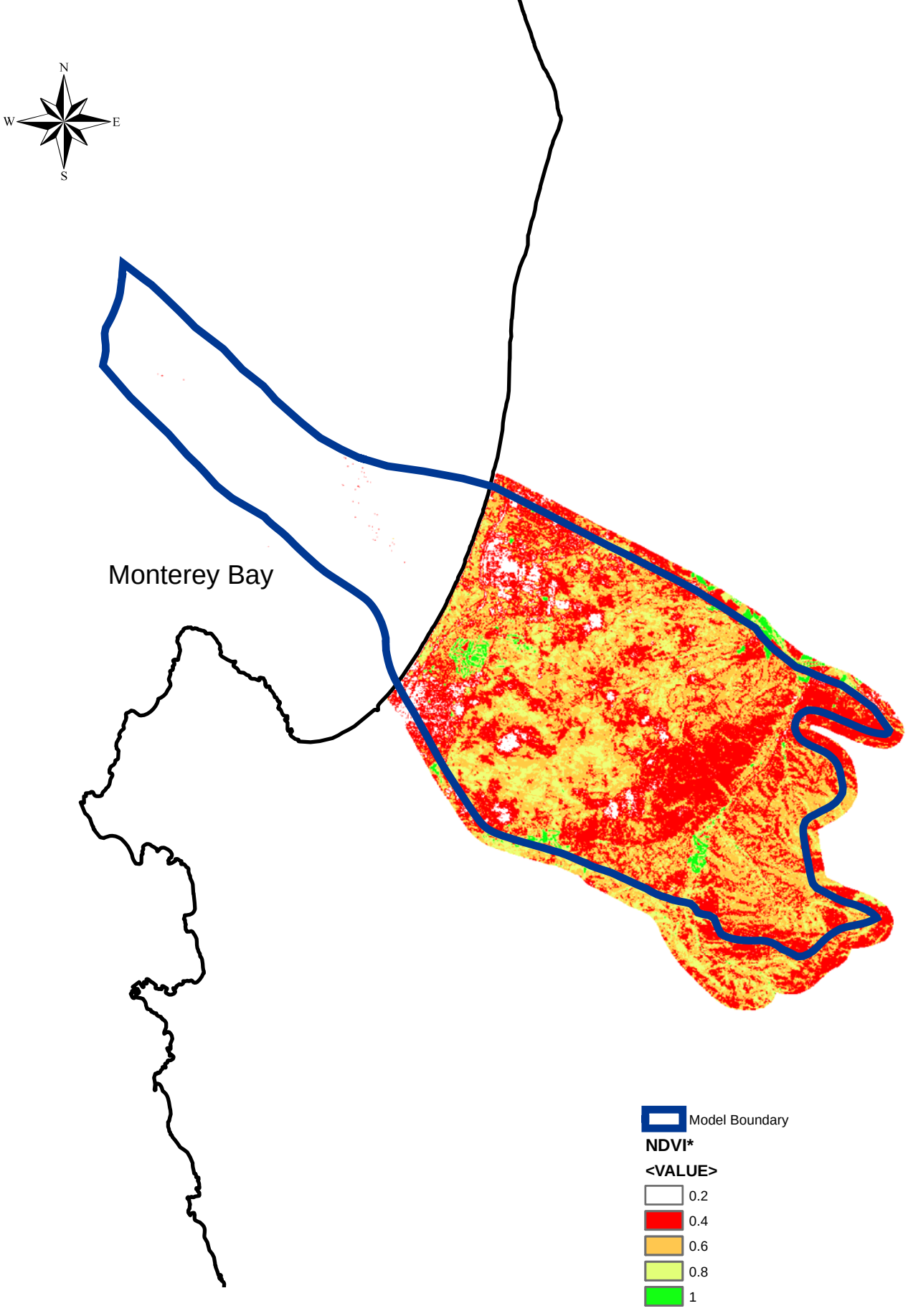

Figure 2.3d Geographic Distribution of NDVI*, August 1993

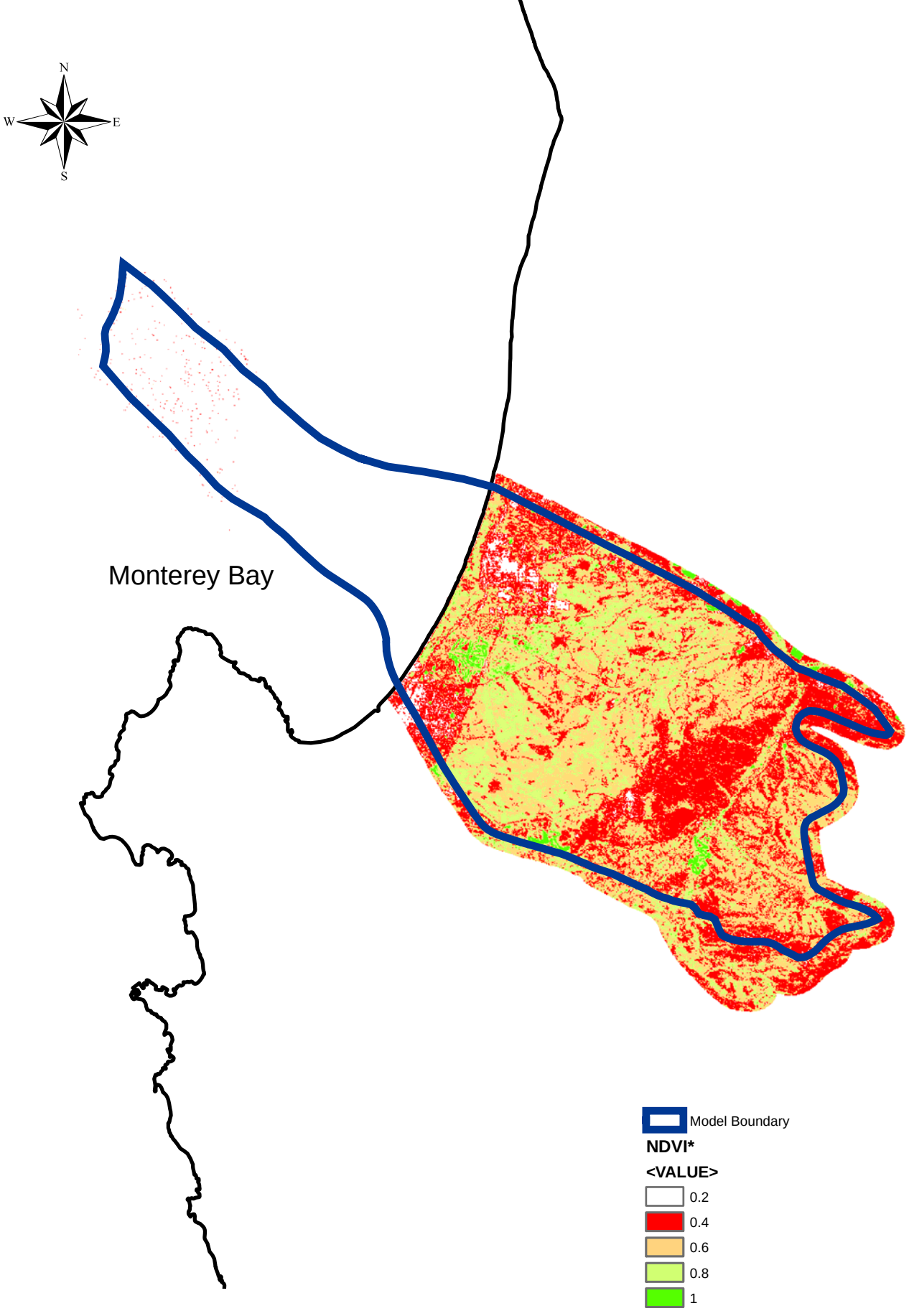

Figure 2.3e Geographic Distribution of NDVI*, October 1993

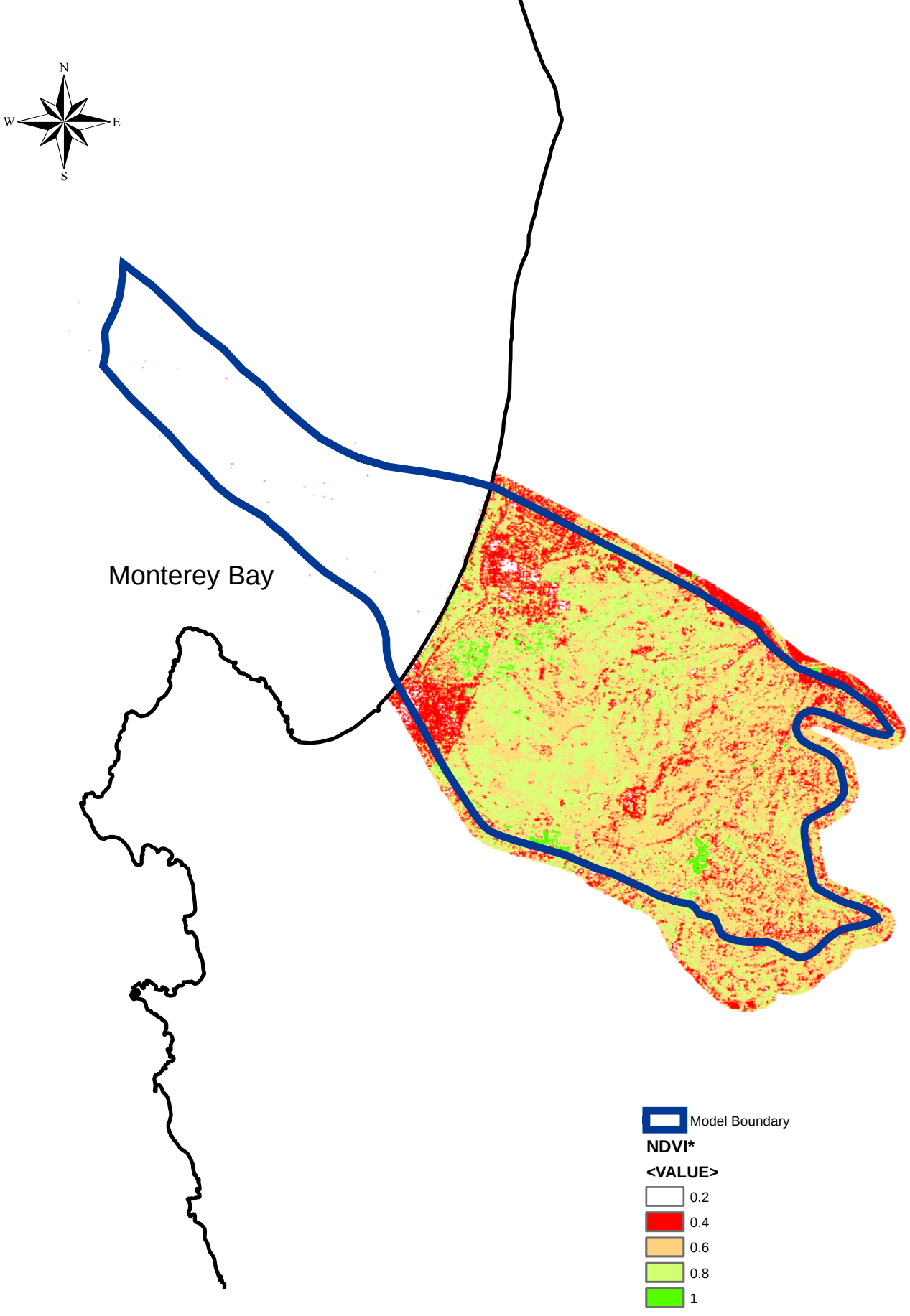

Figure 2.3f Geographic Distribution of NDVI*, December 1993

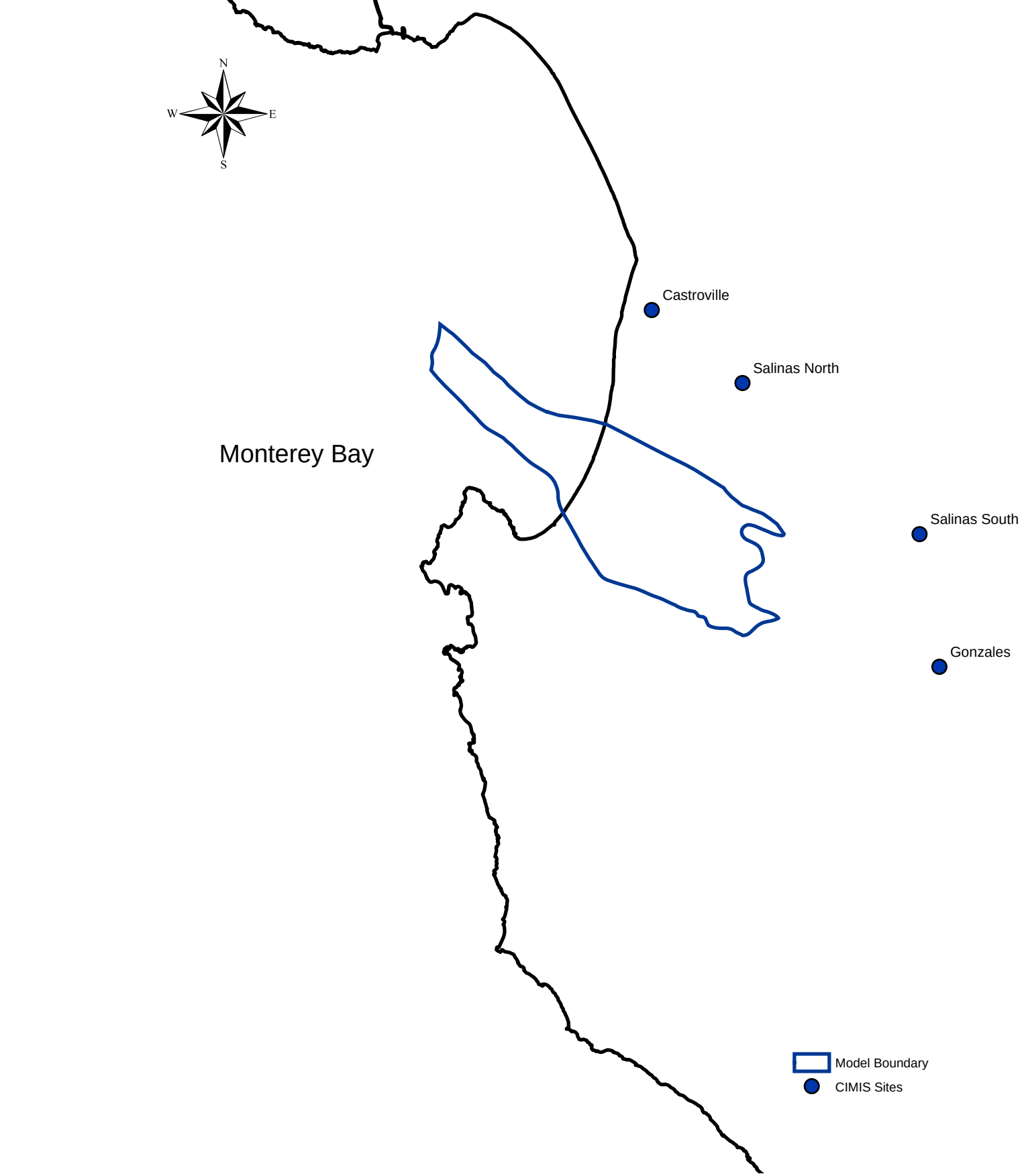

Figure 2.4 Location of CIMIS Sites

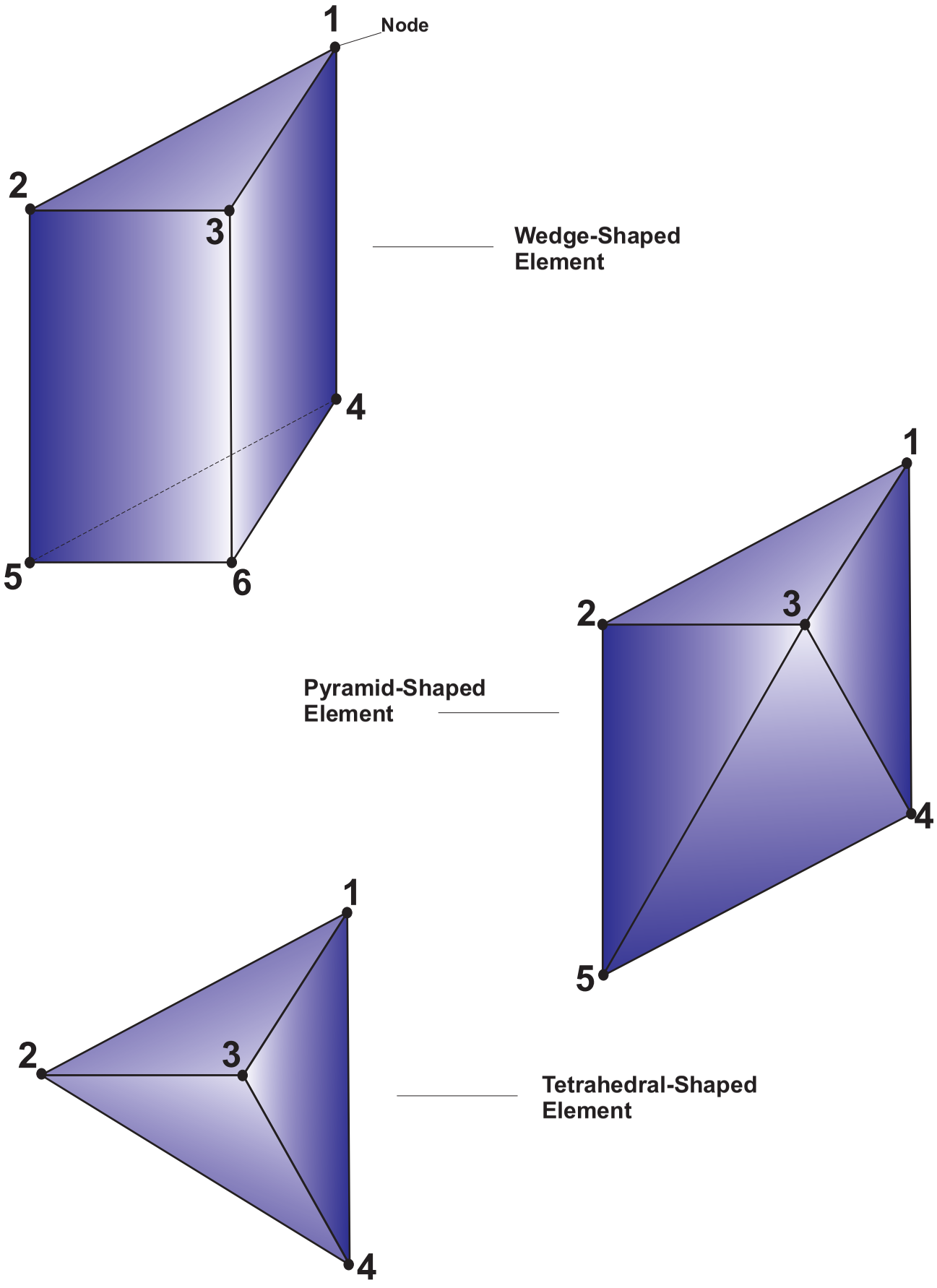

Figure 3.1 Element Types Used to Construct Finite-Element Mesh

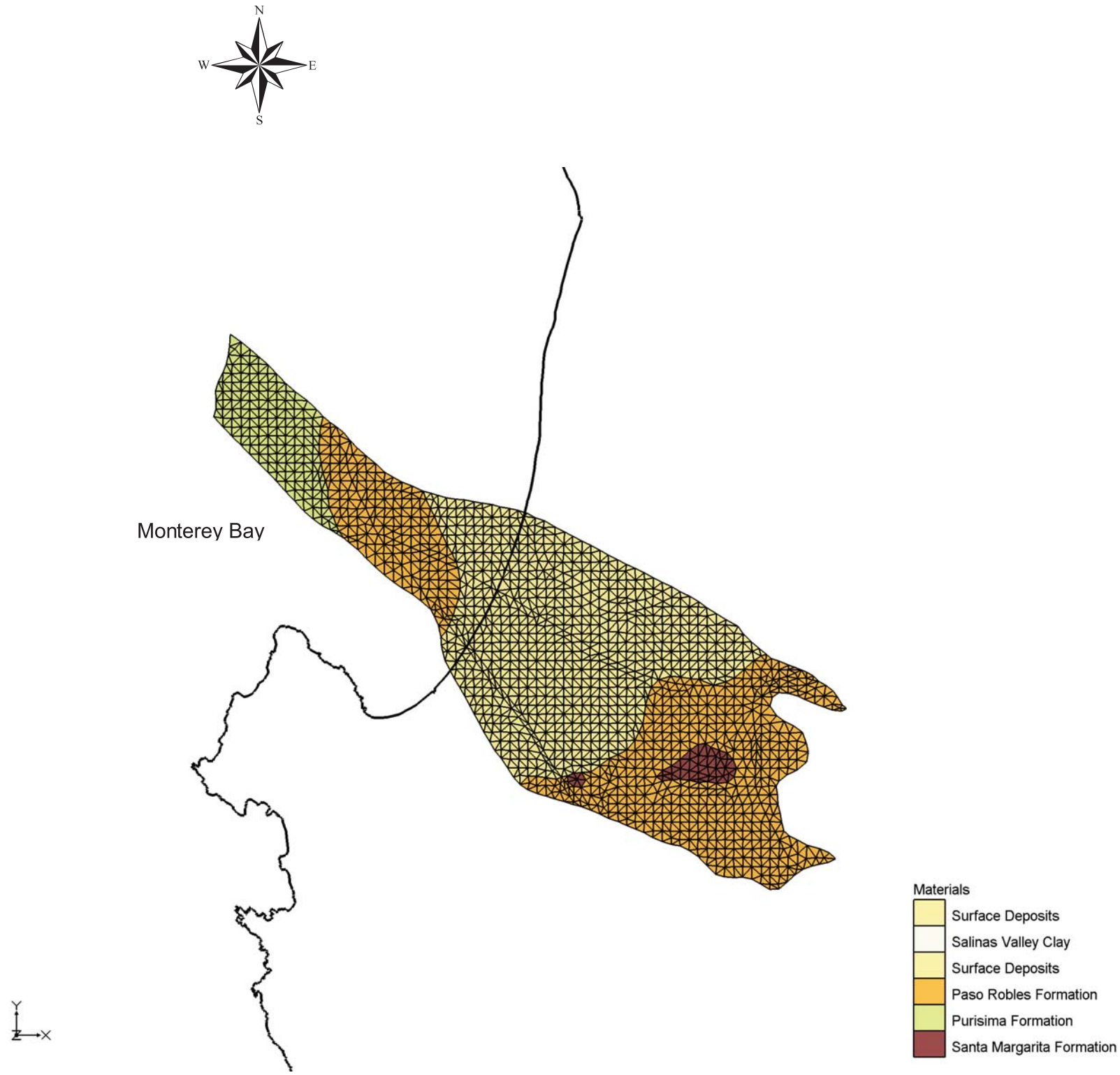

Figure 3.2 Finite-element Mesh

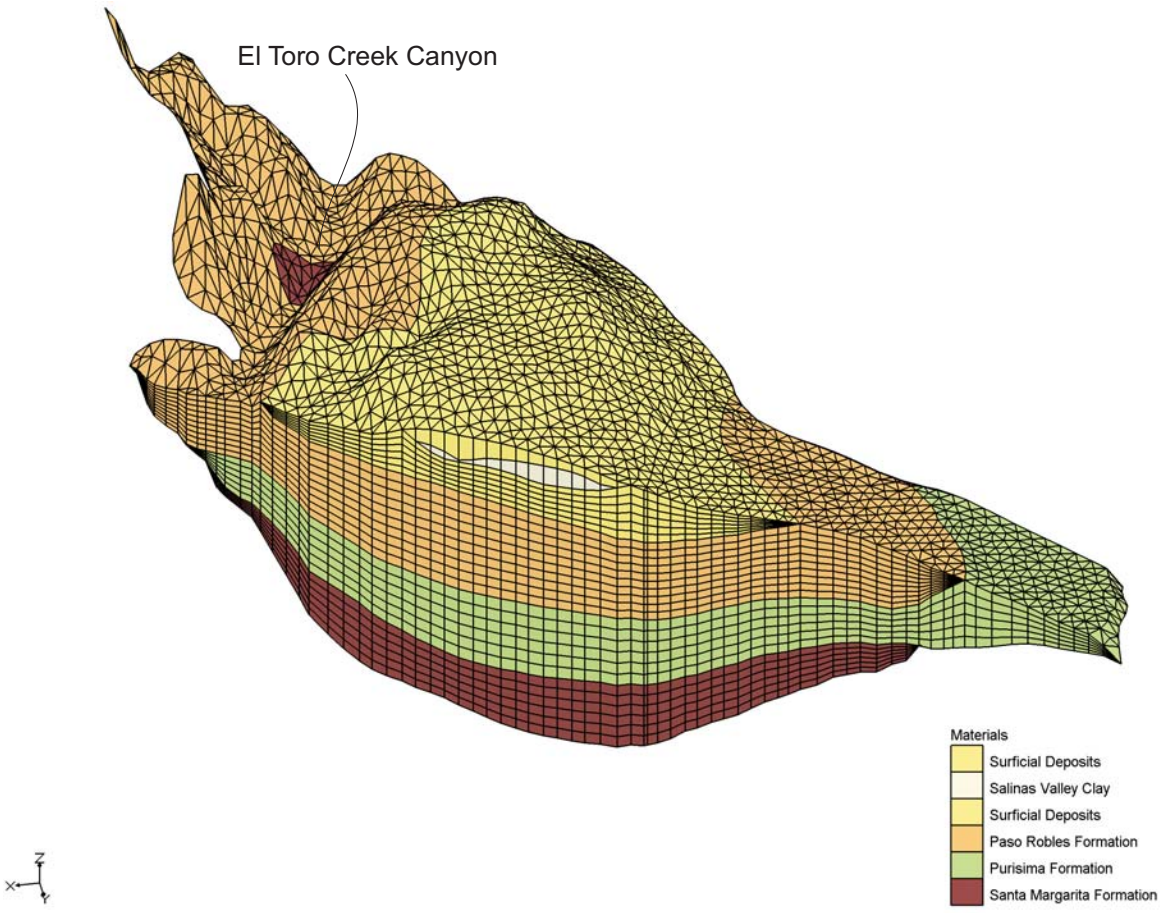

Figure 3.3 Oblique View of Finite-Element Mesh

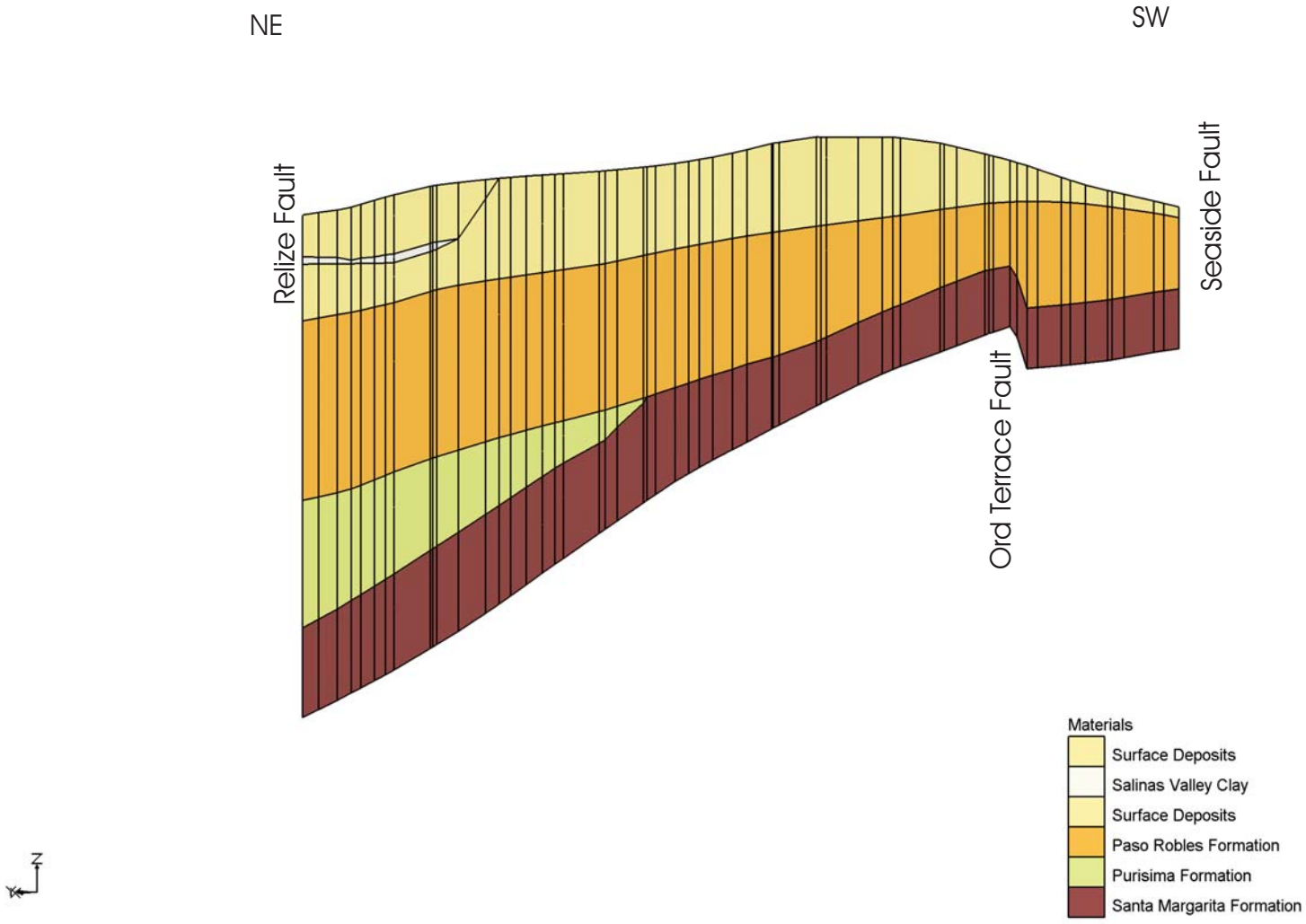

Figure 3.4a South-North Cross-Section of Finite-Element Mesh

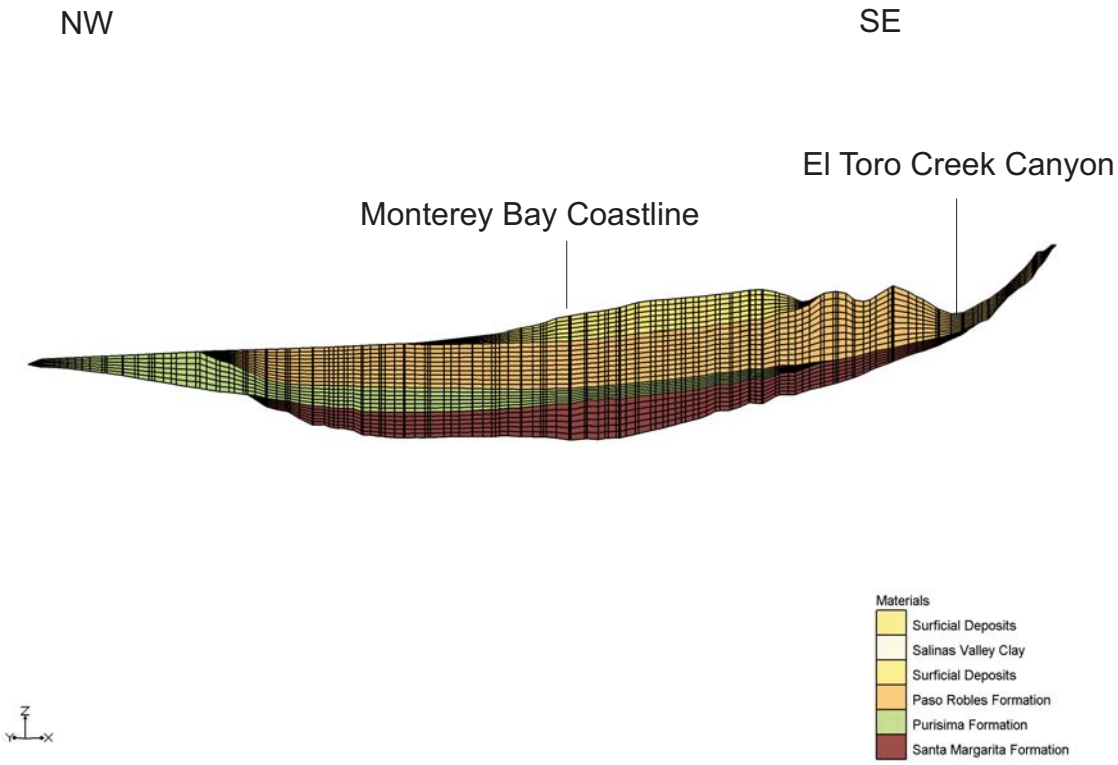

Figure 3.4b Northwest-Southeast Cross-Section of Finite-Element Mesh

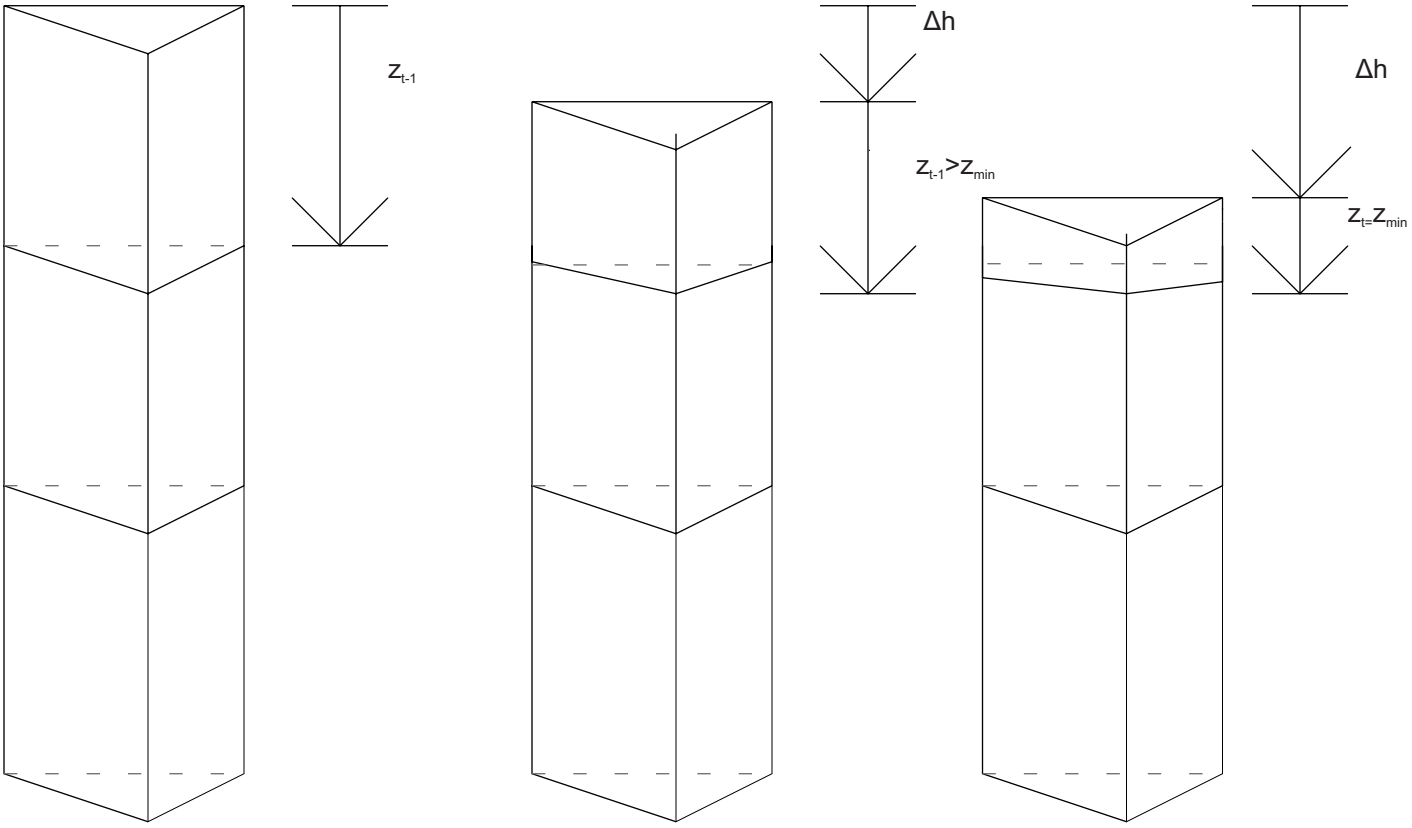

Figure 3.5 Contraction of Element Column

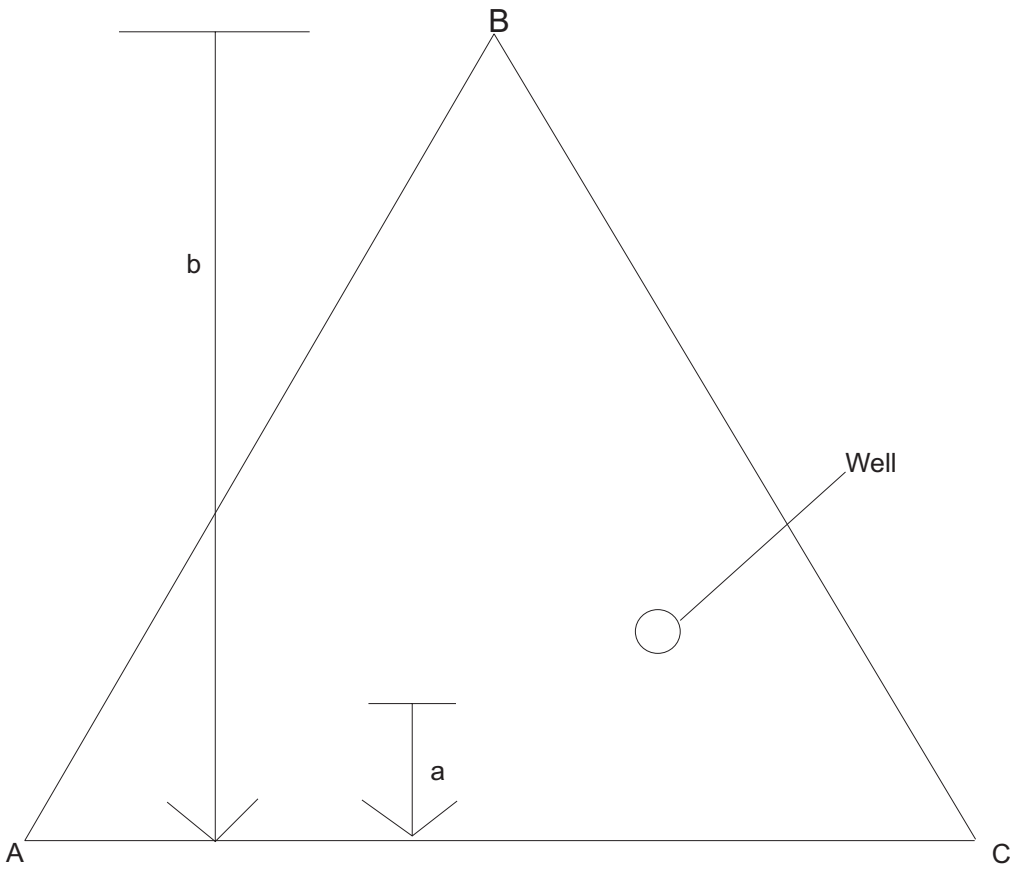

Figure 3.6 Horizontal Weighting of Pumping From a Well to a Node

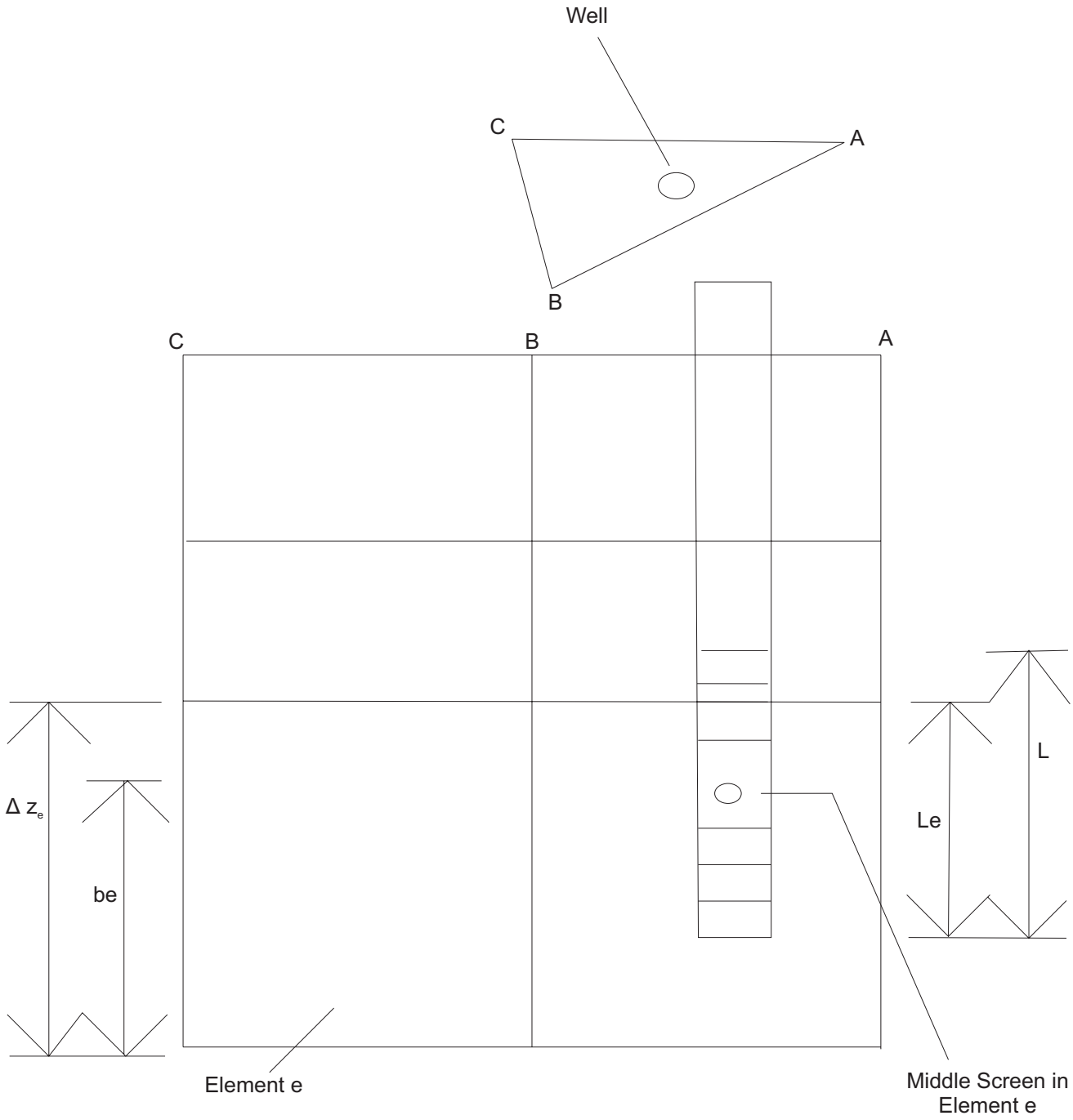

Figure 3.7 Vertical Weighting of Pumping From a Well to a Node

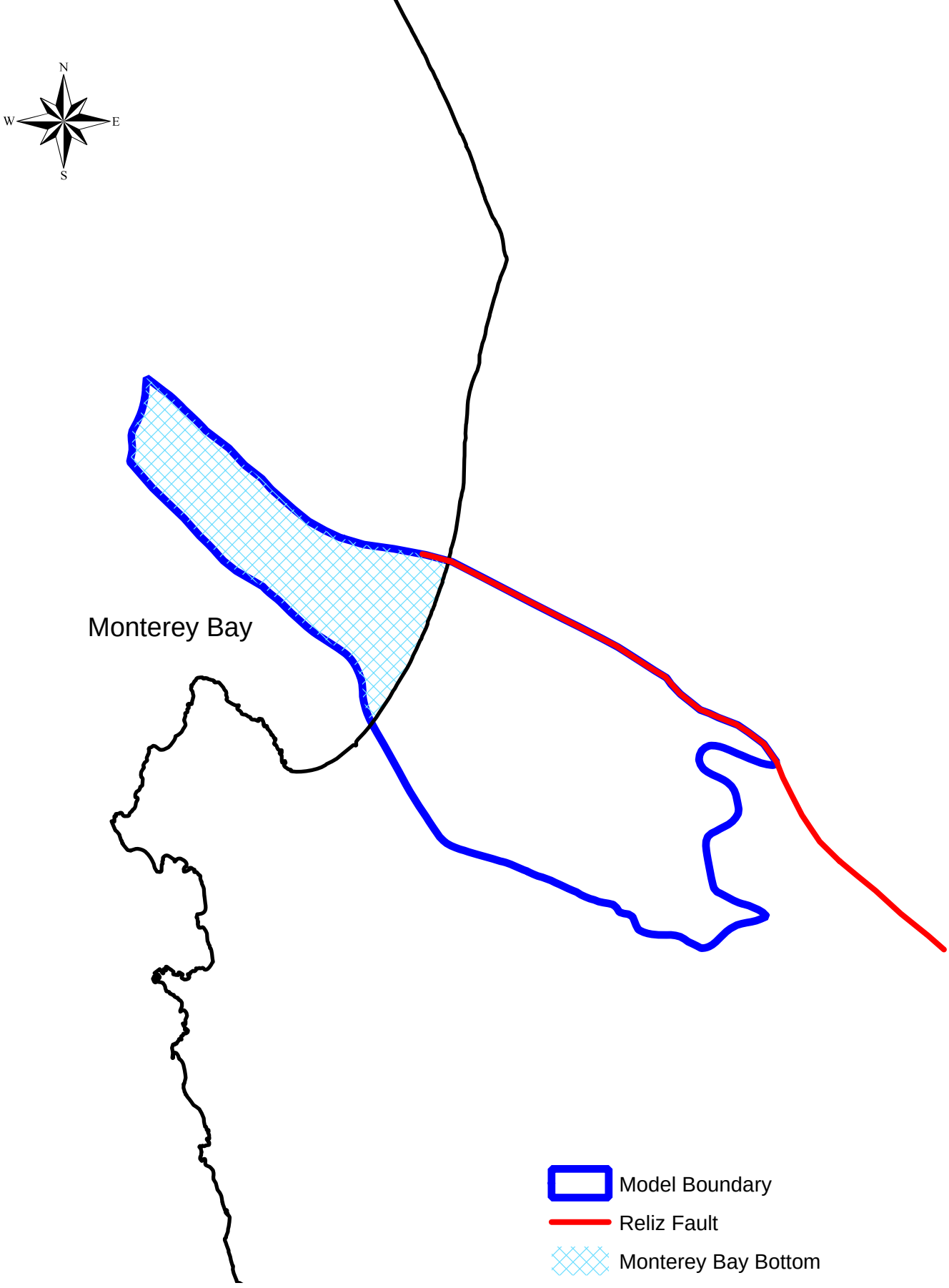

Figure 3.8 Location of Specified-Head Boundaries

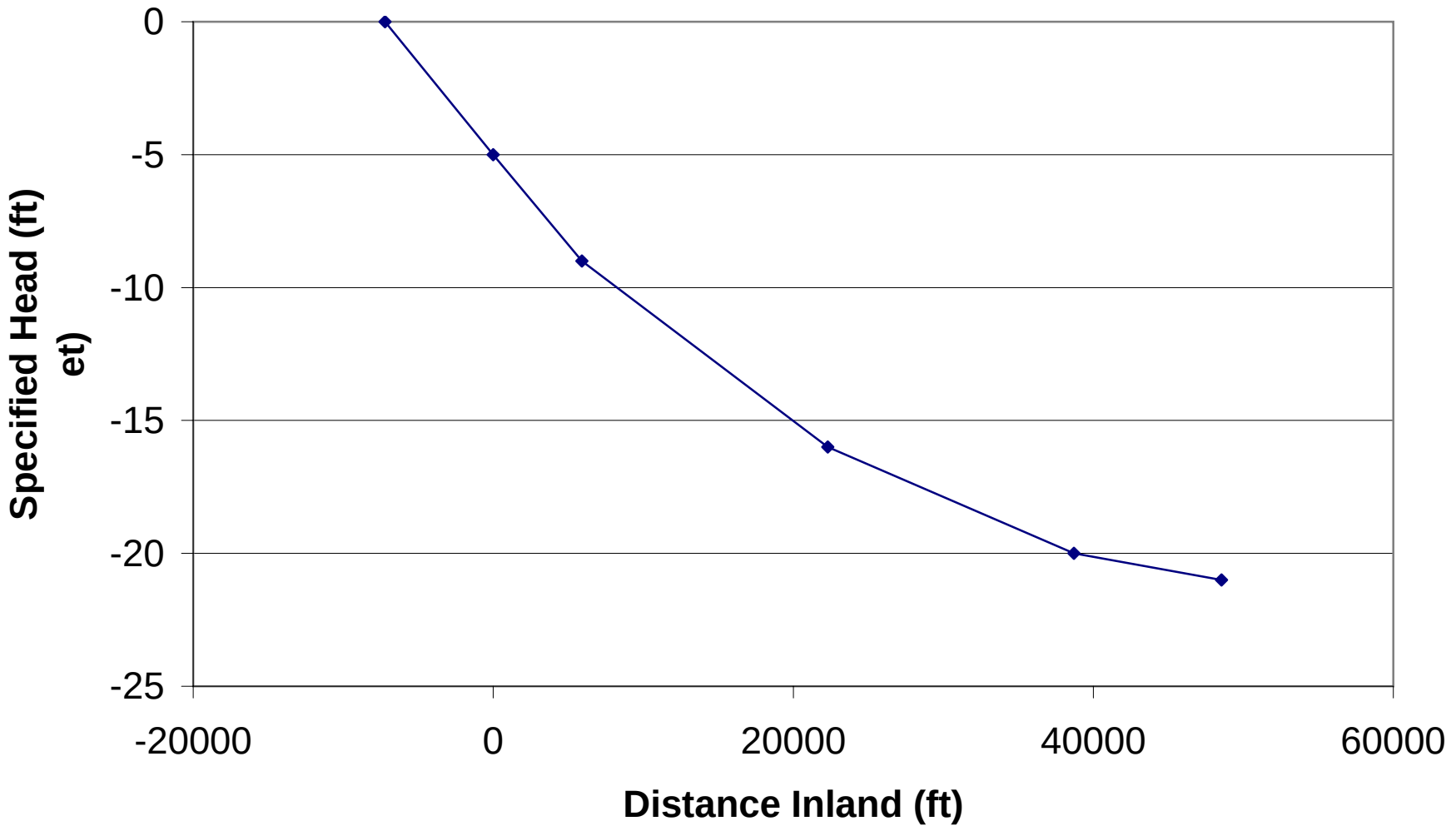

Figure 3.9 Specified Heads Along Reliz Fault

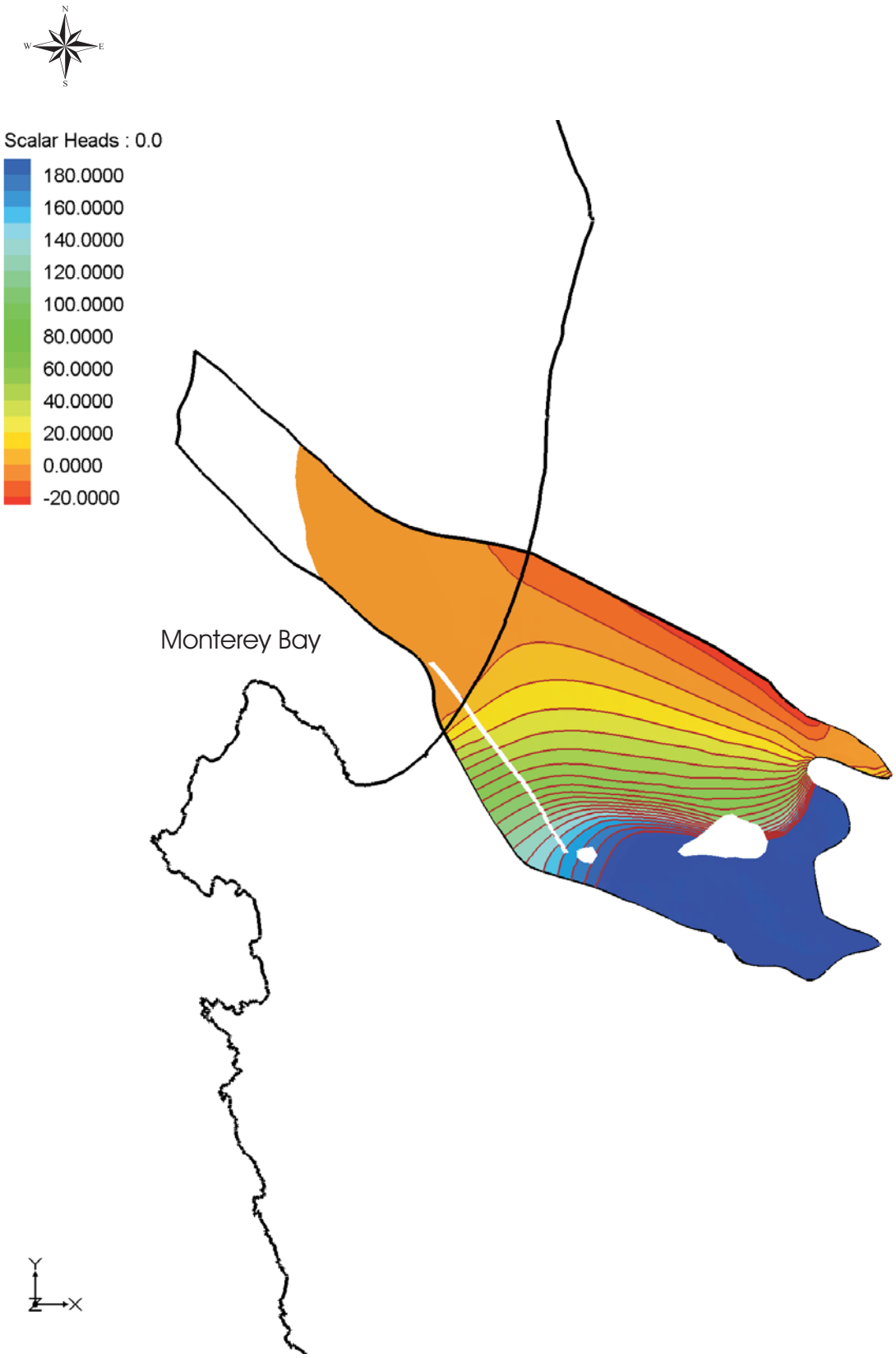

Figure 3.10a Initial Heads Assigned to Model, Paso Robles Formation

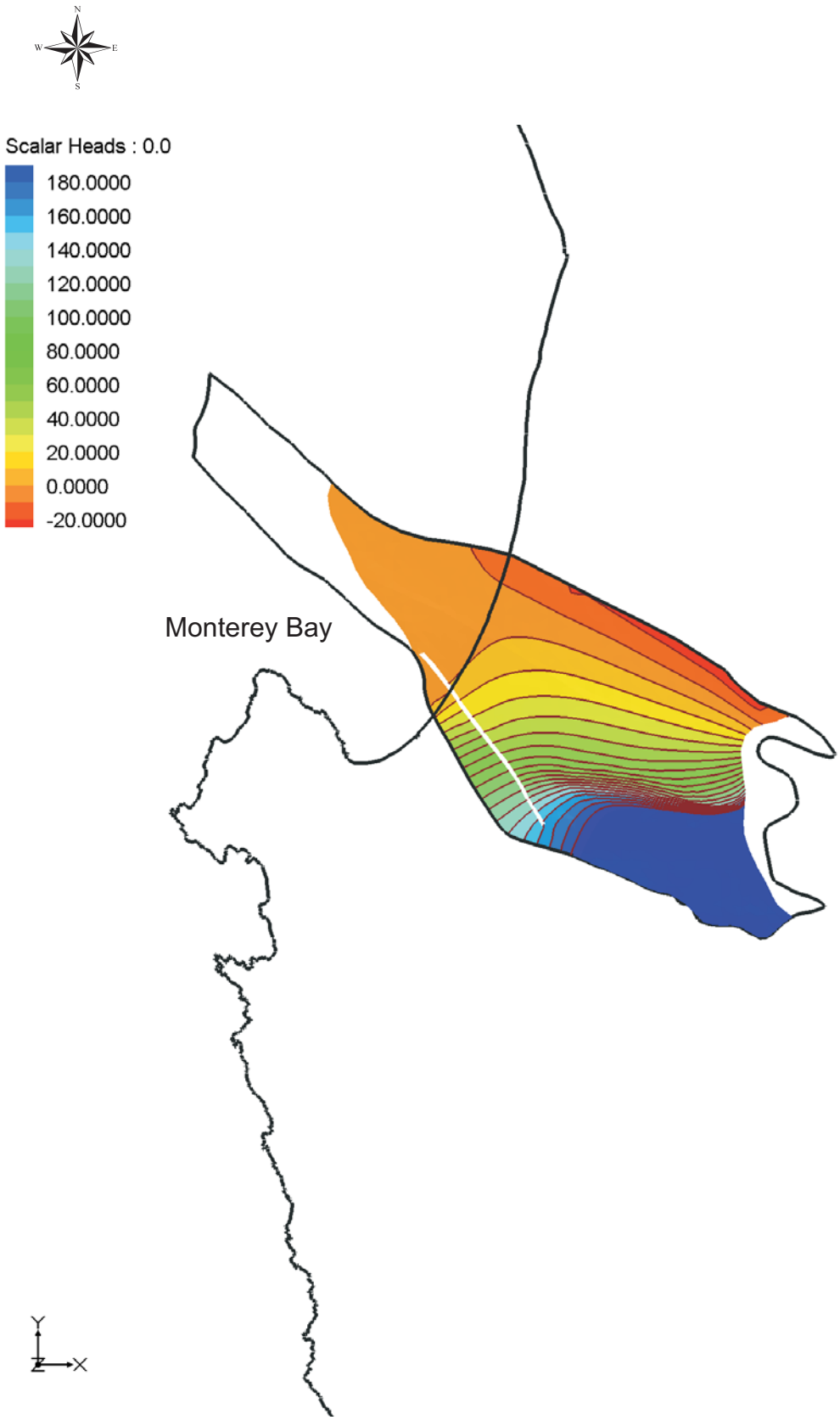

Figure 3.10b Initial Heads Assigned to Model, Santa Margarita Formation

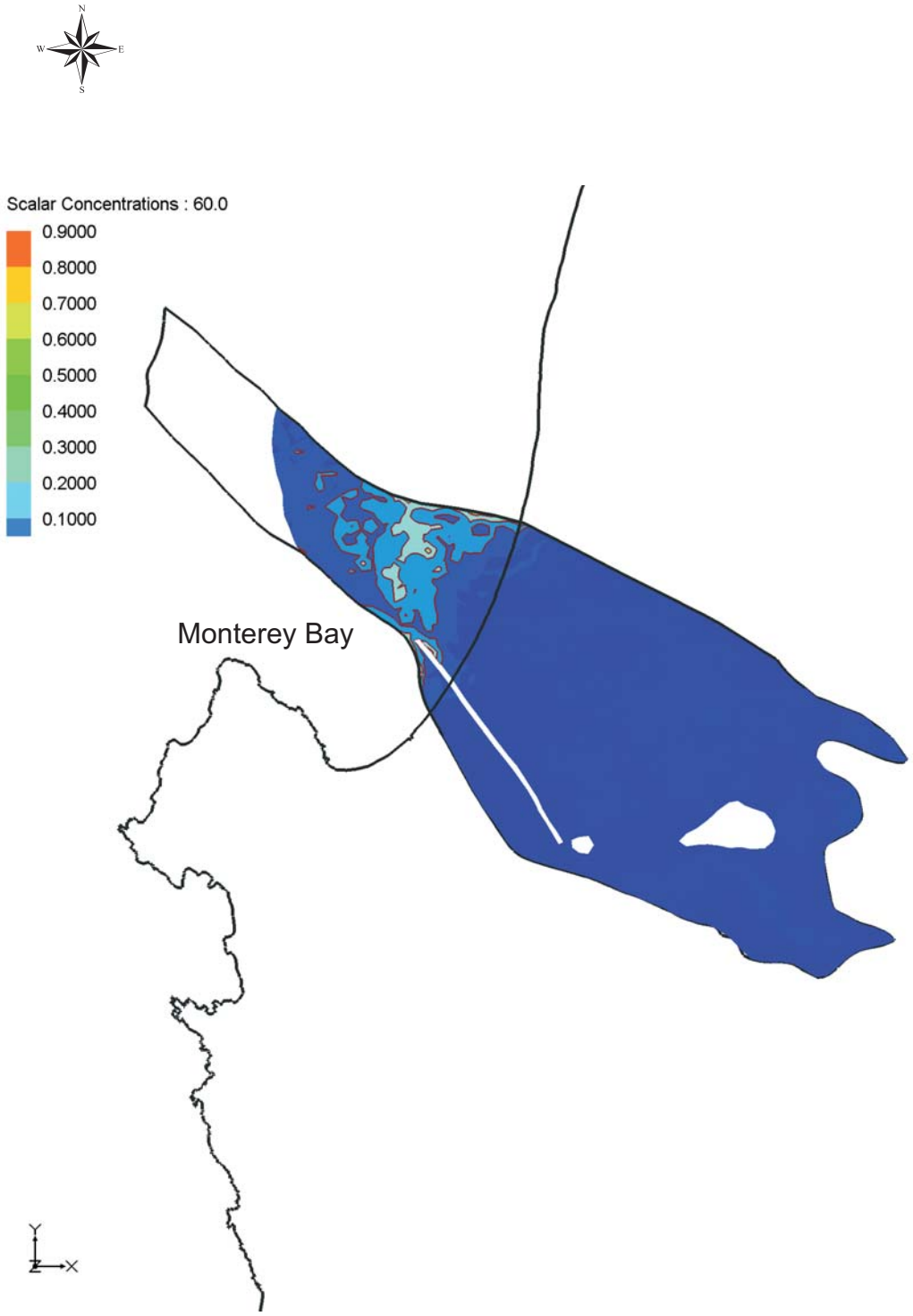

Figure 3.11a Initial Salinity Assigned to Model, Paso Robles Formation

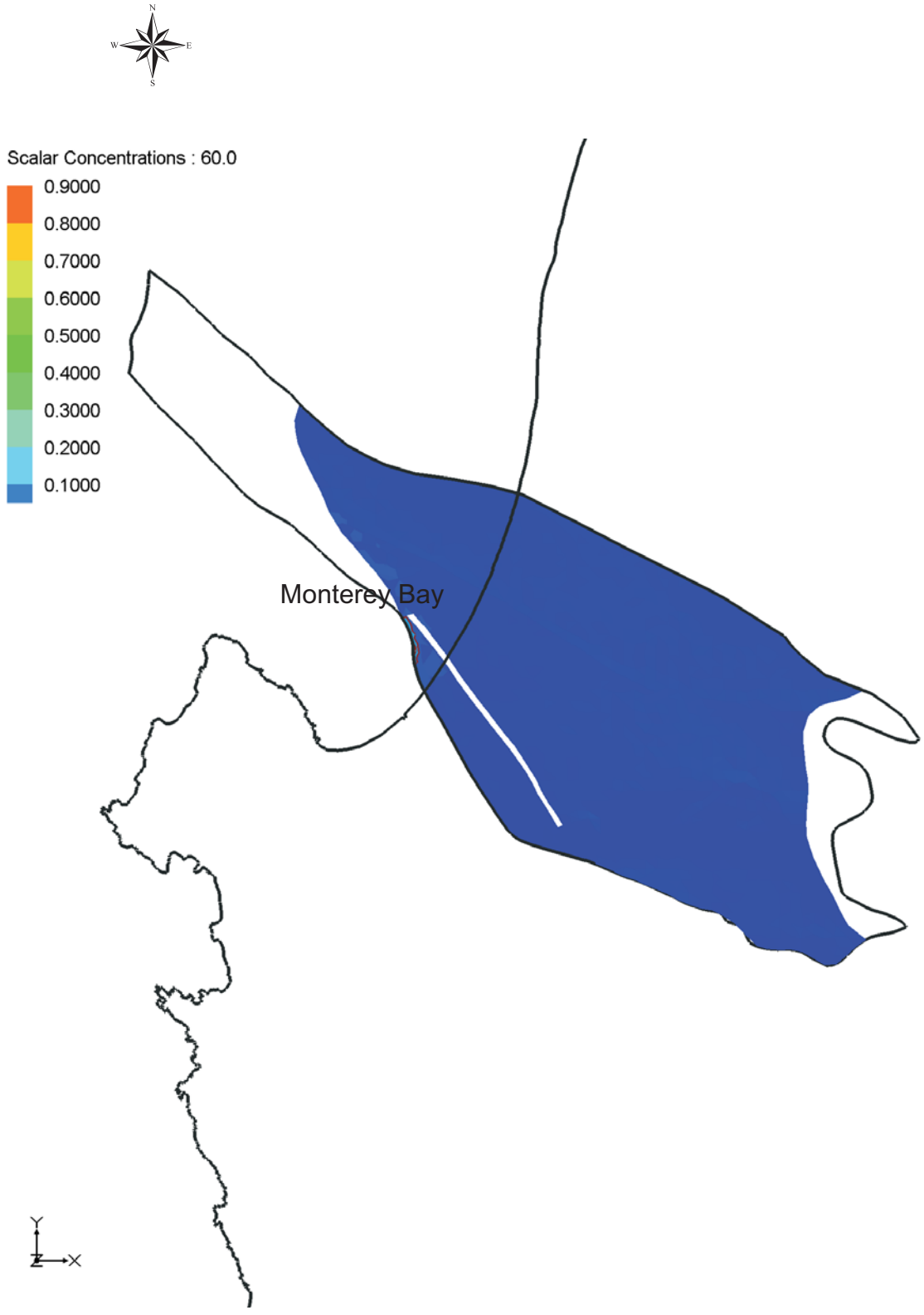

Figure 3.11b Initial Salinity Assigned to Model, Santa Margarita Formation

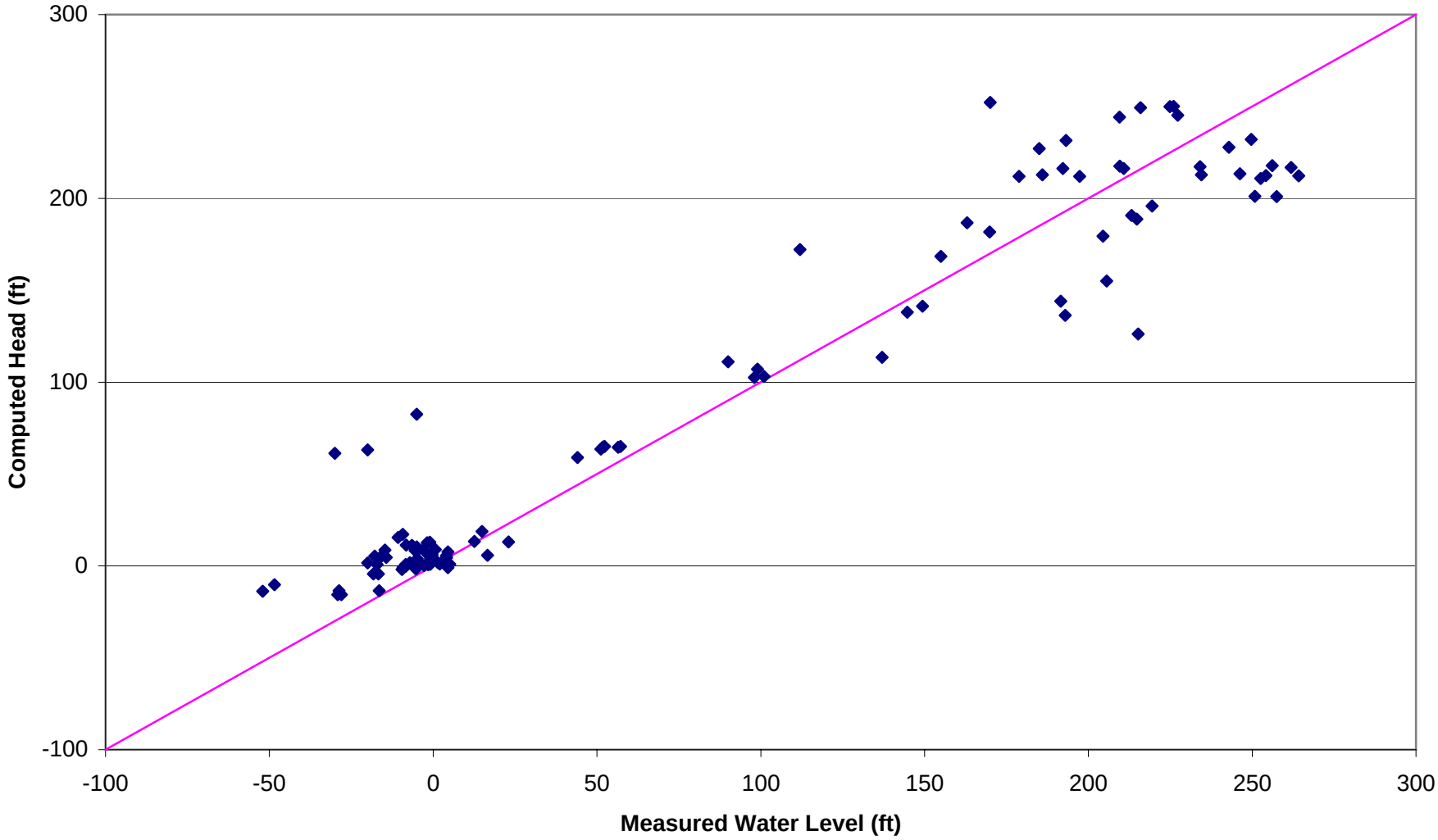

Figure 3-12a Comparison of Computed Heads and Measured Groundwater Levels, Unweighted Residuals

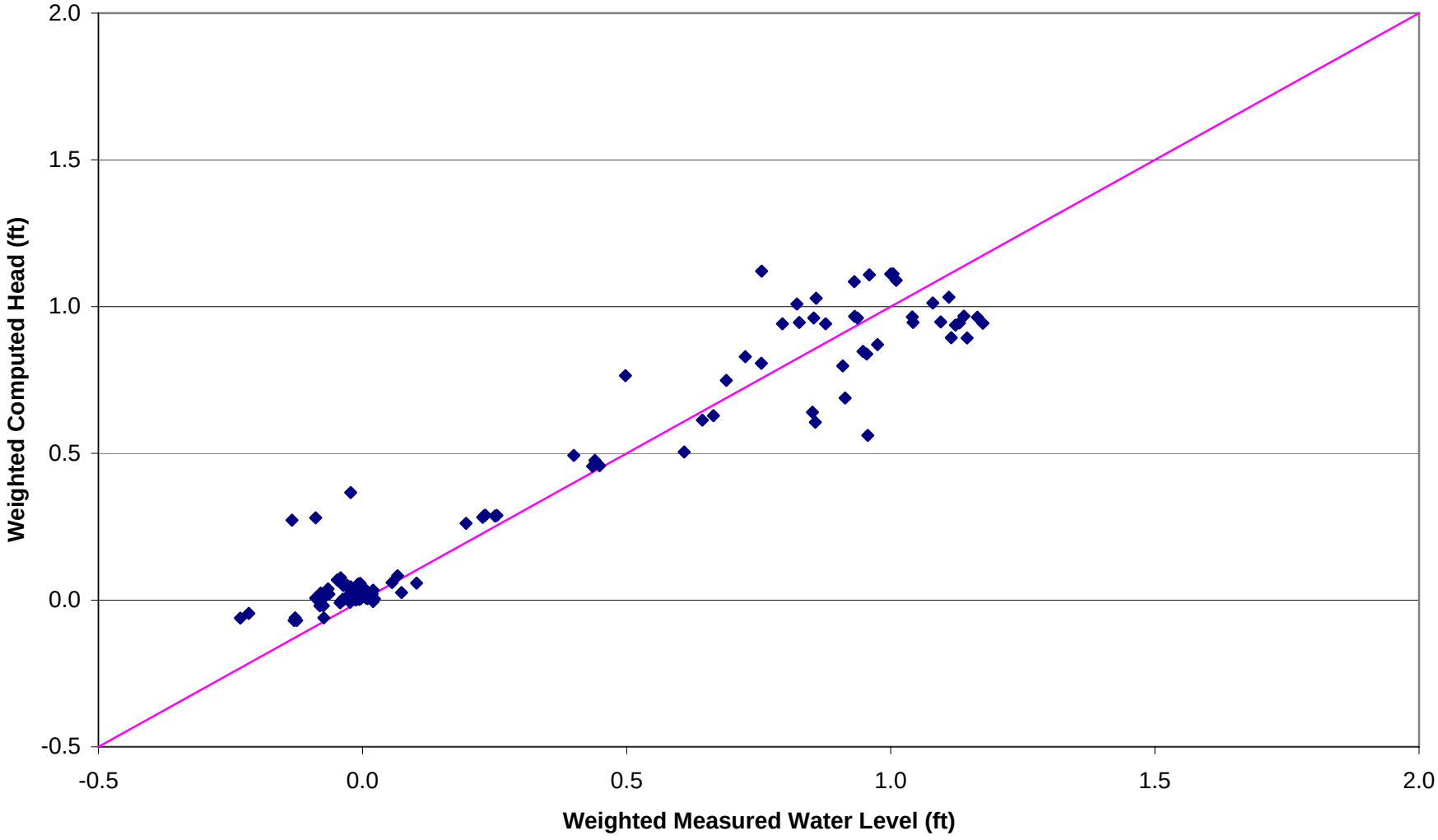

Figure 3-12b Comparison of Computed Heads and Measured Groundwater Levels, Weighted Residuals

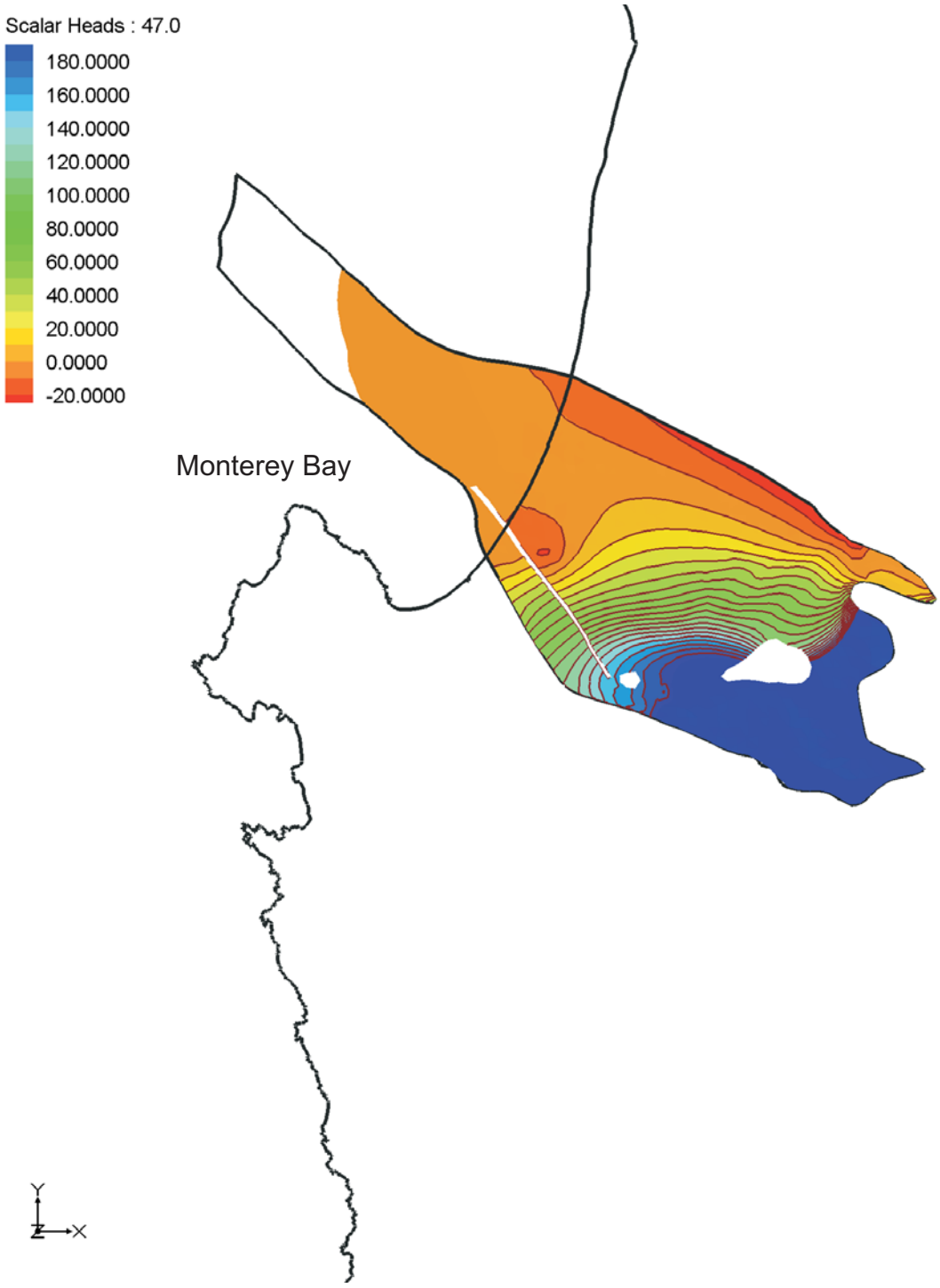

Figure 3.13a Computed Heads for 2002, Paso Robles Formation

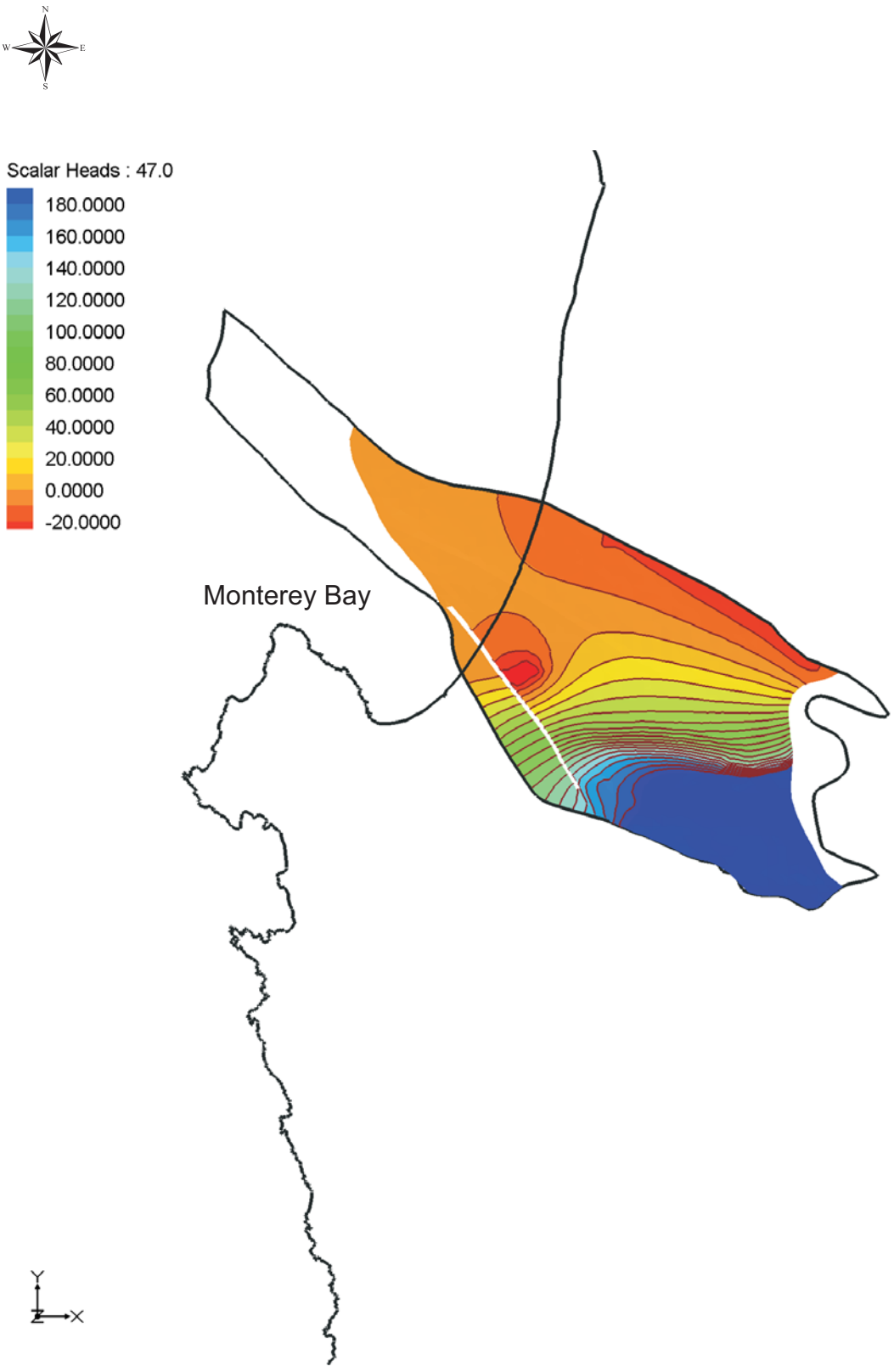

Figure 3.13b Computed Heads for 2002,Santa Margarita Formation

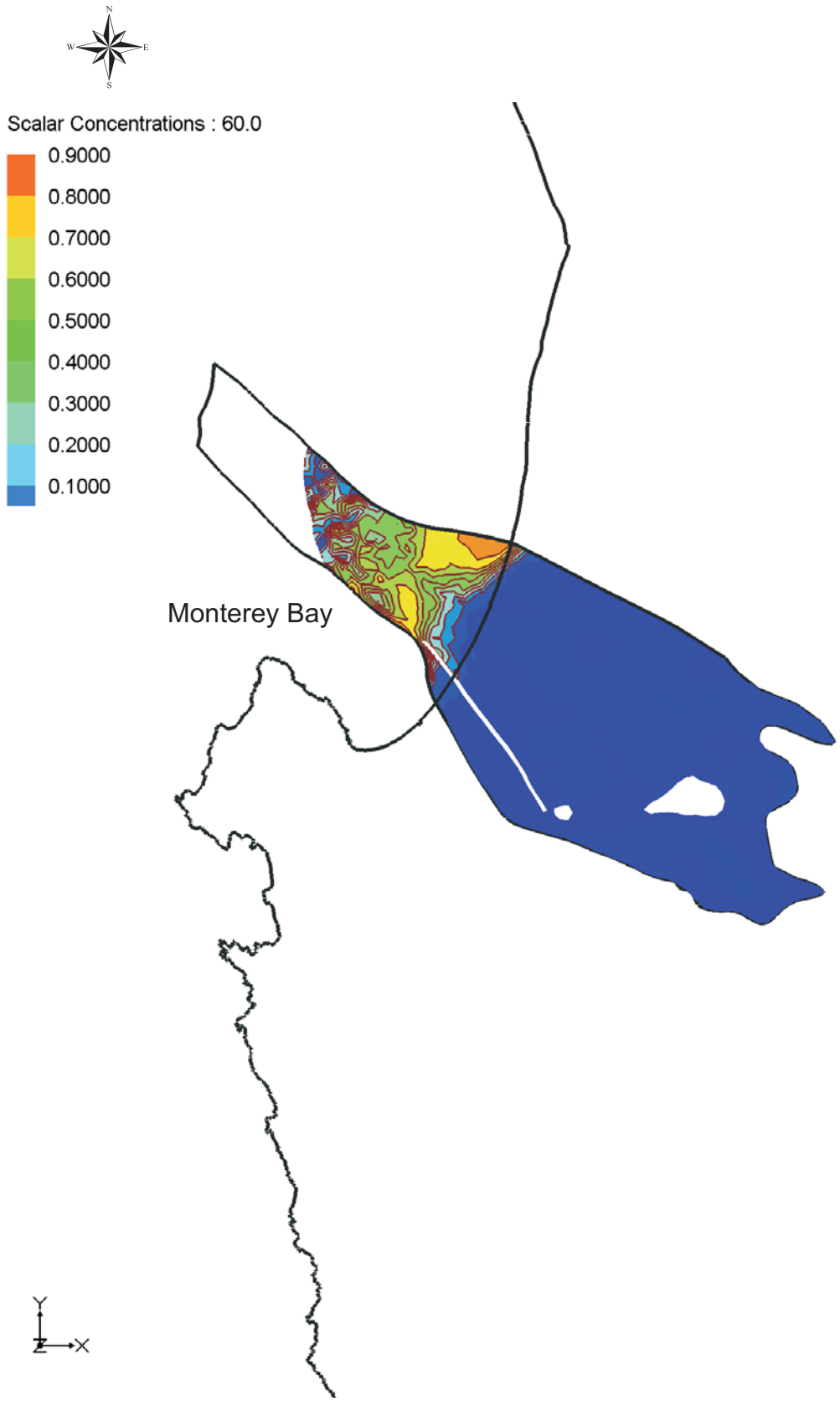

Figure 3.14a Computed Salinity for 2002, Paso Robles Formation

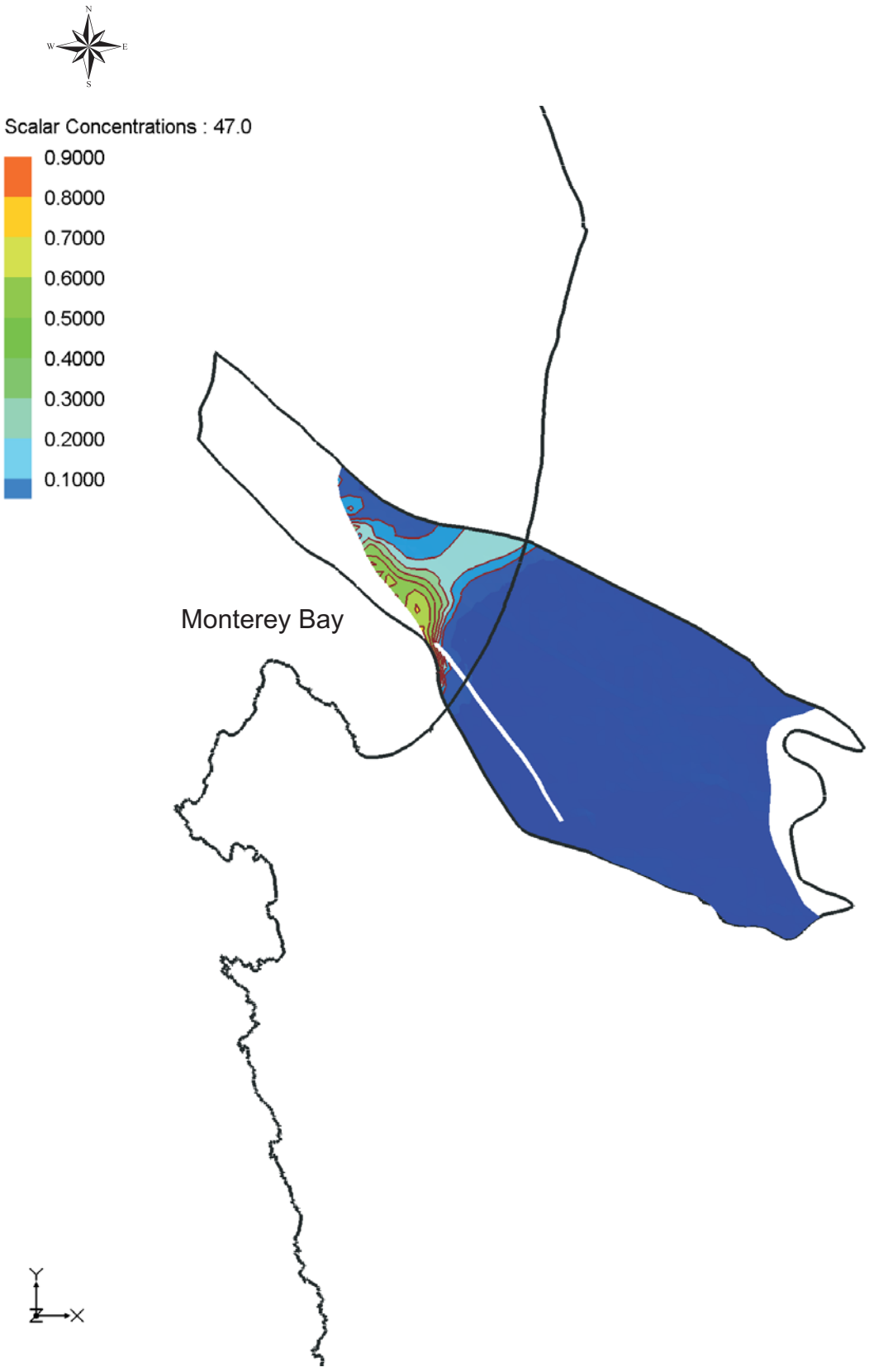

Figure 3.14b Computed Salinity for 2002,Santa Margarita Formation

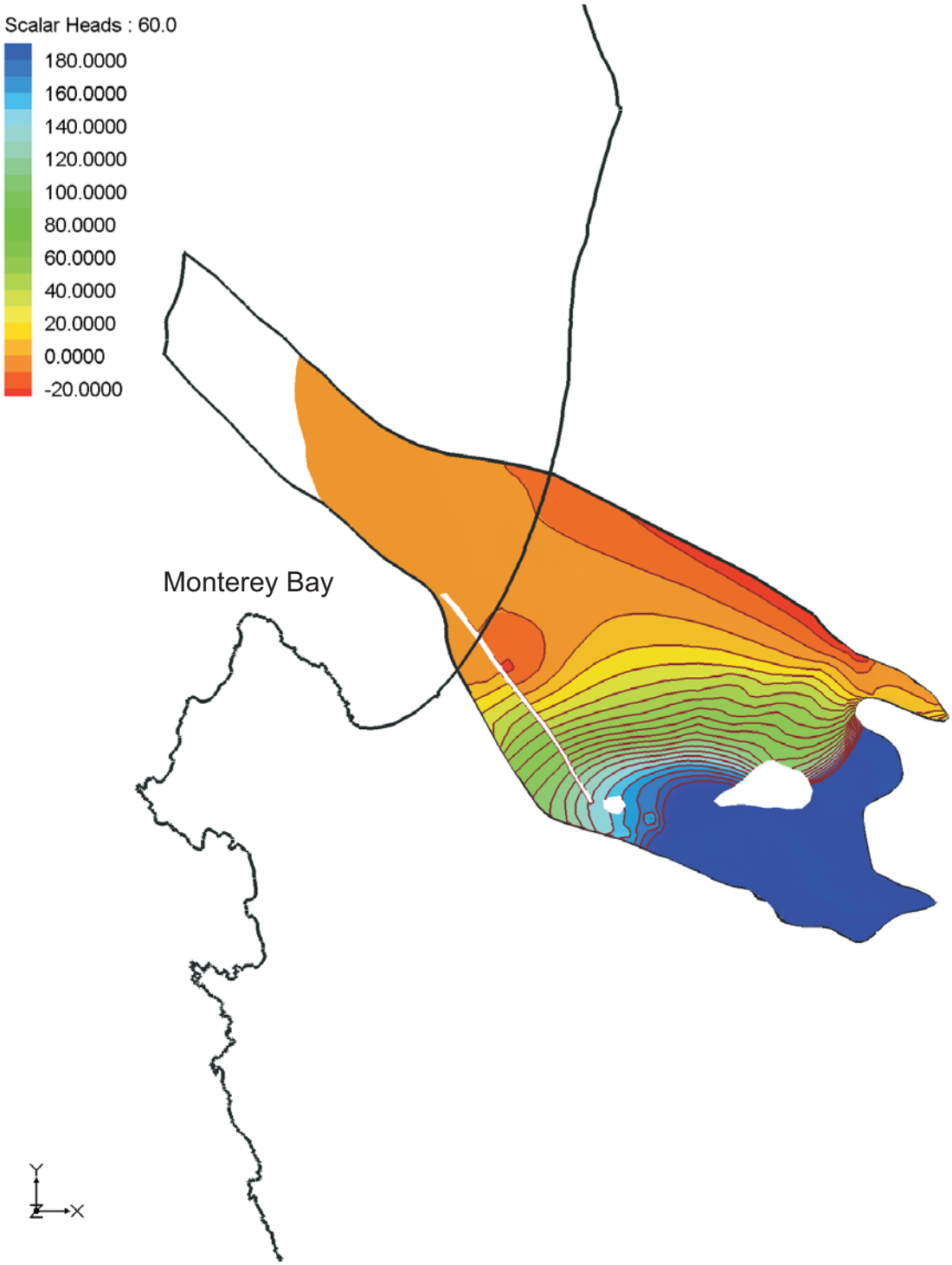

Figure 4.1a Computed Heads for 2015
with Continued Pumping, Paso Robles Formation

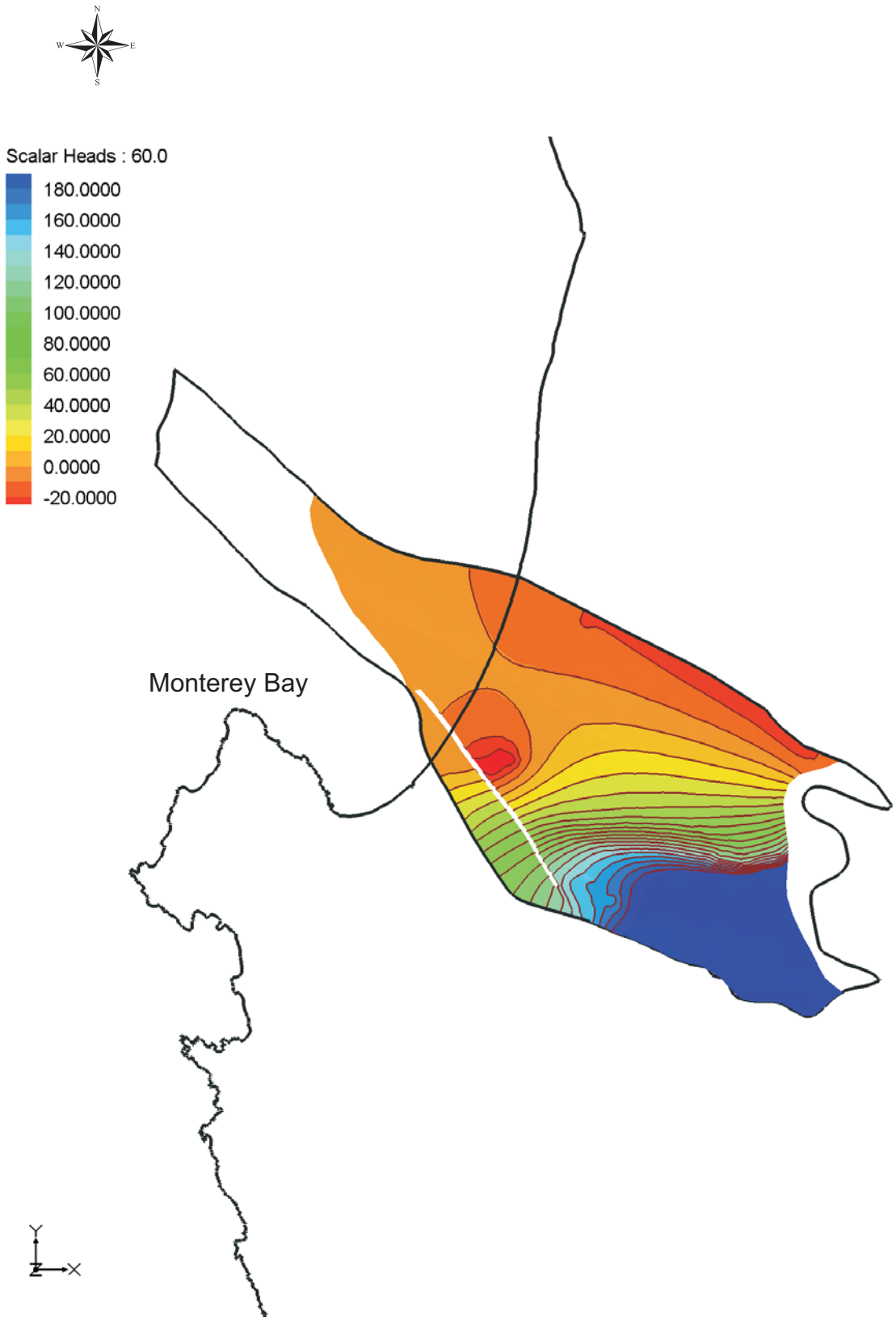

Figure 4.1b Computed Heads for 2015
with Continued Pumping, Santa Margarita Formation

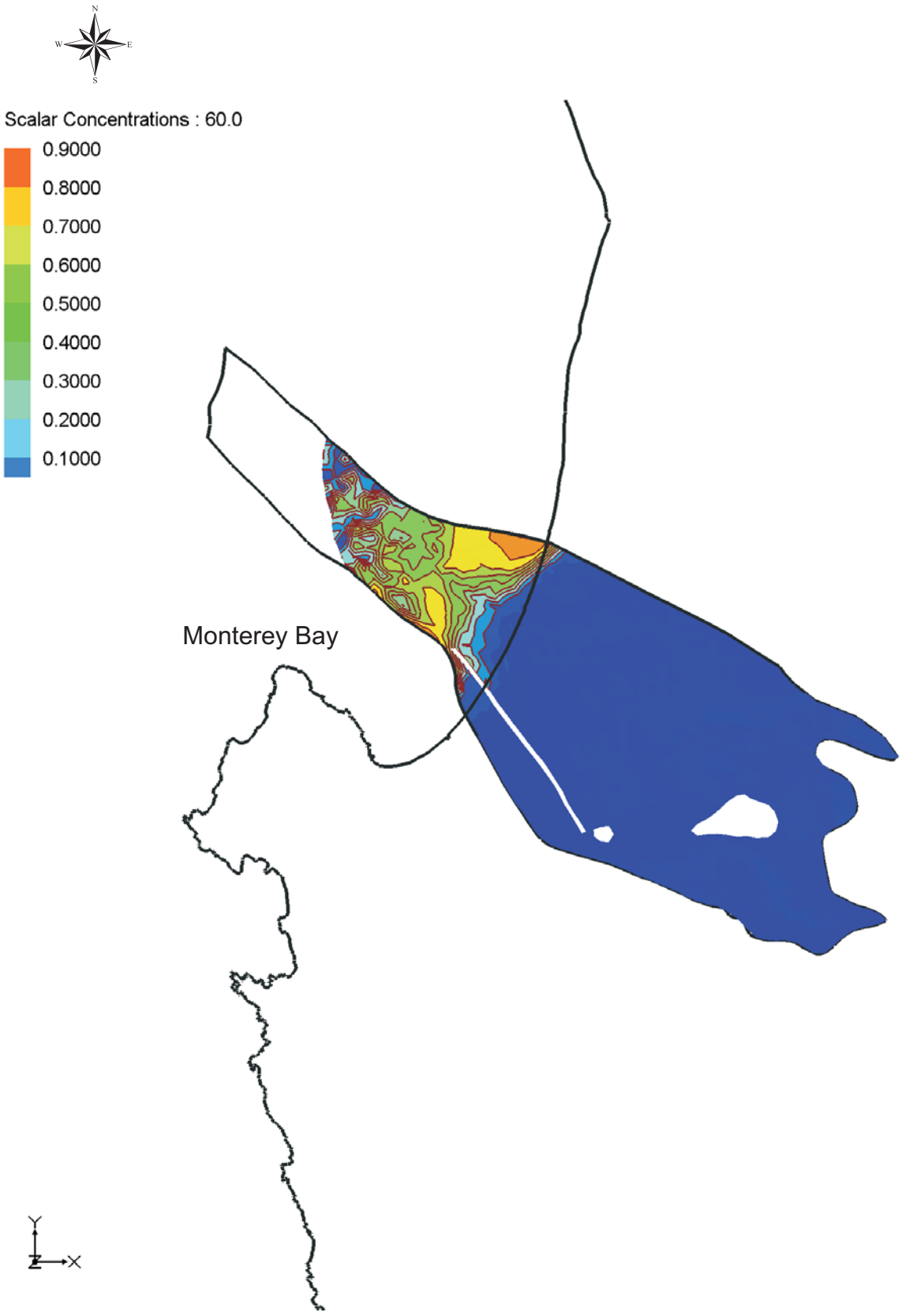

Figure 4.2a Computed Salinity for 2015
with Continued Pumping, Paso Robles Formation

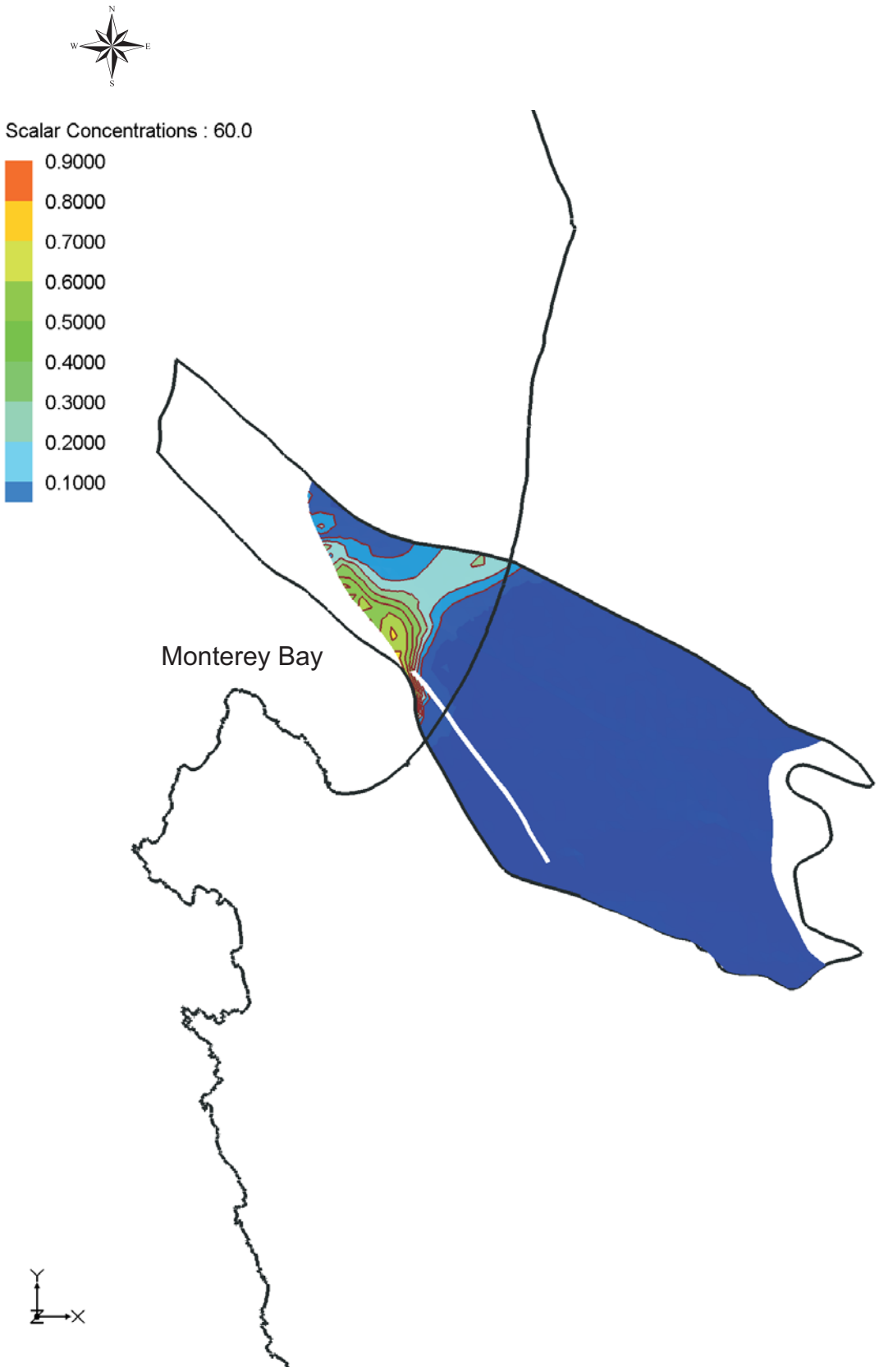

Figure 4.2b Computed Salinity for 2015
with Continued Pumping, Santa Margarita Formation

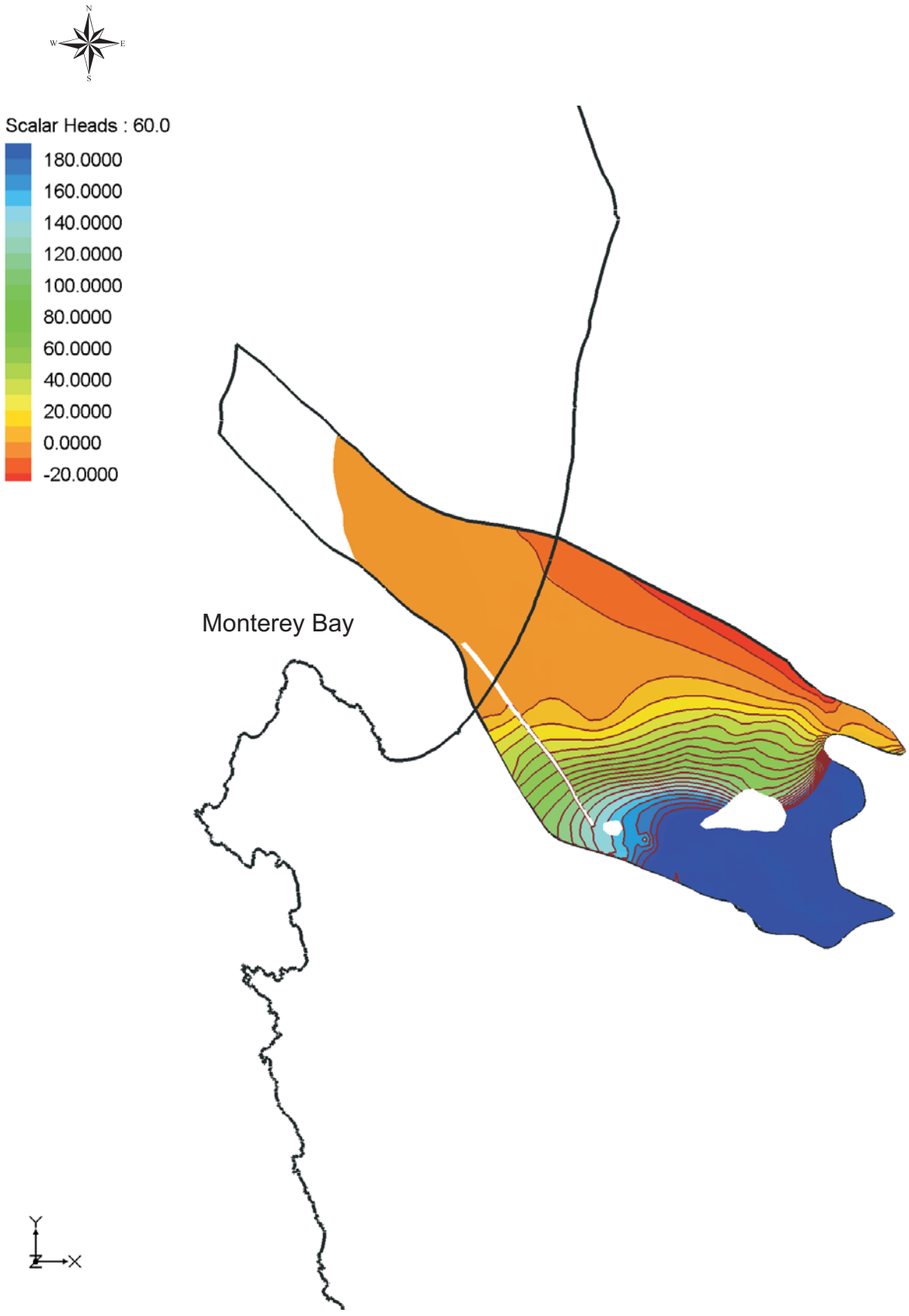

Figure 4.3a Computed Heads for 2015
with Relocated Pumping, Paso Robles Formation

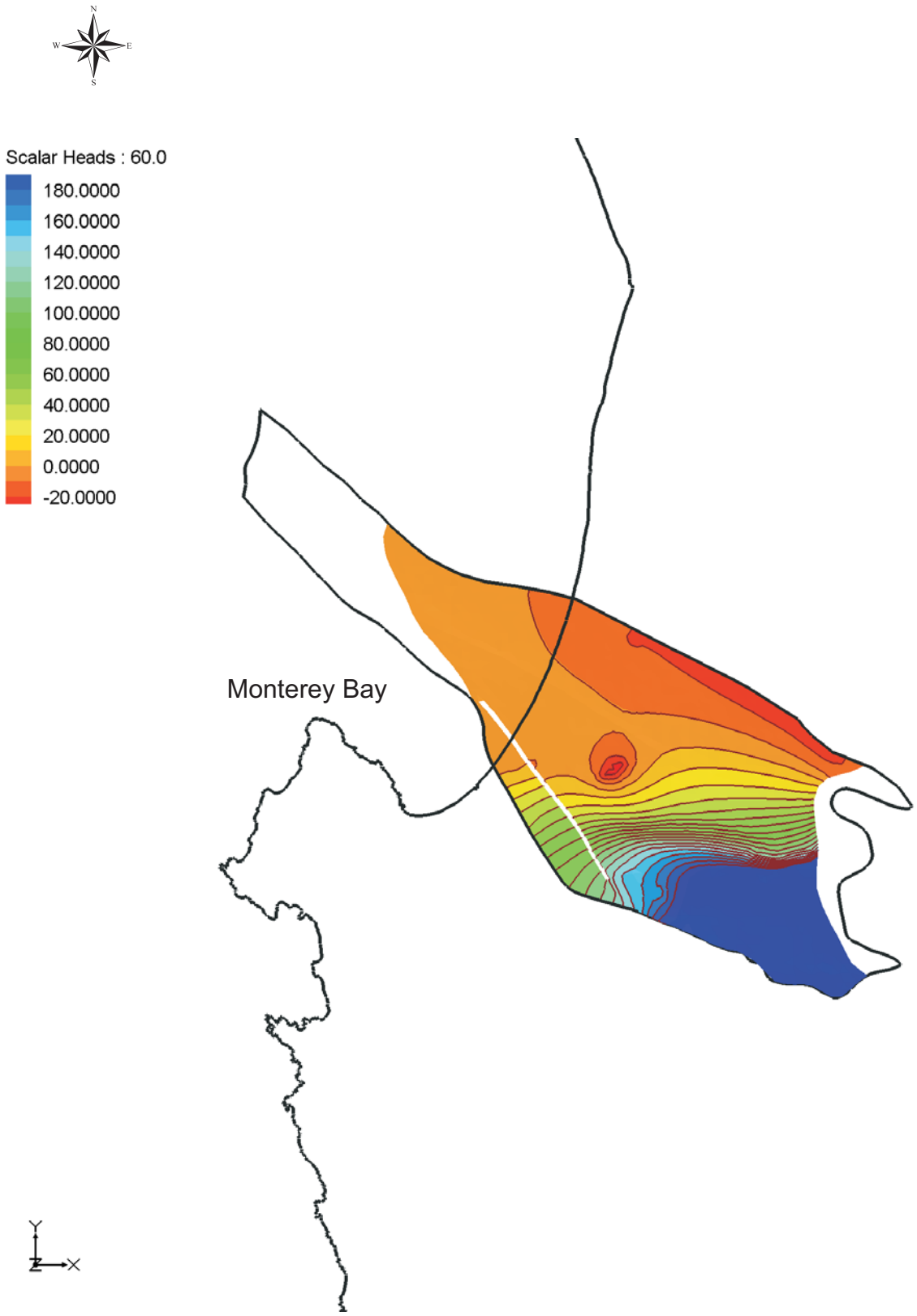

Figure 4.3b Computed Heads for 2015
with Relocated Pumping, Santa Margarita Formation

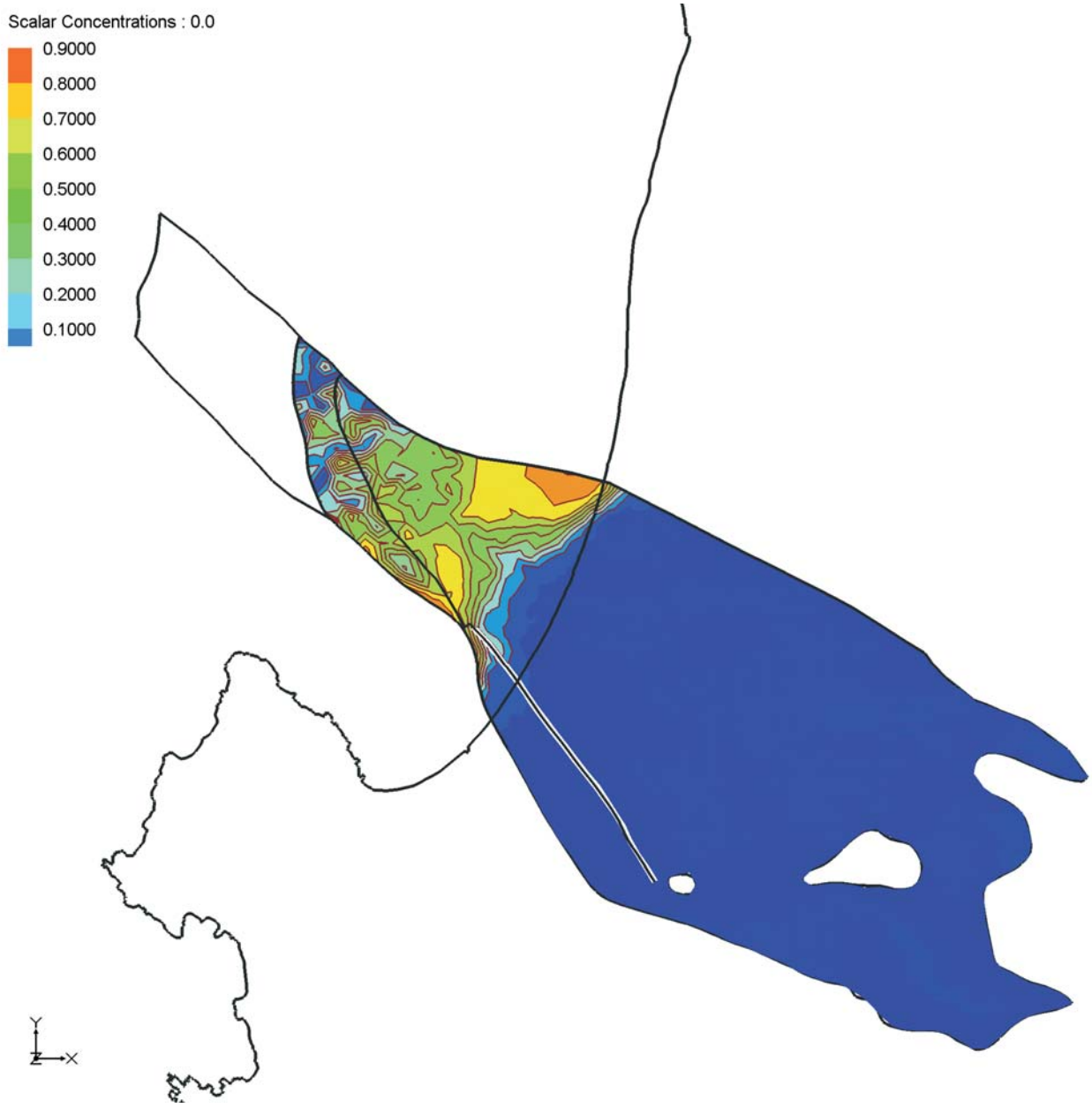

Figure 4.4a Computed Salinity for 2015
with Relocated Pumping, Paso Robles Formation

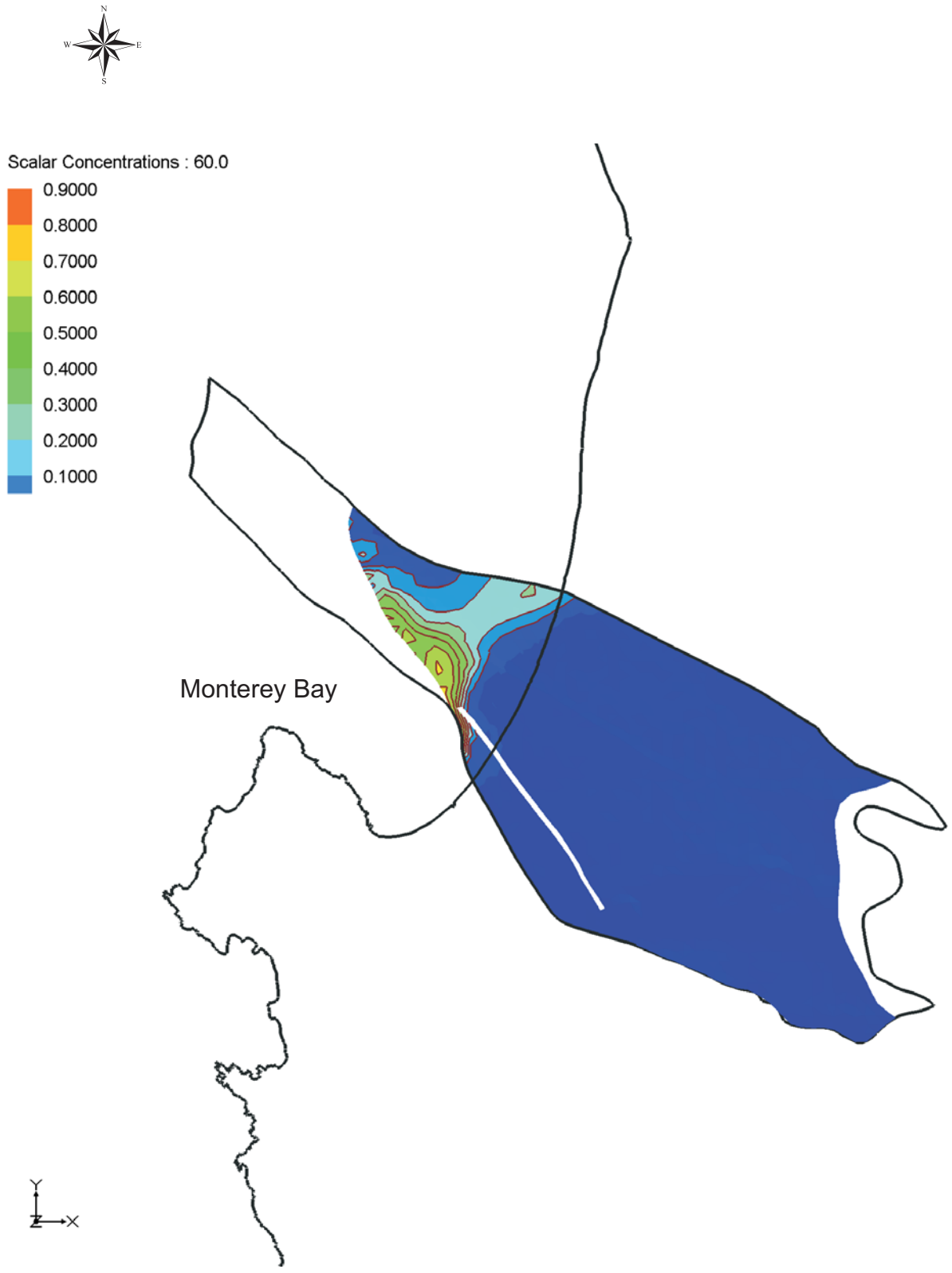

Figure 4.4b Computed Salinity for 2015
with Relocated Pumping, Santa Margarita Formation